MARIA S. MERIAN–Berichte

The Jøtul hydrothermal field – Magma-sediment interaction at the ultraslow-spreading Knipovich Ridge

Cruise No. MSM131

18 August – 28 September 2024
Reykjavik (Iceland) – Emden (Germany)
Jøtul Field

Bohrmann, Gerhard; Anagnostou, Eirini; Asatrian, Kristina; Barrenechea Angeles, Inés; Bergenthal, Markus; Berger, Frederik; Büttner, Hauke; Diehl, Alexander; Feddersen, Greta; Franke, Rosalia; Jain, Apoorvi; Kienitz, Tim; Knutsen, Stig Morten; Kopiske, Eberhard; Malnati, Janice; Marcon, Yann; Meckel, Eva-Maria; Meyer, Maximilian; Pilot, Matthias; Rehage, Ralf; Reuter, Christian; Ribeiro, Pedro; Röhler, Aaron; Römer, Miriam; Schillai, Sophia; Schlindwein, Vera; Schröder, Marcel; Spiesecke, Ulli; Streuff, Katharina; Strmic-Palinkas, Sabina; von Wahl, Till

Gerhard Bohrmann

University of Bremen, MARUM

2025

Table of Contents

1 Cruise Summary ……. 2
1.1 Summary in English ……. 2
1.2 Zusammenfassung …… 2
2 Participants…….. 3
2.1 Principal Investigators …….. 3
2.2 Scientific Party ……..…… 3
2.3 Participating Institutions …….. 5
2.4 Crew Members from Briese ……..…… 5
3 Research Program …….. 6
3.1 Description of Work Area …… 6
3.2 Aims of the Cruise …….. 11
3.3 Agenda of the Cruise …….. 12
4 Narrative of the Cruise …….. 12
5 Preliminary Results ……...
5.1. Hydroacoustic Operations……...……. 18
5.2 Passive Seismology Around Jøtul Vent Field, Knipovich Ridge …… 21
5.3 Oceanographic Data……..……... 25
5.4 MAPR and ORP Sensor…….. 31
5.5 Remotely Operated Vehicle (ROV) MARUM QUEST 4000 …… 37
5.5.1 ROV Operations …….. 37
5.5.2 Dive Reports …… 40
5.5.3 Optical Seabed Surveys and Photo-Mosaicking …….. 69
5.5.4 Temperature Measurements in the Sediments (T-Stick)…….. 71
5.5.5 KIPS Sampling …… 74
5.5.6 IGT Sampling of Fluids and Gases ……. 77
5.6 Gas Analysis……..……... 79
5.7 Sediment Sampling ……..…… 84
5.8 Foraminifera from Jøtul Vent Field…….…….. 87
5.9 Outreach Activities …….. 91
6 Station List MSM131……..……... 92
7 Data Sample Storage and Availability ……... 97
8 Acknowledgements …… 97
9 References …….. 98
10 Appendix …… 100

1 Cruise Summary

1.1 Summary in English

During the expedition with RV MARIA S. MERIAN MSM131, investigations were carried out on the sea floor and in the water column at hydrothermal vents of the Knipovich and Molløy Ridges. On the 500 km long Knipovich Ridge, an active hydrothermal field was discovered for the first time during MSM109 in 2022. Dives with ROV QUEST 4000 were used during MSM131 to investigate the various active hydrothermal vents of the Jøtul field, known by name as Fenris and Gyme Smoker, Yggdrasil and Nidhogg. In addition to fluid sampling with gas-tight sampling devices, the structures were imaged and partially photographed in 3D using photo-mosaicking. The methane and carbon dioxide contents in the sampled fluids were surprisingly high, documenting the interaction of volcanism with the sediments in the subsurface of the hydrothermal field. By repeatedly visiting individual hydrothermal vents, we were able to detect very rapid growth of precipitates in the form of chimneys. To record the hydrothermal plume structure and its drift due to the current to the North, 15 Tow-Yo-CTD profiles were carried out. In addition to continuous temperature and Eh sensors, water samples were taken and analyzed for methane, CO_2 and hydrogen concentrations to record the signals. In addition, samples were taken to examine the helium isotope. Furthermore, 35 surface sediment samples were taken with the mini-corer to investigate the drift of the hydrothermal components of the Jøtul field.

1.2 Zusammenfassung

Während der Expedition mit FS MARIA S. MERIAN MSM131 wurden Untersuchungen am Meeresboden sowie in der Wassersäule zu hydrothermalen Quellen des Knipovich und Molløy Rückens durchgeführt. Tauchgänge mit ROV QUEST 4000 wurden während der MSM131 genutzt, um die verschiedenen aktiven Hydrothermalquellen des Jøtul Feldes, namentlich bekannt als Fenris und Gyme Smoker, Yggdrasil und Nidhogg. Neben der Fluid-Beprobung mit gasdichten Probennahme-Geräten wurden die Strukturen fotografisch dokumentiert und teilweise durch Foto-Mosaicking 3D-mäßig erfasst. Überraschend hoch waren die Methan- und Kohlenstoffdioxid-Gehalte in den beprobten Fluiden, welche die Wechselwirkung von Vulkanismus mit den Sedimenten im Untergrund des Hydrothermal-Feldes dokumentieren. Durch Mehrfach-Aufsuchung einzelner Hydrothermalquellen, konnten wir zum Teil sehr rasches Wachstum von Präzipitaten in Form von Schornsteinen feststellen. Zur Erfassung der hydrothermalen Plume-Struktur und ihrer Verdriftung durch die Strömung nach Norden wurden 15 Tow-Yo-CTD Profile durchgeführt, wobei zur Signalerfassung neben kontinuierlicher Temperatur- und Eh-Sensorik, Wasserproben genommen und auf Methan-, CO_2- und Wasserstoff-Konzentrationen analysiert wurden. Zusätzlich wurden Proben zur Untersuchung der Helium-Isotopie genommen. Weiterhin wurden 35 Oberflächen-Sedimentproben mit dem Mini-Corer beprobt um die Verdriftung der hydrothermalen Komponenten des Jøtul Feldes zu untersuchen.

2 Participants

2.1 Principal Investigators

Name	Institution
Bohrmann, Gerhard, Prof. Dr.	MARUM, GeoB
Römer, Miriam, Dr.	MARUM
Pape, Thomas, Dr.	MARUM, GeoB
Diehl, Alexander, Dr.	MARUM

2.2 Scientific Party

Name	Leg	Discipline	Affiliation
Anagnostou, Eirini	2	KIPS, fluid chemistry	CoUB
Asatrian, Kristina	1	OBS recovery	AWI
Barrenechea Angeles, Inés, Dr.	2	Foraminifers	UiT
Bergenthal, Markus	1	ROV	MARUM
Berger, Frederik	1 + 2	Hydroacoustics	MARUM
Bohrmann, Gerhard, Prof. Dr.	1 + 2	ROV / Chief Scientist	MARUM, GeoB
Büttner, Hauke	1 + 2	ROV	MARUM
De Azevedo Ribeiro, Pedro, Prof.	2	ROV dives	UiB
Diehl, Alexander, Dr.	2	IGT, ROV dives	MARUM
Feddersen, Greta	1 + 2	ICOS, hydroacoustics	MARUM
Franke, Rosalia	2	Media	GeoB
Jain, Apoorvi	2	Hydroacoustics	MARUM
Kienitz, Tim	1 + 2	ROV	MARUM
Knutsen, Stig Morten, Dr.	1 + 2	ROV dives	NOD
Kopiske, Eberhard	1	CTD, Mini-corer	MARUM
Malnati, Janice	2	ICOS, GC, CTD	GeoB
Marcon, Yann, Dr.	1	ROV dives, mosaics	MARUM, GeoB
Meckel, Eva-Maria, Dr.	2	KIPS, fluid chemistry	CoUB
Meyer, Maximilian	1 + 2	Hydroacoustics	GeoB
Pape, Thomas, Dr.	2	CTD, GC, ROV dives	GeoB
Pilot, Matthias	1	OBS recovery	AWI
Rehage, Ralf	1 + 2	ROV	MARUM
Reuter, Christian	1 + 2	ROV	MARUM
Röhler, Aaron	1	ROV dives	MARUM
Römer, Miriam, Dr.	1 + 2	MAPR, ROV dives	GeoB, MARUM
Schillai, Sophia	1 + 2	ROV	MARUM
Schlindwein, Vera, Prof. Dr.	1	OBS recovery	AWI
Schröder, Marcel	1 + 2	ROV	MARUM
Spiesecke, Ulli	1 + 2	ROV	MARUM
Streuff, Katharina, Dr.	1	MBES, PARASOUND	GeoB
Strmic-Palinkas, Sabina, Dr.	1	ROV dives	UiT
von Wahl, Till	2	ROV	MARUM

Fig. 2.2.1 Scientific crew onboard RV MARIA S. MERIAN during MSM131-1.

Fig. 2.2.2 Scientific crew onboard RV MARIA S. MERIAN during MSM131-2.

2.3 Participating Institutions

MARUM Center for Marine Environmental Sciences, University of Bremen, Leobener Straße 8, D-28359 Bremen, Germany, http://www.marum.de

GeoB Fachbereich Geowissenschaften der Universität Bremen, Klagenfurter Straße 2-4, D-28359 Bremen, Germany, https://www.geo.uni-bremen.de

AWI Alfred-Wegener-Institut, Helmholtz-Zentrum für Polar- und Meeresforschung, Postfach 12 01 61, 27515 Bremerhaven, Germany, https://www.awi.de

UiT The Arctic University of Norway, PO Box 6050 Stakkevollan N-9037 Tromsø, Norway, https://en.uit.no/startsida

UiB University of Bergen, Institut for geovitenskap, Postboks 7803, N-5020 Bergen, Norway, https://www.uib.no/en/deepsea

CoUB Constructor University, Bremen gGmbH, Campus Ring 1, 28759 Bremen, Germany, https://constructor.university/

NOD Norwegian Offshore Directorate, Professor Olav Hanssens vei 10, 4021 Stavanger, Norway, https://www.npd.no/en/

Briese Briese Schiffahrts GmbH & Co KG, Abteilung Forschungsschifffahrt, Hafenstr. 12, D-26789 Leer, Germany, https://briese-research.de/

2.4 Crew Members from Briese Shipping Operator

Name	Discipline
Maass, Björn	Master
Bruns, Bastian	Chief Officer
Muenchau, Wiebke	1st Officer
Ulferts, Geert Harm	2nd Officer
Wagner, Sven	Chief Engineer
Schmidt, Samuel	2nd Engineer
Kuehne, Nils	Electrician
Hermann, Denny Klaus	Sysop
Herrmann, Jens	Electronics
Plink, Sebastian	Bosun
Peters, Karsten	Ship’s Mechanik
Hampel, Ulrich	Ship’s Mechanik
Rutenbeck, Birk Lars Winfried	Ship’s Mechanik
Altmann, Detlef	Ship’s Mechanik
Peschkes, Peter	Ship’s Mechanik
Werner, Andre	Ship’s Mechanik
Grüger, Christoph	2nd Cook
Kluge, Sylvia	Stewardess
Brehm, Matthias	1st Cook
Lehmbecker, Jonathan Paul	3rd Engineer
Ederleth, Tom Wilko	Motorman
Friesenborg, Helmut	Fitter
Staak, Ludwig	Ship’s Surgeon

3 Research Program

3.1 Description of Work Area

The proposed study sites at Knipovich Ridge is one segment of the Mid-Atlantic Ridge, north of the Arctic Circle (66°N), which are considered the Arctic Mid-Ocean Ridge (AMOR; Pedersen et al., 2010a). The AMOR consists of the Kolbeinsey, the Mohns, the Knipovich, and the Molløy Ridges, the Lena Trough, and the Gakkel Ridge (Fig. 3.1).

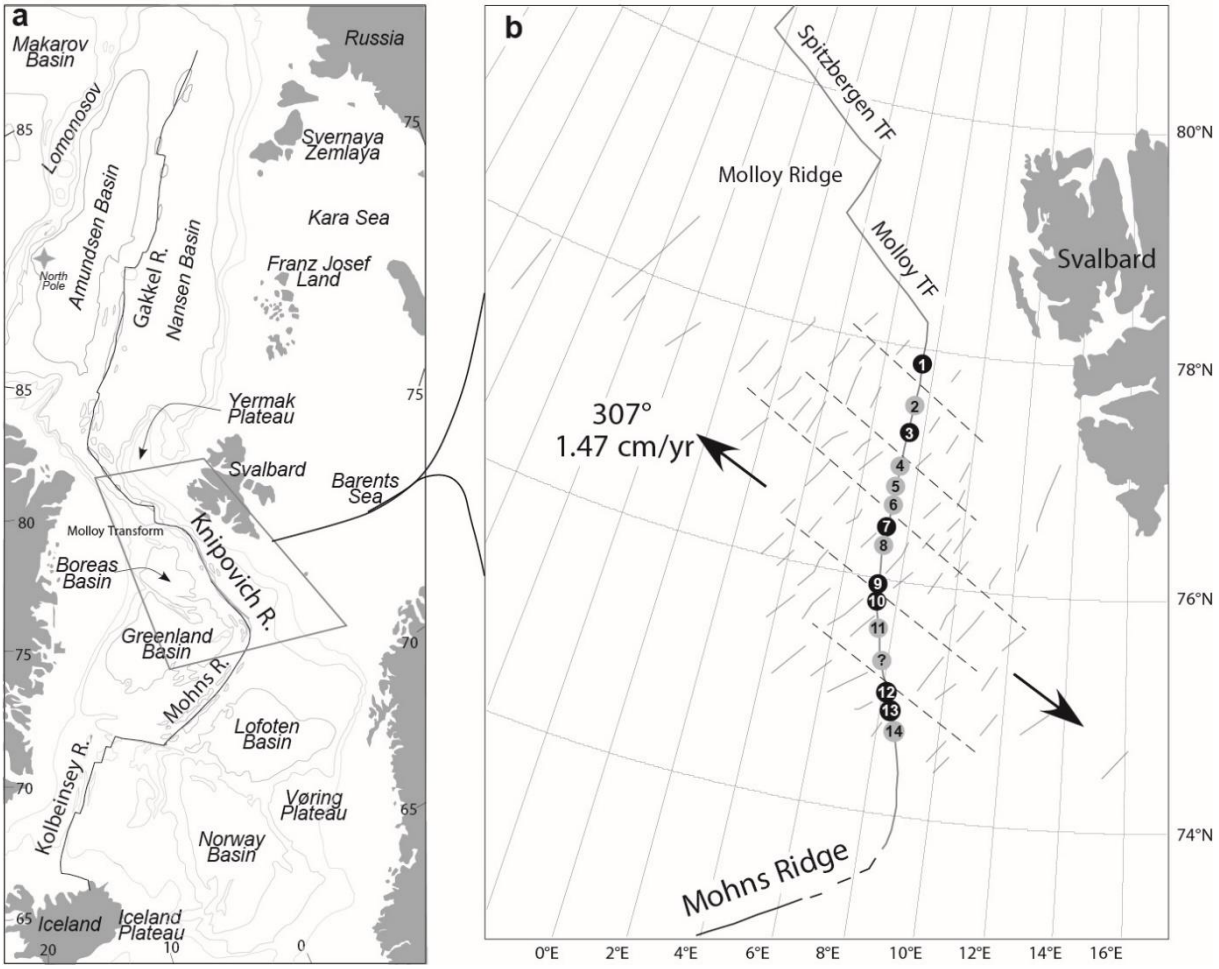

Fig. 3.1. a) Locations of Arctic Mid-Ocean Ridges, continental land masses, and Knipovich Ridge north of Mohns Ridge. Contour lines of the ocean basin depths in 1,000 m intervals. **b)** Segmentation of Knipovich Ridge and tentative magnetic lineations. The numbered circles indicate centres of spreading segments. Black circles correspond to segments that lie at the intersection of off-axis seamount chains with the ridge. Those segments are characterized by pronounced relief, sonar reflectance, and mantle Bouguer anomalies. Gray circles correspond to weaker spreading segments (from Curewitz et al., 2010).

The Knipovich Ridge is situated asymmetrically between Svalbard and NE Greenland, and extends from 73°30'N to 78°40'N. It is bordered by the Molløy Fracture Zone in the North and the Greenland-Senja Fracture Zone at the Mohns-Knipovich Ridge Bend in the South. With a spreading rate of <1.5 cm/yr it is one of the slowest and most obliquely spreading mid-ocean ridges on the planet (Fig. 3.1a). Magnetic and gravimetric surveys along the ultraslow-spreading Gakkel Ridge and Mohns Ridge (Crane and Solheim, 1995) showed ongoing sustained and continuous sea

floor spreading. Investigations in the past, that were predominantly performed by international scientists, have shown that Knipovich Ridge is characterized by a rather complex structure (Okino et al., 2002; Chamov et al., 2010, Curewitz et al., 2010, Zarayskaya, 2017). A bathymetry grid originating from sea floor mapping and other comprehensive investigations was collected during four Russian cruises with R/V AKADEMIK NIKOLAI STRAKHOV (2006, 2007 and 2009). Based on the morphology and specifically on the morpho-structural segmentation, major tectonic elements of Knipovich Ridge have been classified. These investigations revealed that the formation of this active plate boundary was accompanied by the alteration of geodynamic settings with the predominance of strike-slip and normal faults. These processes still compete in the formation of the ridge's rift zone (Okino et al., 2002). The Knipovich Ridge is uninterrupted by transform faults even though the available bathymetric and gravity data have been interpreted to indicate the presence of seven magmatically strong and seven magmatically weak segments (Fig. 3.1b).

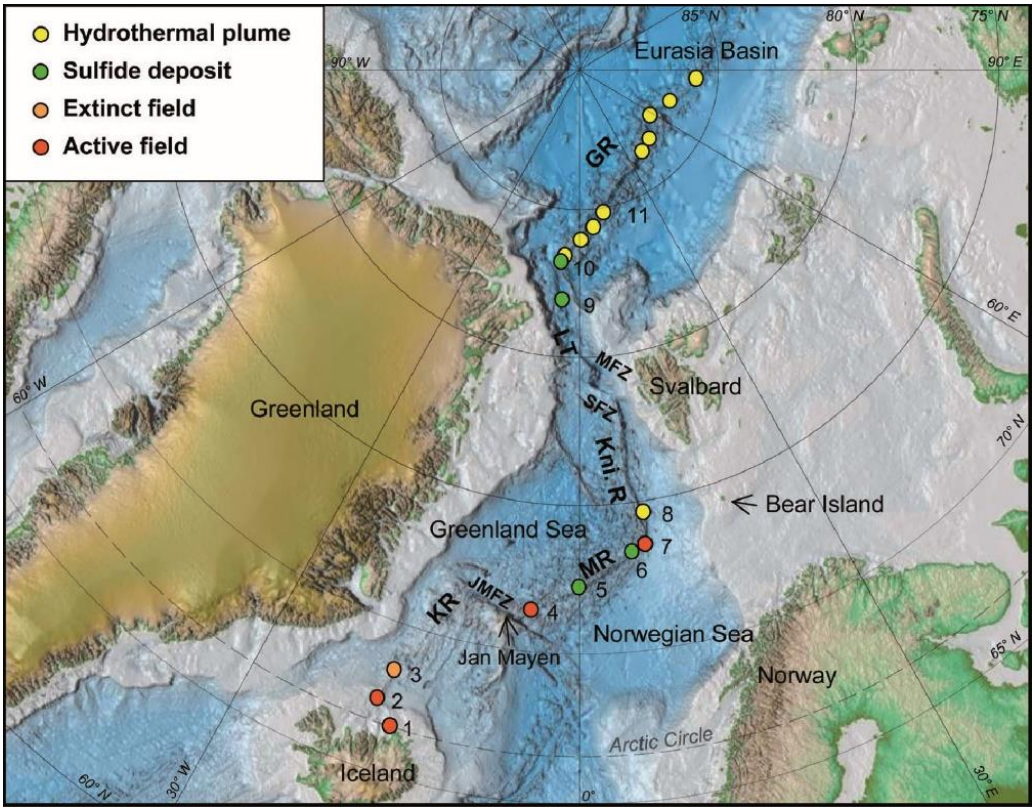

Fig. 3.2 Arctic Mid-Ocean Ridges (AMORs) showing locations of active and extinct hydrothermal vent fields. Grimsey (1), Kolbeinsey (2), Squid Forest extinct field (3), Jan Mayen, Soria Moria, and Troll Wall (4), Copper Hill (5), Mohn's Treasure (6), Loki's Castle (7), hydrothermal plume (8), sulfide deposits (9), sulfide deposits (10), hydrothermal plume (11) from Pedersen et al., 2010a). GR-Gakkel Ridge, LT-Lena Trough; MFZ-Molløy Fracture Zone; SFZ-Spitsbergen Fracture Zone; Kni. R-Knipovich Ridge; MR-Mohns Ridge; JMFZ-Jan Mayen Fracture Zone; KR-Kolbeinsey Ridge.

The rift zone of Knipovich Ridge is generally formed in a transtension environment. Focusing of the melt possibly caused by the presence of spreading cells was firstly shown by Okino et al. (2002) and revised by Jokat et al. (2012). First evidences of these mechanisms were reported by Schlindwein et al. (2016), who showed a seismic gap beneath a cluster of axial volcanic

cones.Until recently, Arctic mid-ocean ridges and their hydrothermal systems were some of the least explored elements of the global ridge system. In contrast, there is considerable scientific interest in these systems, e.g., because of their ultraslow spreading rates, the high density of mantle-derived peridotites, their proximity to continental margins, and voluminous accumulations of organic-rich sediments with high hydrocarbon generation potential on parts of the ridges. Systematic exploration of the spreading ridges north of Iceland (i.e., AMOR) during the past 25 years documented a large number of active and inactive venting sites. Locations of approximately 20 active and extinct vent areas have been either identified during sea floor observations, or inferred from physicochemical anomalies of the seawater that are caused by hydrothermal plumes and from dredge sampling of hydrothermal precipitates (Fig. 3.2).

Decreasing spreading rates and decreasing influence of the Icelandic hot spot toward the North along the AMOR result in a south-north change from shallow and magmatically-robust to a deep and magmatically-starved ridge system (Pedersen et al., 2010a). This contrast gives rise to a large variability in the geology of the ridges and in the formation and geochemistry of associated hydrothermal vent fields. The known vent sites at the southern part of AMOR are either low-temperature or white smoker fields. At the deep, northern parts of AMOR, large black smoker vent fields have been located. North of Iceland hydrothermal vent fields are known from Kolbeinsey Ridge, from Mohns Ridge, from Lena Trough and from Gakkel ridge. Between Mohns Ridge and Knipovich Ridge Loki's Castle is well known (Pedersen et al., 2010b), which was intensively investigated. (No.7 in Fig. 3.2). The field is located in the vicinity of the area where the striking of Mohns Ridge changes about 80° to a more northerly trend and merges into the Knipovich Ridge. It is additionally situated near the summit of a large AVR. Venting from Loki's Castle Vent Field occurs from the top of two hydrothermal mounds that are around 20–30 m high and approximately 200 m across. Venting causes a hydrothermal plume in the water column that rises 300–400 m above the sea floor and is characterized by anomalies in Eh, CH_4, and H_2 (Pedersen et al., 2010b; Baumberger et al., 2016). Although Loki's Castle Vent Field is underlain by volcanic rocks, the influence of sediments from the nearby Bear Island sedimentary fan is observed in the fluid chemistry (e.g., high concentrations of methane and ammonia).

During excellence-cluster expedition using research vessel MARIA S. MERIAN MSM109 (6 July – 3 August, 2022 (Tromsø - Reykjavik) new insights into hydrothermal activities of the Knipovich Ridge could be gained. Based on a high-resolution AUV backscatter map of the Norwegian Petroleum Directorate (NPD), a young volcanically active area could be identified north of the prominent Axial Volcanic Ridge (AVR) near Logachev Seamount. Based on this information, 3 dives were conducted with ROV QUEST 4000, in two cases in the area of a volcanic hill at 76 °49'N showed hydrothermal precipitates. On the top of a volcanic mound in a 10 m deep fissure several chimneys were visible in a hydrothermal area, from which a sulfide smoker was sampled. No evidence of recent hydrothermal activity was seen. A second site in the northeast foot region of the volcanic mound showed patchy yellowish-reddish precipitates that were associated with igneous rocks and most likely also represents hydrothermal activity.

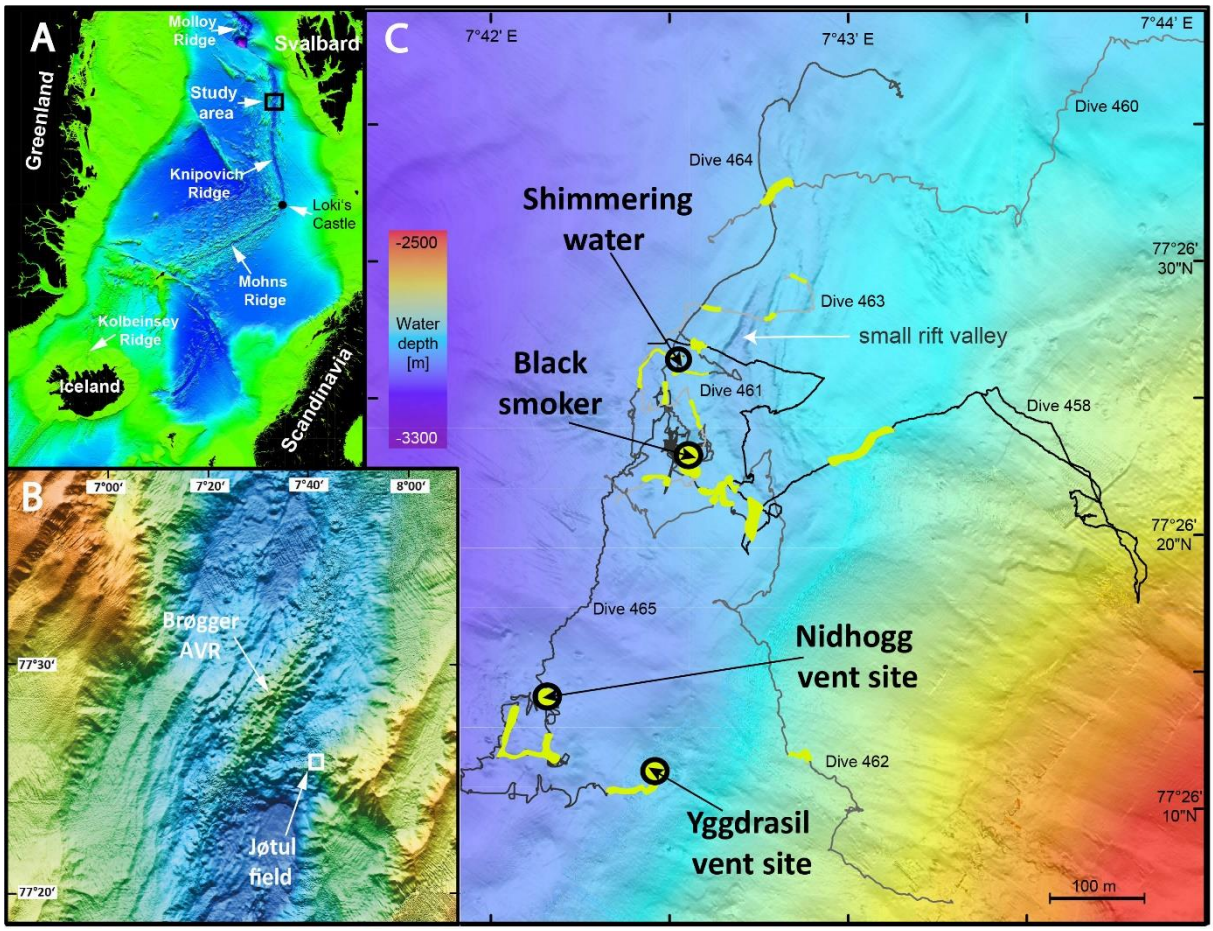

Fig. 3.3 **A**, Map of the Norwegian-Greenland Sea with locations of active sea floor spreading centers and the study area. **B**, Detailed map of the study area including the Brøgger Axial Volcanic Ridge (AVR) and the newly discovered hydrothermal active area called Jøtul hydrothermal field. **C**, AUV-based bathymetry of the Jøtul hydrothermal field (data acquired during cruise MSM109 and provided by NPD). Track lines of ROV dives are shown and track portions, where hydrothermal activity was visually observed, are marked in yellow. Four sites were sampled for fluids during MSM109 and are indicated by circles (Bohrmann et al. 2024).

Numerous indicators of low-temperature to high-temperature hydrothermal activity were found north of a very prominent AVR we named the Brøgger AVR at 77° 26' N west. Evidence of surface hydrothermal activity was derived from Eh anomalies and methane concentrations in the water column. Seven ROV dives were used to locate active vent sites and to document the extension of hydrothermal activity primarily to the West and East (Fig. 3.3). Most common were patches of white staining on sediment surfaces and at the margins of igneous rocks, which are certainly due to white microbial filaments mostly attached to Siboglinid tubeworms. The white staining at the edges of the hard rocks are often associated with white precipitates of barite and amorphous silica. These patchy features have been classified as minor hydrothermal manifestations without detailed investigations being conducted. Other vent locations are characterized by the outflow of bright but shimmering fluids with temperatures between 8 – 272°C or are typical black smokers with black sulfide fluids having temperatures higher than 300°C.

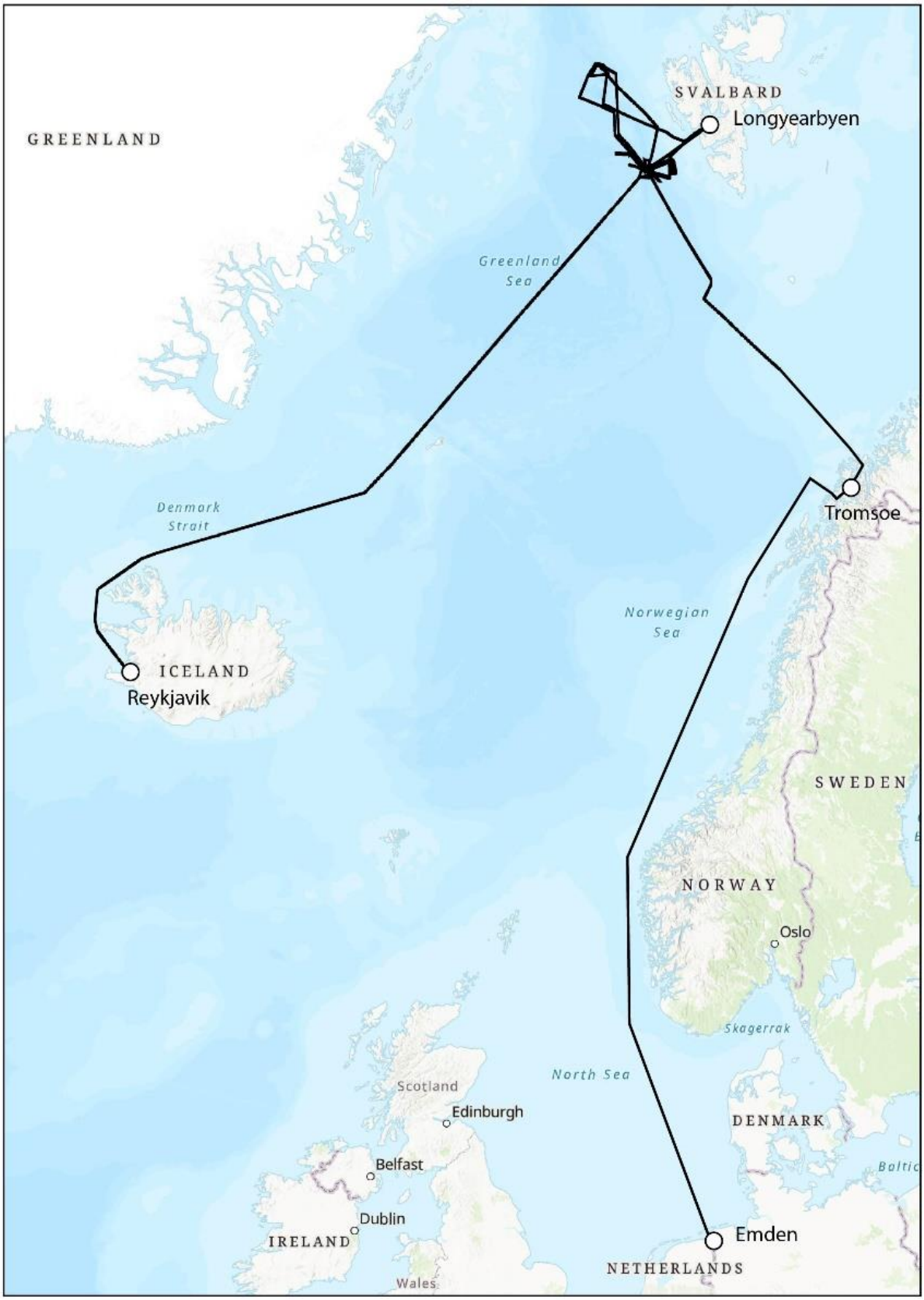

Fig. 3.4 Ship track of RV MARIA S. MERIAN cruise MSM131 from Tromsø to Reykjavik.

Several of the vent structures are complex with various chimneys and flanges and show extensive diverse mineral precipitates in their immediate vicinity which were sampled during MSM109 (Fig. 3.4). The analyses reveal that the black smoker precipitate is mostly composed of chalkopyrite, spahlerite, pyrrhotite and anhydrite. Other hydrothermal edifices are composed of dolomite mixed with chalkopyrite, pyrite and other lower temperature precipitates (Bohrmann et al. 2024). The discovered hydrothermal field was named Jøtul field during expedition MSM109. ROV dives to date show that the hydrothermal area has a north-south extent of at least 1 km, but the boundaries to the North and South are not yet covered by surveys. The east-west extent of the Jøtul field is approximately 200 m, with this area of hydrothermal activity broadening significantly to the South. Overall, the Jøtul field runs along the lower slope between 3,000 and 2,800 m water depth on the eastern flank of the Knipovich Graben.

High methane levels are reported from hydrothermal areas such as Loki's Castle, Escanaba or Guaymas (Baumberger et al. 2016) where there are interactions between magmatism and sediments. This is also true for the Jøtul field, as the hydrothermal activity is not tied to the AVR of the Brøgger Ridge in the center of the Central Graben, but occurs on the eastern flank where the magmatic activity interacts with the sediments of the Svalbard continental margin. The isotopic composition of hydrogen and carbon indicate a thermogenic origin for the methane. East and southeast of the southernmost hydrothermal vents of Nidhogg and Yggdrasil the sea floor shows a strange morphology in the microbathymetric AUV map with a corrugated surface, reminescent of an outcroping flat part of a detachment fault. The surface corrugations reveal NW/SE striking lines, which are parallel to the spreading direction. Cut-off structures are lying perpendicular to the spreading direction. Two highly weathered rock samples collected during an ROV dive partly covering the detachment fault plane revealed are totally composed of talc and have high contents of chrome and nickel which is more enriched in mantle rocks. Thin sections of these rocks showed a mesh structure which is typical for serpentinite altered from mantle rocks. Based on these new observations and recent data, the existence of an oceanic core complex (OOC) is expected. The relationship of the OCC to the hydrothermal activity is therefore very interesting and has to be investigated during the cruise.

3.2 Aims of the Cruise

The main objective of the research expedition is to study the Jøtul hydrothermal field in detail, characterize its various hydrothermal vents on the seafloor and the north and south extension of the field. In addition to the mapping work, the precipitates and the fluids from the emission sites will be sampled and investigated to understand the connection between the newly discovered hydrothermal circulation at the eastern rim of the Knipovich Ridge. The interaction of the magmatic intrusions with the sediments of Svalbard margin are of special interest because of the release of hydrocarbons. Further investigations will include exploration in a young volcanic area north of Logachev AVR. The objectives also include the formation of hydrothermal plumes in the water column and the distribution of hydrothermal components in the surrounding sediments. Our research questions and hypotheses are:

1) How diverse are the hydrothermal fluids between the vents in the Jøtul field and what are the volcanic and faulting controls of this diversity at the rim of the graben system? We hypothesize

that magmatic intrusions in sediments from the Svalbard margin are important for the mobilization of hydrocarbons.

2) How are metals transformed within the rising and neutrally buoyant parts of the hydrothermal Jøtul plume and how is the fate of metals controlled by primary differences in metal:sulfide and metal:carbon ratios?
3) How is the relationship of the Jøtul hydrothermal field to the nearby detachment fault? Small-sized elevations in the AUV-based micro-bathymetry of the potential ocean core complex could represent hydrothermal mounds? Are these mounds of different hydrothermal precipitates than the precipitates from the Jøtul field? Is the detachment fault and the potential oceanic core complex (OOC) east of the Jøtul field involved in the hydrothermal circulation of the field, and what are the connections?
4) Which hydrothermal activities exist in the area of the young volcanic field north of the Logachev AVR, where hydrothermal precipitates were found during MSM109. Is there an active hydrothermal circulation or are all hydrothermal systems inactive? In case we can find active hydrothermal fluids, are they different form fluids of the Jøtul field? How are these related to the different host rocks in a completely different part of the ultra-slow spreading ridge?

3.3 Agenda of the Cruise

As part of the research unit "The Ocean Floor as Reactor" of the Bremen Cluster of Excellence "The Ocean Floor – Earth's Uncharted Interface" we used RV MARIA S. MERIAN cruise MSM131 to investigate hydrothermal fields of the Knipovich Ridge and Molløy Ridge in the Norwegian Greenland Sea west of Svalbard. The newly found Jøtul hydrothermal field was of special interest and multidisciplinary investigations were planned. The use of Multibeam Kongsberg EM133 and the sub-bottom sediment echosounder PARASOUND were planned for bathymetry, backscatter imaging of the sea floor and for the search of gas emission sites. CTD rosette water sampling combined with self-contained miniature autonomous plume recorders (MAPR) should be used for detecting the distribution of the hydrothermal plume water. For detailed investigations at hydrothermal vent areas ROV QUEST 4000 was available and should be used for high-resolution imaging and sampling of hydrothermal fluids with the gas-tight fluid samplers (IGTs). In total 28 working days have been available after 4 days transit from Reykjavik to the working area and 8 days transit to Emden at the end of the cruise.

4 Narrative of the Cruise

On **Sunday, 18 August**, 2024, RV MARIA S. MERIAN left the "Grandabryggja" pier in the Old Port of Reykjavik at 08:36 local time to set off for the Norwegian Sea. Investigations on the so-called Knipovich Ridge to determine the distribution of hydrothermal vents on the seabed are the main objective of the research mission MSM131. The departure on Sunday was preceded by 4 days of intensive unloading and loading work in the port of Reykjavik. After the ship arrived in Reykjavik around noon on Wednesday, the three packed containers from the previous cruise MSM130 were unloaded, and the ship's crew began loading three Bremen containers of the "Remotely Operated Vehicle", MARUM ROV QUEST 4000. The start of the assembly of MARUM ROV QUEST 4000 on the ship was a top priority, as an additional port day is required

to integrate the ROV into the ship's operations. Thanks to the good port logistics in all 8 containers from Germany, 6 from MARUM in Bremen and 2 from AWI Bremerhaven, were delivered to Reykjavik on time, and on Thursday the remaining 5 containers were placed onboard MARIA S. MERIAN. Most of the scientists also arrived on board on **Friday, 16 August** while the ROV team was already busy installing the various ROV components from the first day in port. Saturday was the day for setting up the ship's laboratories, for which the ship's crew had already emptied the two containers with the laboratory equipment packed in transport boxes and the consumables.

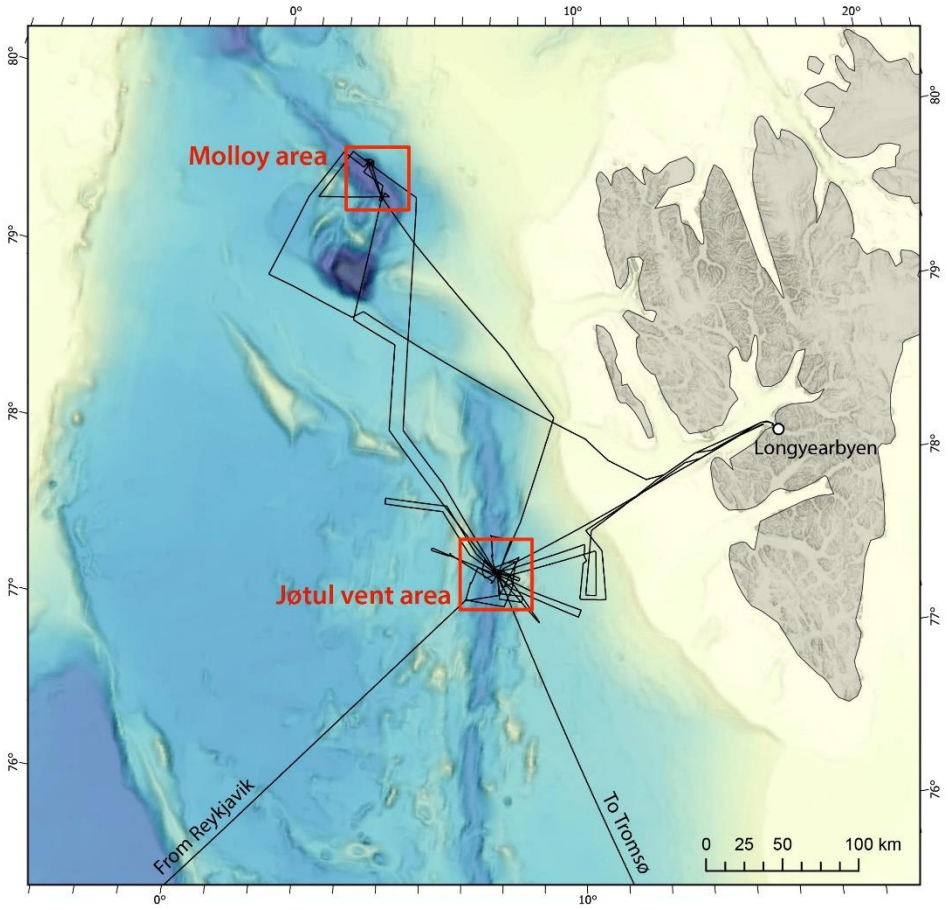

Fig. 4.1 Track lines of RV MARIA S. MERIAN during MSM131 and the two areas of detailed investigations.

The port work was completed on **Saturday, 18 August** evening and the ship was ready to set sail on Sunday morning. The ship sailed north through the Denmark Strait on the west side of Iceland and then, after the passage, almost directly for the Jøtul hydrothermal field on the northern Knipovich Ridge, west of Svalbard (Fig. 4.1). On **Tuesday, 20 August**, we reached the Norwegian EEZ at 12:16 p.m. and were able to start recording the hydroacoustic devices. Further preparations for the expedition's scientific work program took place during the daily science meetings in the afternoon on the transit route to the work area. Our working area was the Knipovich Ridge at 77° 27’ north, where we discovered the first hydrothermal field of the 500 km long Knipovich Ridge two years ago with this ship. In the middle of the graben there is a narrow ridge made of volcanic pillow lava basalts. The hydrothermal field we found, which we named Jøtul Field after a giant in Norse mythology, is not tied to this volcanic ridge as originally expected, but is located 5 km east of the ridge at the foot of the eastern rift shoulder at a water depth of 3,000 m. After reaching the working area on **Thursday evening, 22 August**, we started with an acoustic survey of the water

column on the eastern shoulder of the Knipovich Ridge. On Friday morning we started with the first CTD station, whose changes in temperature and Eh data showed very clear hydrothermal signals near the bottom and at a higher level. The rest of the day and the first half of the night were used to record 7 ocean bottom seismometers. In total, Vera Schlindwein and her working group at the AWI, Bremerhaven, placed 15 OBS on the sea floor in the area of the Jøtul field and its surroundings. Last year, 7 OBS were deployed during the RV POLARSTERN cruise PS137, and 8 further short-term OBS were deployed by a Norwegian research vessel about 2 months before our cruise. They register micro-seismic earthquakes, the analysis of which allows us to identify structures in the subsurface and may give us clues about the structure of the Jøtul fluid system within the earth's crust.

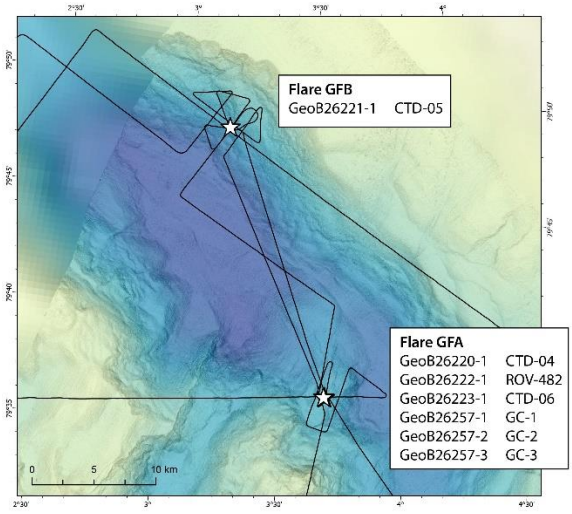

Fig. 4.2 Northern part of the Molløy Ridge area with ship tracks and sampling locations close to the Flare GFA and GFB positions.

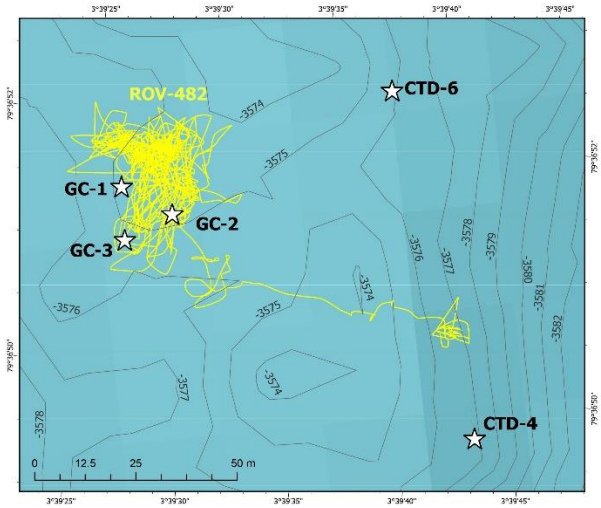

Fig. 4.3 Sea floor track of ROV dive 482 and positions of GC and CTD locations close to Flare GFA on the northern Molløy Ridge.

On **Saturday morning, 24 August**, the time had come for MARUM ROV QUEST 4000 to make its first dive. In the last few days, numerous repairs had to be carried out on the deep-sea robotic system, as the vehicle had suffered a number of injuries during transport in the container from Bremen to Reykjavik. We had initially noticed this on the transport container, which had suffered relatively major transport damage. However, as the vehicle was being upgraded on deck of the MARIA S. MERIAN, injuries were gradually noticed, which we attempted to repair using on-board equipment. Unfortunately, the 481st dive of the ROV QUEST 4000 (Fig. 4.4) was also delayed due to further technical problems, and it was not until around 5:00 p.m. local time that the seabed at a depth of 3,000 m could be reached. Thanks to our previous knowledge and very good maps, we were able to find a black smoker immediately, and a beacon was placed on the sea floor for quick retrieval. A short survey of the sea floor about 120 m to the West showed that there was plenty of hydrothermal activity due to the numerous bacterial mats distributed in patches. Unfortunately, a rapid loss in one of the four oil circuits forced us to abort the dive and ascend after a relatively short time. During the night of **Sunday, 25 August**, the OBS group was able to collect another 6 OBS from the sea floor. The CTD is currently in the water and after further successful repairs to the ROV, we can continue the program with the next dive tomorrow, if the weather permits. The third week unfortunately began with slightly worse weather than before, so that we could not dive in the Jøtul hydrothermal field, which is located at 77°26' north latitude, on **Monday 26 August**. A look at the various weather forecasts told us that wind and sea conditions

further north would allow more favorable conditions for station work, and so we steamed to our northern study area at almost 80° north. This was mainly possible because our three colleagues from the Alfred-Wegener-Institute had already recovered their 15 ocean bottom seismometers during three night-shifts, so that this work, which was tied to the region, could be successfully completed during the first leg of the cruise.

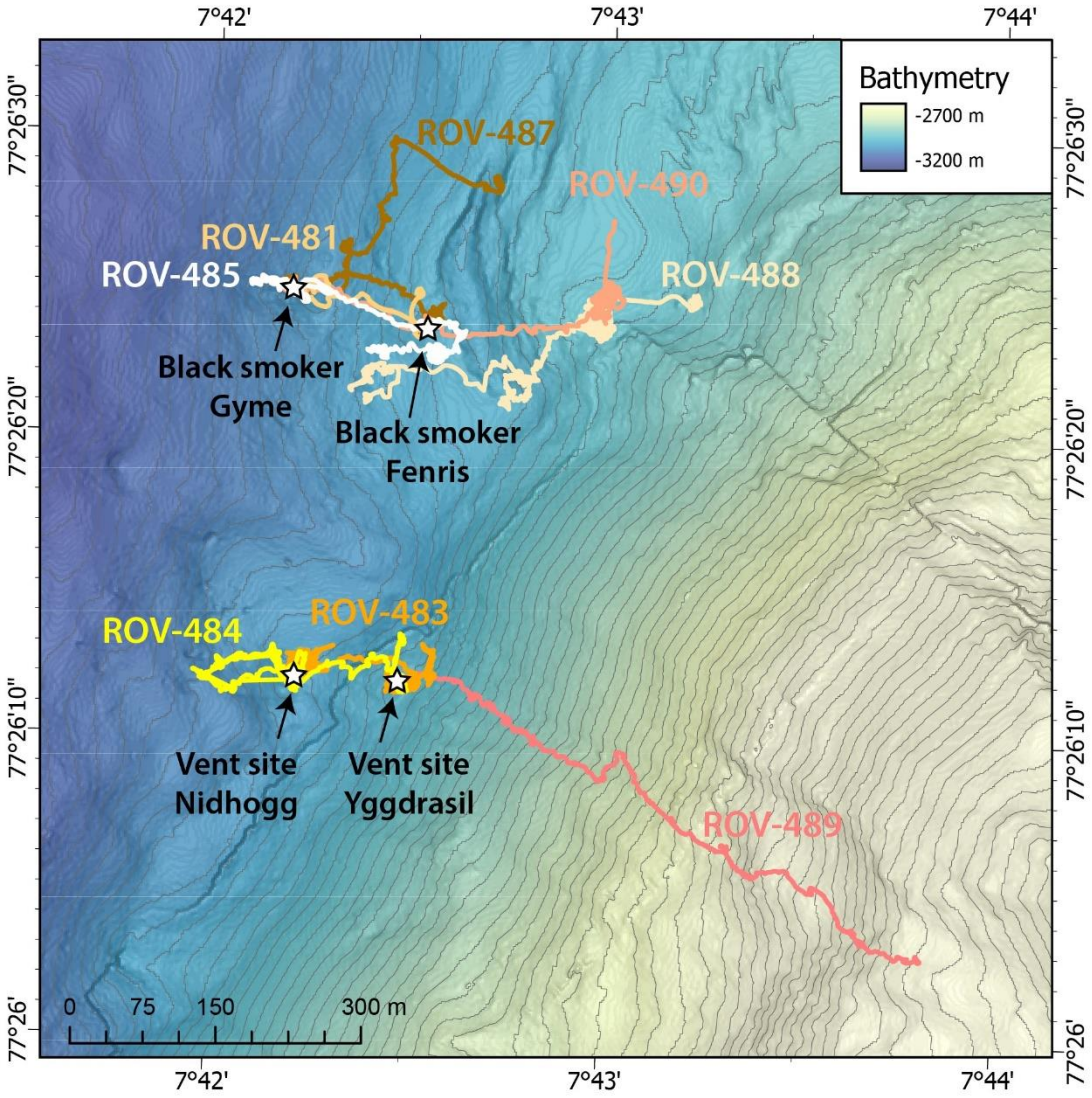

Fig. 4.4 Main hydrothermal venting structures of the Jøtul field and tracks of ROV dives performed during MSM131.

At the northern end of the ridge and north of the Spitsbergen Fracture Zone, two gas flares in the water column are described in the literature, which are confirmed by our hydroacoustic measurements (Fig. 4.2). During our measurements with the ship's hydroacoustic systems, we were able to identify the two flares and carried out a CTD station at both exit points with sampling of the water column and examined for methane concentrations. We were able to detect higher methane concentrations in the area of the gas flare of the northern Molløy Ridge. This finding and information from colleagues in Tromsø prompted us to conduct a dive to the seabed there on **Wednesday 28 August**. Similar to what we know from other regions of the world's oceans, at this depth of 3,500 m on the sea floor, massive gas hydrates are formed from the methane bubbles bubbling out of the sea floor, which form hill-like structures due to their increased buoyancy. We

were able to excellently and persistently investigate this during the 482nd dive of ROV QUEST 4000 (Fig. 4.3). We combined a survey with the ship's own Multibeam and sediment echo sounder on the following **Thursday 29 August**, with the transit to Longyearbyen, where we were able to dock at the coal port pier on Friday at 9:00 a.m. sharp for about 8 hours. This short port stay was planned for a partial change of scientists. Within 12 hours we were back to the Jøtul hydrothermal field, where we were unable to dive on **Saturday, 31 August** due to the weather, but used the day to take sediment samples in the area around the hydrothermal vents.

Dives on **Sunday, 1 September** (Dive 483) and **Tuesday, 3 September** (Dive 484), were spectacular (Fig. 4.4). We investigated two hydrothermal hills whose characteristic appearance led us to name them Yggdrasil and Nidhogg two years ago. These terms, like the word Jøtul, originate from Nordic mythology, and since these are important objects of investigation for us, we like to use their names and not just numbers. We were able to suck in one such hydrothermal fluid, which had a temperature of at least 289°C, under a flange with our intake nozzle and sample it in the KIPS container. A second fluid sample was obtained with one of the two pressure-tight IGT samplers. While the flange samples come from mid-height of the structure, a second location, namely an outlet channel at the summit of Yggdrasil, was visited. This escaping fluid also had a temperature of 282°C, so it can be assumed that the escaping fluids come from the same source. Two years ago, we also measured a temperature of 272°C at Yggdrasil. The second part of the dive took us to Nidhogg hydrothermal mound, about 120 m further west. Compared to two years ago, when we only measured temperatures of up to 33°C, the values this time are significantly higher.

In addition to the ROV dives, the fourth week of the expedition was also characterized by an intensive sampling program of the hydrothermal plume in the water column and its effect on the sea floor. So-called Tow-Yo CTD profiles were carried out mainly at night, with the CTD and its water samplers being hoisted and lowered in a zigzag manner along one stretch while the ship was traveling very slowly in the depth range occupied by the hydrothermal cloud. The input of metals from the hydrothermal sources and the distribution via the hydrothermal plume in the Jøtul hydrothermal field will be determined using chemical measurements on surface sediments. To this end, we have set up a large network of 22 mini-corer stations on several days this week, which will be expanded in the coming days. The use of simple sampling devices is sometimes necessary because we unfortunately often have technical problems with the ROV that have to be solved on board by the ROV crew. For example, on Tuesday evening when ROV QUEST was brought in, the latch system was damaged, which unfortunately could not be repaired on board. It is thanks to several colleagues, and in particular one colleague who arrived by plane, that a spare part was brought from Bremen to Longyearbyen by **Friday, 6 September**.

The 5th week of our research cruise was generally characterized by worse weather conditions than before, so that we were only able to dive to the sea floor on two days. Although the daily forecasts did not predict bad weather, the actual wind speeds were at least one Beaufort force higher, but often even two Beaufort force higher. We used these times to complete our sea floor surveys with the Multibeam echo sounder and the sediment echo sounder. We were able to survey a longer distance on **Monday, 9 September**, on the way to the Molløy Ridge, where we carried out station work with a gravity corer the following day and then steamed back to the area of Jøtul hydrothermal field. On **Wednesday, 11 September** and T**hursday, 12 September** of this week, the station work was mainly carried out to investigate the hydrothermal plume above the Jøtul

field. On **Friday, 13 September**, the weather had calmed down and ROV QUEST 4000 was finally able to dive again. Dive number 486 of ROV QUEST 4000 began at Nidhogg hydrothermal mound. The new sampling with KIPS and IGT sampler was carried out precisely at a constant temperature of 214°C. ROV QUEST 4000 then moved 300 m north along the 3,020 m isobath to the Black Smoker. It is the first black smoker discovered in the Jøtul field in 2022 and we therefore named it by the Norwegian name Fenris, which stands for the famous strong wolf in Norse mythology. Sampling with IGT and KIPS samplers were easily carried out in the vent opening of Fenris at maximum temperatures of 314°C. We then moved with ROV QUEST 4000 about 100 m west towards a west/east facing narrow ridge of hydrothermal rocks and reached a second active black smoker, which we named Gyme, another figure from Norse mythology. To round off the week, we made our 487th dive on **Sunday, 15 September** in relatively calm weather, which took us back to the two smokers Gyme and Fenris, where we recorded extensive video mosaics of the structures and their surroundings. Despite its shortness, the sixth week was the most successful one for our science. It was only 4 days long for our work, because on Thursday evening we stopped station work and set off for the return journey to Germany. Due to significantly better weather conditions than in the previous week, we were able to dive on 3 out of 4 days. Only **Tuesday, 17 September**, did we not have the opportunity to use our diving robot due to the high swell and a strong wind of Beaufort 6-7. During that day, the surface sampling program in the Jøtul hydrothermal field and the area of the hydrothermal plume to the North was completed with three mini-corer stations. With a total of 35 stations, a great set of samples was obtained on our cruise, the analysis of which will show an image of the drift of hydrothermal particles through the plume.

The three dives of the week mainly worked on profiles that began in the West at a water depth of more than 3,000 m and examined the sea floor up the slope to the East. The almost daily growth changes on the two smokers of the Jøtul main field Gyme and Fenris were usually at the beginning of the investigation programs. During the two dives 488 on **Monday, 16 September** and 490 on **Thursday, 19 September** we examined a sea area at a water depth of 2,935 m that contained numerous indications of cold seep outlets (Fig. 4.4). We investigated a completely different question on the penultimate dive 489 (Fig. 4.4) on **Wednesday, 18 September** by examining and sampling an oceanic core complex (OCC) that is located immediately east of the Jøtul hydrothermal field and whose relationship to the hydrothermal field is completely unclear. During dive 489 we selectively collected 11 different rock samples from the sea floor along a 600 m long profile, and the petrographic analyses in the Bremen laboratories will give us information about the rock diversity and its relationship to the OCC. After finishing the station work in the Jøtul hydrothermal field, the MARIA S. MERIAN headed for our next port of call, Tromsø. It left the shelf of the Barents Sea during the night of **Sunday, 22 September**, to enter the fjord landscape of Flugløysundet and, after about 25 km, the wide passage of Grøtsundet, so that we could berth in the port of Breivika/Tromsø on time at 8:00 a.m. In addition to our Norwegian scientists, several other scientists also left the ship, and three employees from the Kula company came on board to prepare for the shipyard period that would follow this cruise on the way to Emden. After two hours, we set off again at 10:00 a.m. and MARIA S. MERIAN steamed to Emden, where we arrived on **Friday, 27 September**, one day earlier than planned, after a passage across the Ems.

5 Preliminary Results

5.1 Hydroacoustic Operations

(K. Streuff, M. Römer, F. Berger, G. Feddersen, M. Meier)

Knowledge of the topography and stratigraphy of the sea floor can be obtained via hydroacoustic methods and is necessary to understand submarine processes, such as, e.g., past sedimentary processes and the composition of the sea floor. In the study areas of the MSM131 cruise they provide information about the morphology of the Mid-Atlantic Ridge as well as its surrounding sea floor and can therefore indicate suitable sites for mini coring and ROV operations. During MSM131, the hydroacoustic systems were operational throughout transits and bathymetric surveys, accumulating new data covering about 30,000 km^2.

Hydroacoustic data were gathered using the hull-mounted Kongsberg Maritime Simrad EM122 and the Atlas PARASOUND parametric sediment echosounder installed aboard the MARIA S. MERIAN. Acquisition started on the 20.08.2024 at 10:48 UTC, after leaving the EEZ of Iceland, and ended on the 21.09.2024 at 22:56 UTC when entering the territorial waters of Norway. Data acquisition was interrupted during recovery of the ocean bottom seismometers, during ROV operations, and twice while entering the territorial waters of Spitsbergen. Acquisition speed was mostly around 10 kn, but was reduced occasionally due to bad weather, close to sites of station work, and where higher-resolution bathymetry was needed. Water column data were logged throughout.

Methodology

All bathymetry was gathered using the EM122 and the Kongsberg Seafloor Information System software to log and visualise the collected data. Bathymetric and backscatter data were stored as *.all and water column data as *.wcd files. The EM122 is a deep-water system, operating in water depths between 20 and 11,000 m, making it suitable for the study areas' water depths, which mostly exceeded 3,000 m. It uses two linear transducer arrays that are configured in a Mills Cross alignment. The EM122 operated at acoustic frequencies of about 12 kHz with a beam number of 576, a beam width configuration of 2° by 2° and a beam spacing set to high-density quasi-equidistant. The ping mode was generally set to automatic, but was occasionally adapted to a shallower setting to improve the imaging of the water column. The dynamic dual-swath mode of the EM122 was used throughout, providing up to 864 soundings per ping. To ensure maximum coverage, the opening angle was kept at the maximum of 150°. An overview of the new data collected with the hydroacoustic systems is given in Fig. 5.1.1.

The multibeam echosounder was frequently calibrated, using sound velocity profiles from CTD casts and from the WOA13 Atlas Model during transit from Iceland and to Norway.

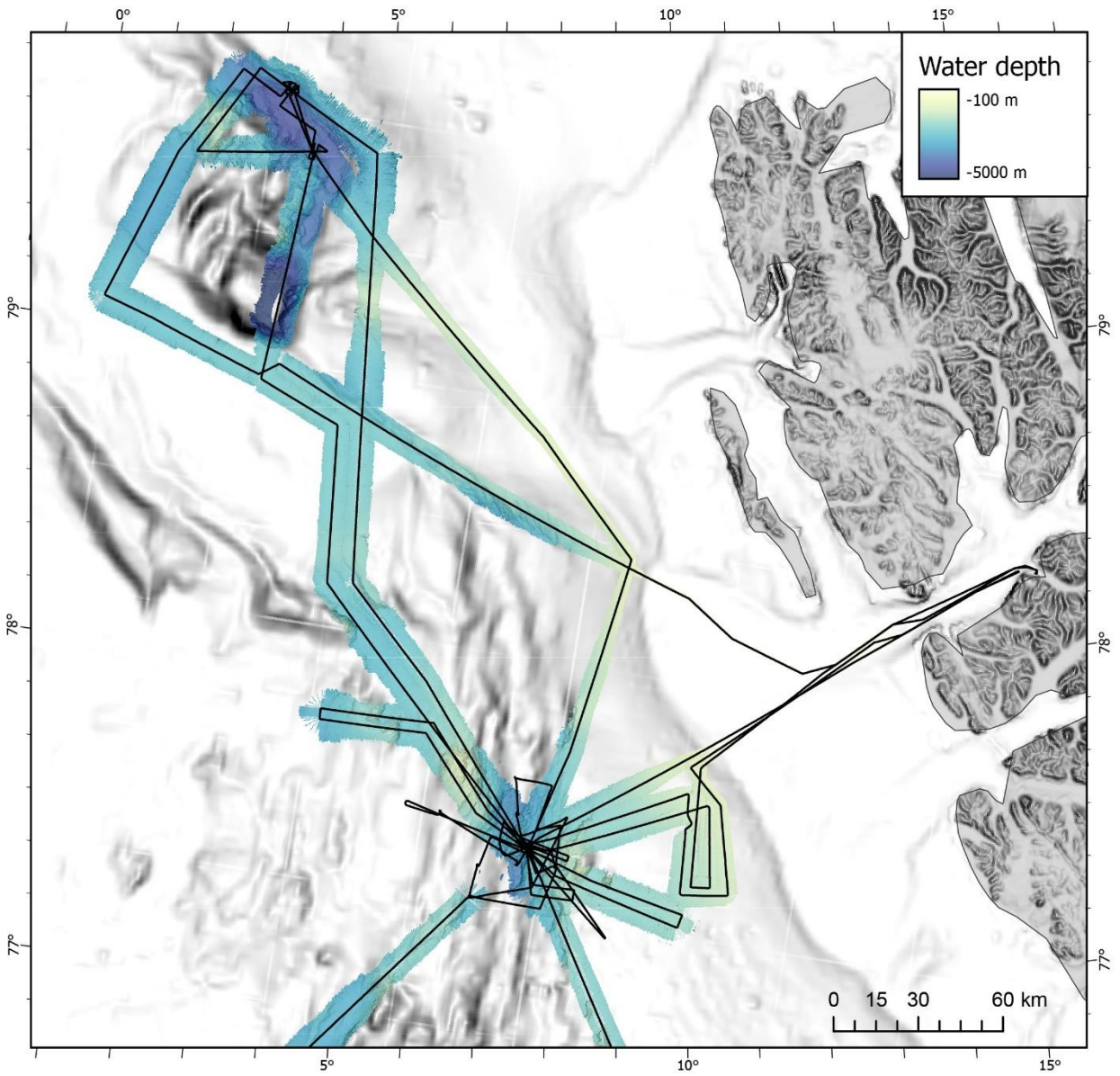

Fig. 5.1.1 Overview of the on-board-processed bathymetry obtained during MSM131. Water depths are color-coded according to the scale in the upper right-hand corner. The vessel's track is shown as a black line.

The ATLAS PARASOUND echosounder uses the principle of acoustic wave propagation to identify differences in sediment properties. These include density and sound velocity, which permit the visualization of lithological changes in the sediment column. Compared to conventional echo sounders, the PARASOUND system offers an improved lateral and vertical resolution of sedimentary structures. This is due to the parametric effect on the one hand, and a much smaller opening angle (4° compared to 20°) on the other. The software programs ATLAS PARASTORE and ATLAS Hydromap Control Center were used to modify the PARASOUND settings throughout MSM131. The sediment echosounder was operated at two main frequencies, a primary high (PHF, 18 kHz) and a secondary low frequency (SLF, 4 kHz), in order to obtain information about the water column and the sea floor stratigraphy. The transmission was set to single pulse throughout the entire cruise, to facilitate the identification of acoustic features in the water column. The pulse type was set to continuous wave and the number of pulses to 1. Data storage occurred as raw .asd files and both, pre-processed .ps3 and .sgy files. Due to their superior quality, only the

.ps3 files were used; they were converted into UTM-corrected envelope .sgy files with the software tool PS32SGY (courtesy of Hanno Keil, University of Bremen). The resulting output files were then imported into SMT The Kingdom Suite v. 2020 for visualization and interpretation.

Preliminary Results

The area of MSM131 was pretty well-mapped during previous cruises by MARUM and the University of Bremen (MSM109, MSM56, MSM57), as well as by our Norwegian colleagues, providing ship's bathymetry as well as high-resolution AUV data. Data acquisition during MSM131 was therefore mostly opportunistic, using the time between ROV, Mini-corer, CTD and OBS recovery operations to fill in gaps in our existing datasets. As the focus of the cruise was placed mostly on the first three of these instruments, there was limited time for mapping surveys. Nevertheless, we acquired new data covering an area of ~30,000 km². Results were as expected, with the Multibeam data clearly showing the hummocky and uneven rift topography of the Knipovich Ridge, both around the Jøtul hydrothermal field, as well as around the Molløy deep (Fig. 2). In contrast, areas further away from the main ridge axis were smoother and much more even, suggesting, especially on the Spitsbergen continental shelf and slope, thick sediment coverage of the underlying topography.

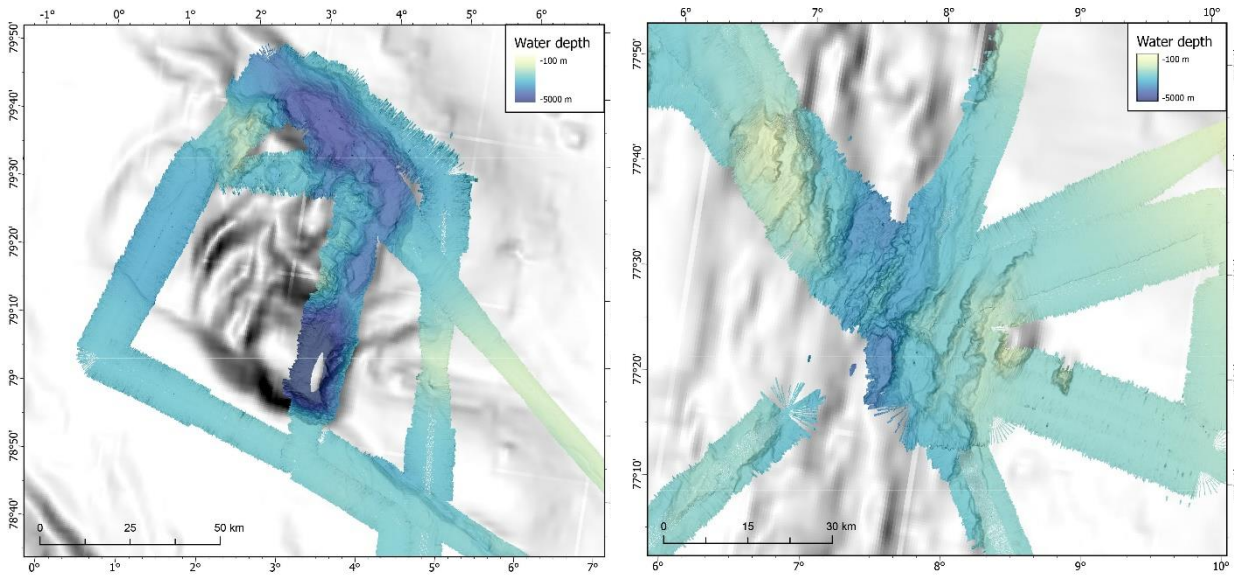

Fig. 5.1.2 Left: Close-up of the on-board-processed bathymetry obtained during MSM131 in the Molløy area. Right: Close-up of the on-board-processed bathymetry obtained during MSM131 in the Jøtul vent area.

Water Column Anomalies

In published records, as well as during the previous cruises, there had been some indication for active gas bubble seepage at several locations on the sea floor in the area mapped during MSM131. In the Molløy area, two very intense and high-reaching flares are known, called GFA and GFB (Chand et al., 2024), which we wanted to image and investigate further during MSM131.

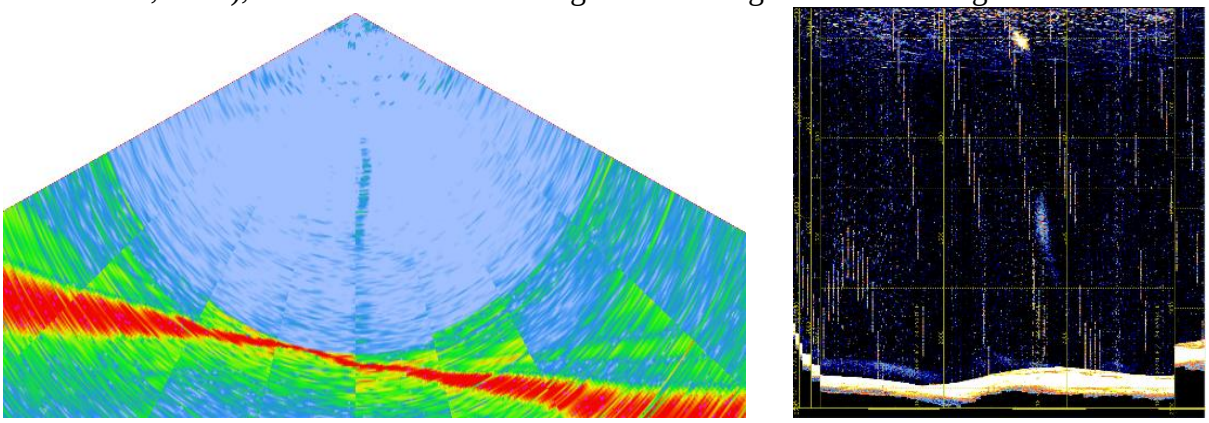

Fig. 5.1.3 Example of one of the flares detected during MSM131, mapped on August 29th at 18:50 UTC. On the left is a screenshot of the water column showing the flare as it appeared in the EM122 water column data in the FM Midwater software. On the right, the corresponding flare is depicted as it showed up in the live PARASOUND data.

Both flares could be detected, however our echosounder records did not image them as flares connected to the sea floor, but starting only at medium water depths. We suspect that this is due to a misalignment between the resonance frequency of the released bubbles close to the sea floor and the frequencies used by the hydroacoustic systems. No flares were detected in the Jøtul area. Although a previous cruise reported a potential flare site close to the Jøtul vent field, our recordings could not confirm active gas bubble release there, despite specific surveying of the area. While transiting between the work areas and to Svalbard, the echosounders also detected a few additional flare sites (Fig. 5.1.3), specifically on the Svalbard shelf, where gas seepage had previously been documented (e.g. Knies et al., 2004; Roy et al., 2014; 2015; Liira et al., 2019).

5.2 Passive Seismology Around Jøtul Vent Field, Knipovich Ridge

(V. Schlindwein, M. Pilot, K. Asatrian)

During cruise MSM109 in summer 2022, a new hydrothermal vent field, called Jøtul, was discovered along the eastern flank of Knipovich Ridge at a subordinate volcanic complex near 77°20’ N (Fig. 5.2.1). Jøtul is special in its geological setting as it is not located directly on an axial volcanic ridge (AVR), like for example Loki’s Castle vent field at the Knipovich-Mohns Ridge Bend, but rather to the east of the AVR at the flanks of the rift valley (Fig. 5.2.2). Recording the seismicity of this vent field will give insights into active fault structures that serve as pathways for fluid circulation and earthquake swarm activity that may point to diking events that provide heat to drive hydrothermal circulation. Furthermore, local earthquake tomography will give information on potential melt reservoirs as heat sources for hydrothermalism.

Ultraslow spreading ridges are known for their high incidence of hydrothermal anomalies (Edmonds et al. 2003). Intensive, deep-reaching hydrothermal circulation may contribute to effective cooling and alteration of the lithosphere in these settings. We have instrumented so far three known vent fields along the ultraslow spreading Arctic Ridge system (Fig. 5.2.2): Loki's Castle vent field in 2019-2020 with 8 OBS in collaboration with the University of Bergen. First results show prominent seismicity along a dipping detachment fault that likely serves as fluid path for the hydrothermal vent field situated on top of an AVR (Pilot et al. 2024). 8 ocean bottom seismometers were installed around Aurora vent field on Gakkel Ridge. Here, the vent field is situated on a basaltic mound near the rift flank and shows indications of fluids circulating through mantle rocks despite basalts at the seafloor. A heat source in form of a close-by AVR is not obvious at this location (German et al. 2022). Jøtul vent field is the third vent field that we instrumented and yet different to the other two. We expect that the comparative analysis of the three locations with three similar passive seismic data sets will give an unprecedented view of the different geological settings and hydrothermal circulation styles.

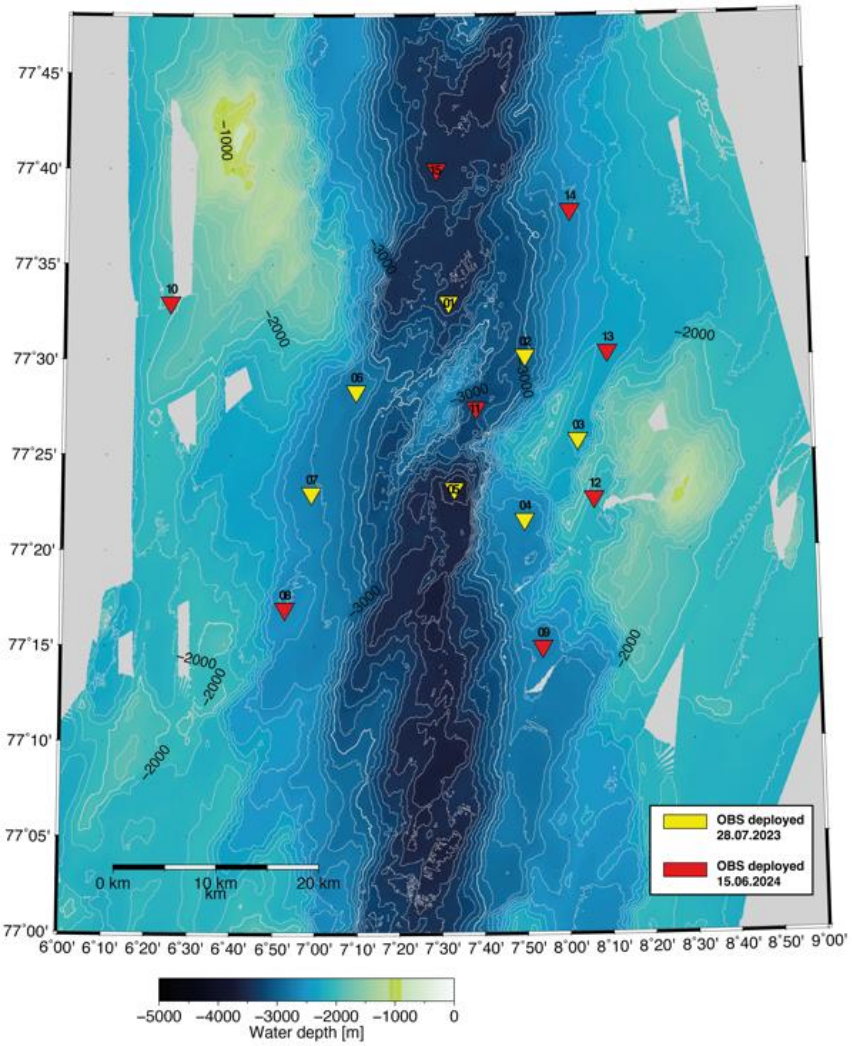

Fig. 5.2.1 Ocean Bottom Seismometer Network around Jøtul Vent Field

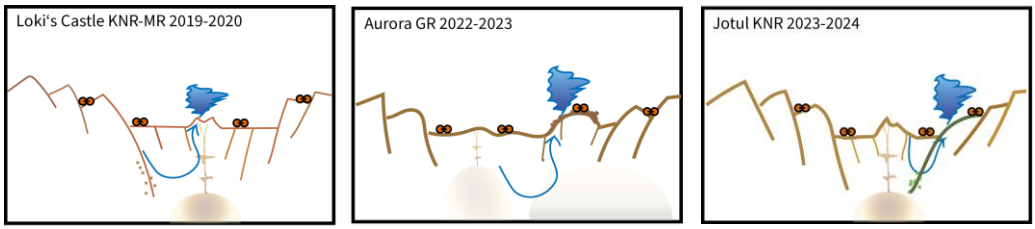

Fig. 5.2.2 Different geological settings of Loki's Castle, Aurora and Jøtul vent field. Comparable passive seismic networks were installed for a period of one year at each of the vent fields

Method and Work at Sea

A dense inner network of 7 ocean bottom seismometers (OBS) of type LOBSTER equipped with KUM 6d6 data loggers and Trillium Compact broadband three component seismometers was deployed in the rift valley near Jøtul vent field on 28 July 2023, when RV POLARSTERN returned from cruise PS137 (yellow, Fig. 5.2.1). At that time, only 7 instruments were available, one of which a prototype. Stations are called JOT01-JOT07 and are marked in grey in Tabs. 5.2.1-3. This network recorded for a period of 13 months and allows to capture also episodic seismicity.

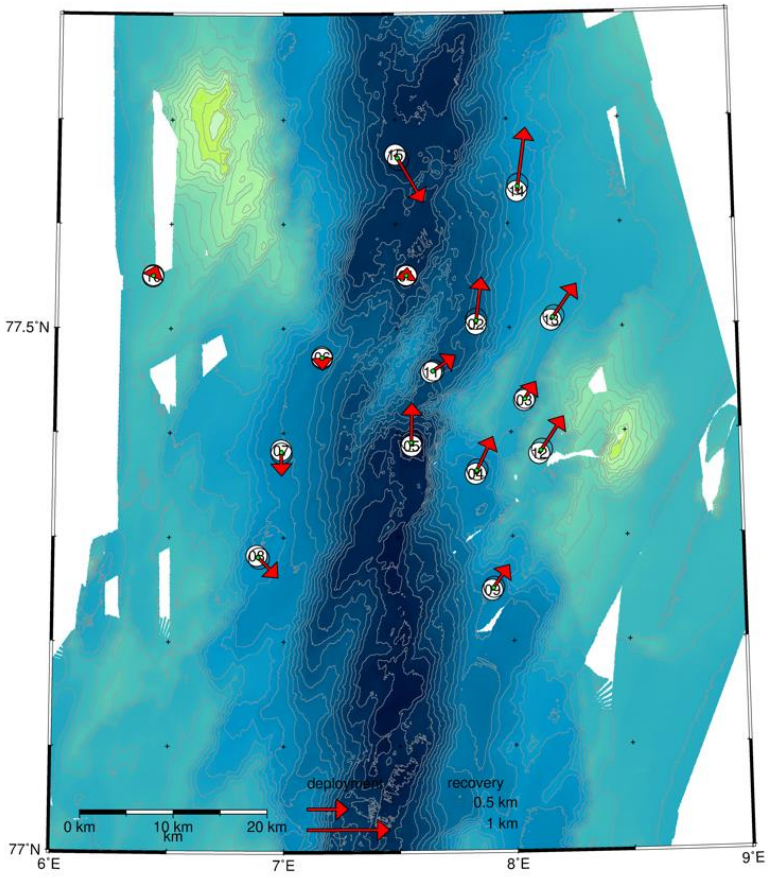

Fig. 5.2.3 Deployment positions of OBS (white, numbered circles), recovery positions (open circles) and likely seafloor positions at two thirds between deployment and recovery position (green dots). Enlarged red arrows indicate the drift of the seismic stations between deployment and recovery. Note the systematic north drift on the eastern rift flank.

To improve earthquake location, resolution and depth penetration of seismic tomography, we deployed on 15 June 2024 eight additional OBS (red, Fig. 5.2.1) from board RV HELMER HANSSEN in cooperation with the University of Tromsø. The rationale for the network geometry was to gain a total network aperture of about 50 km (JOT08, JOT09, JOT14, JOT15), cover seismicity beyond the vent field area, especially around the Brøgger axial volcanic ridge (JOT08, JOT11, JOT14), and also study the off-axis area that consists of highly elevated, fault-controlled mountains that display in multichannel seismic data clear signs of faulting (JOT10, JOT12, JOT13). The vent field area itself is surrounded by a triangle of stations (JOT02-05, JOT11, JOT12). Deployment closer to the vent field or the axial volcanic ridge was considered as risky due to the very rugged sea floor.

All instruments were successfully recovered during cruise MSM131 on RV MARIA S. MERIAN between August 23 and 25, 2024. Recovery and deployment positions and an estimate of the instrument drift between the positions are given in Fig. 5.2.3.

Table 5.2.1 summarizes the deployment and recovery positions of the instruments. Table 5.2.2 gives the recording parameters. All stations apart from JOT03 and JOT05 returned a full data set. The battery of station JOT05 was prematurely empty on 31 May 2024. JOT03 stopped recording after about one month for unknown reasons. Tab. 5.2.3 gives the clock synchronization time and the time drift of the records clocks during the deployment.

Preliminary Results

Upon recovery, no preliminary results can be given. Data have not yet been converted into miniseed from the recorder format. Prior to any earthquake detection and location, the clock drift will have to be corrected. Ample records of local earthquakes are highly likely upon a quick inspection of few converted days of data.

Raw data will be archived in PANGAEA. Time corrected miniseed data will be archived and accessible at GEOFON under seismic network code 3S.

Table 5.2.1 Deployment and recovery times and positions of OBS stations JOT01-15

	Deployment		Deployment Position at surface			Recovery		Recovery Position on deck		
Station	Date	Time UTC	Latitude [° N]	Longitude [°E]	Depth [m]	Date	Time UTC	Latitude [° N]	Longitude [° E]	Depth [m]
JOT01	28.07.23	16:04	77° 33.013‘	07° 32.704‘	3477	23.08.24	22:45	77° 33.066‘	07° 32.736‘	3530
JOT02	28.07.23	16:53	77° 30.201’	07° 51.036‘	3055	23.08.24	16:39	77° 30.507‘	07° 51.220‘	3033
JOT03	28.07.23	17:37	77° 25.800‘	08° 03.530‘	2312	23.08.24	11:19	77° 25.917‘	08° 03.896‘	2312
JOT04	28.07.23	18:17	77° 21.621‘	07° 50.448‘	2663	24.08.24	19:59	77° 21.856‘	07° 50.980	2712
JOT05	28.07.23	18:55	77° 23.249‘	07° 33.633‘	3620	25.08.24	16:16	77° 23.533‘	07° 33.667‘	-
JOT06	28.07.23	19:50	77° 28.373‘	07° 10.174‘	2759	25.08.24	05:48	77° 28.293‘	07° 10.190‘	2758
JOT07	28.07.23	20:31	77° 23.014‘	06° 59.366‘	2662	25.08.24	04:05	77° 22.846‘	06° 59.382‘	2668
JOT08	15.06.24	06:49	77° 16.955‘	06° 52.894‘	2601	25.08.24	02:19	77° 16.814‘	06° 53.530‘	2596
JOT09	15.06.24	15:00	77° 14.940‘	07° 54.390‘	2682	24.08.24	23:41	77° 15.102‘	07° 54.913‘	2672
JOT10	15.06.24	08:32	77° 32.990‘	06° 25.111‘	1993	25.08.24	18:54	77° 33.062‘	06° 25.233‘	-
JOT11	15.06.24	13:08	77° 27.466‘	07° 39.058‘	-	24.08.24	00:42	77° 27.576‘	07° 39.794‘	3193
JOT12	15.06.24	14:01	77° 22.746‘	08° 07.313‘	2136	24.08.24	21:35	77° 22.985‘	08° 08.060‘	-
JOT13	15.06.24	12:12	77° 30.397‘	08° 11.048‘	2351	23.08.24	14:00	77° 30.630‘	08° 11.830‘	2348
JOT14	15.06.24	10:58	77° 37.819‘	08° 02.600‘	2641	23.08.24	18:35	77° 38.229‘	08° 02.881‘	2617
JOT15	15.06.24	10:09	77° 39.999‘	07° 30.020‘	3464	23.08.24	22:40	77° 39.690‘	07° 30.868‘	3470

Table 5.2.2 Recording parameters of OBS stations JOT01-15

Recording					Sample Rate	Gain	Seis. meter	Hydro phone	6d6	Temp-sensor
Station	Start date	End time	End Date	End time	(Hz)	HXYZ	Type	Inv. (I)	SN	SN
JOT01	28.07.23	15:20:51	23.08.24	22:55:37	100	4 1 1 1	TC	H	61607087	1854377
JOT02	28.07.23	15:52:43	23.08.24	16:47:50	100	4 1 1 1	TC	H	61607298	1854371
JOT03	28.07.23	16:15:55	23.08.24	14:30:08	100	4 1 1 1	TC	H	61607210	1854370
JOT04	28.07.23	17:03:46	24.08.24	20:11:47	100	2 1 1 1	TC	H	61607102	-
JOT05	28.07.23	17:49:00	31.05.24	19:24:08	100	2 1 1 1	TC	H	61607070	1854207
JOT06	28.07.23	18:28:27	25.08.24	14:44:44	100	2 1 1 1	TC	H	61607190	1854406
JOT07	28.07.23	19:09:30	25.08.24	04:20:07	100	on	-	H	6d7	-
JOT08	15.06.24	06:27:44	25.08.24	02:29:29	250	2 1 1 1	TC	H	61607093	-
JOT09	15.06.24	14:13:31	24.08.24	23:50:25	250	2 1 1 1	TC	H	61607091	-
JOT10	15.06.24	07:40:19	25.08.24	19:16:04	250	2 1 1 1	TC	H	61607197	-
JOT11	15.06.24	12:19:00	24.08.24	00:49:15	250	2 1 1 1	TC	H	61607209	-
JOT12	15.06.24	13:19:51	24.08.24	21:45:40	250	2 1 1 1	TC	H	61607094	-
JOT13	15.06.24	11:04:09	23.08.24	14:07:59	250	2 1 1 1	TC	H	61607085	-
JOT14	15.06.24	10:17:11	23.08.24	18:45:32	250	2 1 1 1	TC	H	61607086	-
JOT15	15.06.24	08:42:56	23.08.24	20:51:18	250	2 1 1 1	TC	H	61607194	-

Table 5.2.3 Clock parameters of OBS stations JOT01-15

	Synchronisation		Skew		Skew [ms]
Station	Date	Time UTC	Date	Time UTC	
JOT01	28.07.23	15:16:44	23.08.24	22:56:11	12856542
JOT02	28.07.23	15:42:04	23.08.24	16:48:12	10317201
JOT03	28.07.23	16:15:33	23.08.24	11:38:29	10474778
JOT04	28.07.23	17:03:27	24.08.24	20:12:25	-9513019
JOT05	28.07.23	17:47:26	26.08.24	12:25:39	-7639404
JOT06	28.07.23	18:28:01	25.08.24	14:45:43	14232497
JOT07	28.07.23	19:09:27	25.08.24	04:21:17	-451756
JOT08	15.06.24	06:22:12	25.08.24	02:30:37	-2663344
JOT09	15.06.24	14:11:54	24.08.24	23:51:19	-495845
JOT10	15.06.24	07:37:20	25.08.24	19:17:11	-102940
				00:51:09	855438
JOT11	15.06.24	12:19:05	24.08.24	00:51:57	-141892
JOT12	15.06.24	13:18:26	24.08.24	21:46:33	-1381982
JOT13	15.06.24	11:02:54	23.08.24	14:09:04	-209748
JOT14	15.06.24	10:17:00	23.08.24	18:46:04	-1093866
JOT15	15.06.24	08:42:56	23.08.24	20:51:47	-1447601

5.3 Oceanographic Data

(T. Pape, M. Römer, E. Kopiske, M. Meyer, J. Malnati, G. Feddersen, F. Berger)

Oceanographic data were collected during 23 hydrocasts (Table 5.3.1) with the CTD/rosette (CTD/ro) system of *RV MARIA S. MERIAN* above the Jøtul hydrothermal field and the northern Molløy Ridge area. Above the Jøtul hydrothermal field they were carried out to delineate the extent of the hydrothermal plume(s) fueled from the hydrothermal emissions. Above the Molløy Ridge

area they were carried out to investigate the methane release through the water column at two known flare sites (GFA and GFB, Chand et al., 2024).

The CTD system consisted of a CTD 911plus deck unit with two conductivity sensors (SBE 4C), two temperature sensors (SBE 3plus), a single pressure sensor (SBE 9plus), and two SBE 5T pumps (all components from Sea-Bird Scientific). The system was also equipped with a dissolved oxygen sensor (SBE 43), a fluorometer/turbidity sensor (WET Labs ECO FLNTURTD), and a Teledyne Benthos PSA-916 altimeter. In addition, an oxidation-reduction potential (ORP) sensor was mounted in the rosette, and a Miniature Autonomous Plume Recorder (MAPR) for recording light-backscattering, oxidation-reduction potential (ORP), temperature, and pressure was attached on the cable 50 m above the rosette. All oceanographic data was recorded and processed with the Seasave (V7.22) and SBE Data Processing (V7.22.0) software programs. The CTD/ro system was veered and heaved with winch EL1 via the small movebar in the ship's hangar. Acoustic underwater positioning was achieved with the ships' own Sonardyne Ranger 2 Gyro USBL HPT 7000 with the transponder being attached to the frame of the rosette.

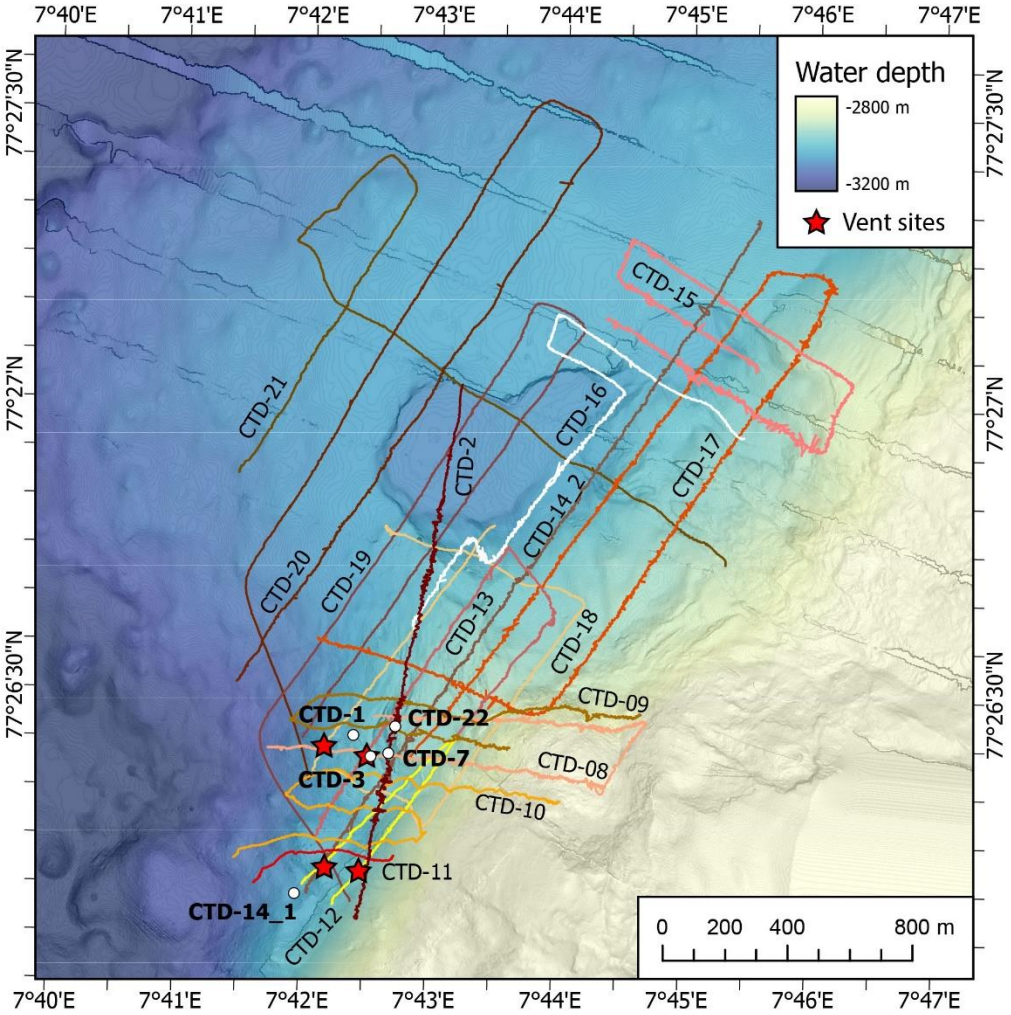

Fig. 5.3.1 Bathymetric map depicting positions of CTD/ro stations conducted in the water column above the Jøtul hydrothermal field. Open circles and bold titles – positions of stationary hydrocasts; colored lines and normal titles– profiles of Tow-Yo casts and the towed deployment.

Table 5.3.1 List of CTD/ro stations conducted during cruise MSM131 (JHF – Jøtul hydrothermal field; TYC – Tow-Yo cast; SHC – stationary hydrocast; TD – towed deployment). n.a. – not applicable

GeoB	Tool CTD-	Type of De-ploy-ment	Dura-tion [hh:mm]	Approx. length of profile [km]	Area / Target / Comment
Leg 1					
26201-1	01	SHC	02:42	n.a.	JHF, N' of Gyme and Fenris
26216-1	02	TYC	06:54	1.77	JHF, NW-SE trending profile, crossing the eastern sector of the hydrothermal field
26219-1	03	SHC	02:33	n.a.	JHF, close to Fenris BS
26220-1	04	SHC	02:24	n.a.	Molløy Ridge area: Flare GFA
26221-1	05	SHC	02:49	n.a.	Spitsbergen FZ: Flare GFB
26223-1	06	SHC	03:22	n.a.	Molløy Ridge area: Flare GFA
		Total	**20:45**		
Leg 2					
26224-1	07	SHC	02:54	n.a.	JHF, on Tow-Yo CTD-02
26229-1	08	TYC	11:07	2.22	JHF, W-E trending profiles in the northern sector around Gyme and Fenris
26234-1	09	TYC	10:46	1.92	JHF, W-E trending profiles in the northern sector around Gyme and Fenris
26241-1	10	TYC	11:35	2.00	JHF, ~W-E trending profiles between Gyme and Fenris as well as Yggdrasil and Niddhog
26246-1	11	TD	03:17	0.44	JHF, ~W-E trending profile north of Yggdrasil and Niddhog
26251-1	12	TYC	09:32	1.38	JHF, ~SW-NE trending profiles crossing Yggdrasil and Niddhog
26253-1	13	TYC	11:14	2.00	JHF, ~SW-NE trending profiles crossing Gyme
26262-1	14-1	SHC	01:35	n.a.	JHF, S' of Yggdrasil and Niddhog; station aborted due to technical problems with the winch
26262-2	14-2	TYC	10:19	2.60	JHF, SW-NE profile across the vent field towards the NE' border of the plume
26267-1	15	TYC	13:44	2.56	JHF, NW-SE trending profiles close to the NE' border of the plume
26270-1	16	TYC	11:00	2.21	JHF, profiles of different orientation in the central plume area
26271-1	17	TYC	15:14	4.58	JHF, SW-NE profile close to the E' border of the plume
26273-1	18	TYC	10:07	2.87	JHF, profiles of different orientation in the central plume area
26275-1	19	TYC	10:17	3.40	JHF, SW-NE profile close to the W' border of the plume
26279-1	20	TYC	11:16	4.17	JHF, SW-NE profile close to the W' border of the plume
26281-1	21	TYC	09:43	3.26	JHF, profiles of different orientation close to the W' border and in the central area of the plume
26283-1	22	SHC	02:31	n.a.	JHF, about 200 m NNE of Fenris Smoker, sampling of water in the plume downstream of Fenris
		Total	**156:13**		

Three types of CTD/ro stations were conducted to survey the water body: 1) stationary hydrocasts for vertical profiling of the water column, 2) Tow-Yo casts, which included continuous lowering and heaving of the CTD/ro system along (a) profile(s) in selected depth ranges, and 3) towed deployments with a defined distance above the seabed (Table 5.3.1). Tow-Yo casts were carried out in water depths between about 2,400 (in exceptional cases up to 2,250 m) and 10 m

above ground over a lateral distance of ranging between 0.4 and 4.6 kilometers. Towed deployments were conducted to tow the system over ground at an altitude ranging between 15 m and 25 m. Tow-Yo deployments and towed deployments were usually carried out with a ship velocity of 0.1 to 0.2 knots (in exceptional cases max. 0.4 knots). During Tow-Yo casts the CTD/ro system was veered and heaved at a speed of 0.5 m/s. Of the 23 hydrocasts, 8 were carried out as stationary hydrocasts, 14 as Tow-Yo casts and one as pure towed deployment. The duration of the stations (except station CTD-14-1, which was aborted), ranged between 02 h 24 min and 15 h 14 min (Tab. 5.3.1). Total deployment time of the CTD/ro system during MSM131 Leg1&2 was almost 177h.

While three CTD/ro stations were carried out in the Molløy Ridge area, the Jøtul hydrothermal field was examined at high resolution at 19 CTD stations (Tab. 5.3.1, Figs. 4.2 and 5.3.2).

Preliminary Results

This report focuses on the temperature and salinity distributions in the deep water body below a water depth of 1500 m, since one of the main goals of cruise MSM 131 was to determine the spatial distribution of fluids discharged from the seabed into the water column.

The Potential Temperature–Salinity (T-S) plots of the three CTD stations in the Molløy Ridge area showed a relatively consistent pattern (Fig. 5.3.2).

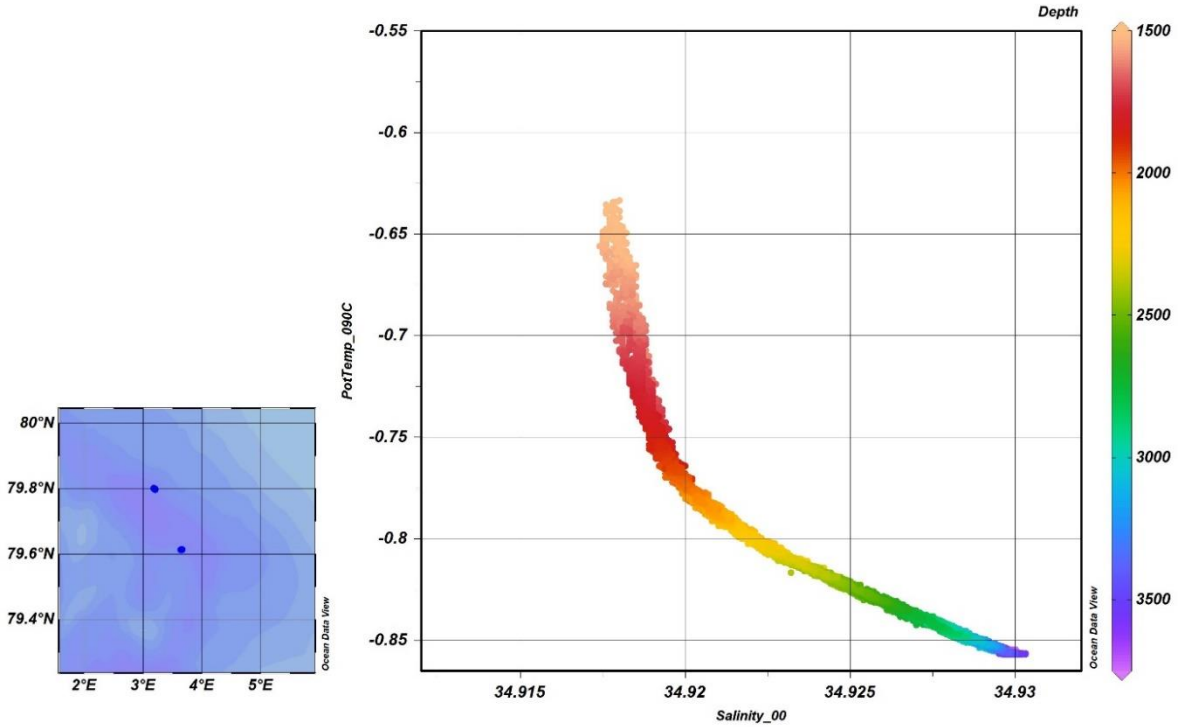

Fig. 5.3.2 Potential temperature – salinity (T-S) diagram for all data pairs below a water depth of 1500 m from stations CTD-04, -05, -06, conducted in the Molløy Ridge area.

At water depths between 1500 m and about 2000 m, salinity increased only slightly with depth from about 34.917 psu to 34.920 psu, while potential temperature decreased from about –0.634 °C to –0.780 °C. Between approximately 2000 m and the maximum depth of 3,772 m (CTD-05), salinity increased with depth to approx. 34.930 psu, whereas the potential temperature continued to decrease with increasing depth (minimum temperature –0.857 °C).

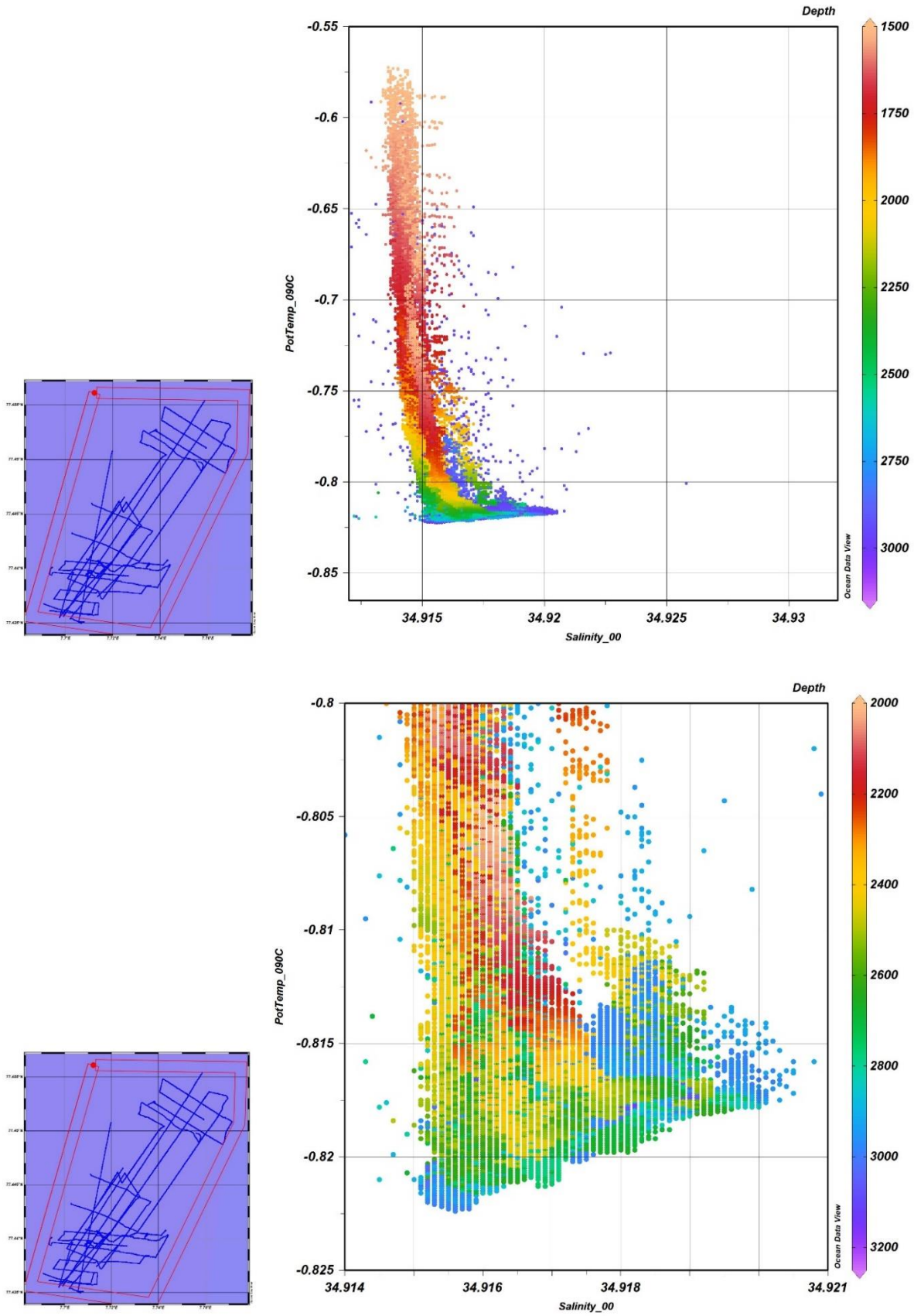

Fig. 5.3.3 Top: T-S plot for all data pairs below a water depth of 1500 m for all stations carried out at Jøtul hydrothermal field. Bottom: Enlargement of the T-S plot for the Jøtul hydrothermal field to the data pairs below 2000 m and a temperature lower than -0.8 °C.

Following the classifications proposed by Schlichtholz and Houssais (2002) and Rudels et al. (2005) water masses would be assigned to the Nordic Seas Deep Water (1500 m to ca. 2000 m water depth) and to the Eurasian Basin Deep Water (below ca. 2000 m water depth). Compared to the stations in the Molløy Ridge area, the T-S plot for the CTD stations at the Jøtul hydrothermal field show a generally larger spread of the data, especially below 2000 m water depth (Fig. 5.3.3). As at the Molløy Ridge area, the mean salinity in the water column above the Jøtul hydrothermal field between 1500 m and 2000 m was relatively homogeneous, but at 34.913 psu to 34.916 psu somewhat lower in comparison (Fig. 5.3.3 top). In addition, the potential temperature in this depth range was -0.573°C and -0.751°C and thus somewhat higher than in the Molløy Ridge area. This may indicate that at Jøtul hydrothermal field the entire water column below 1,500 m is dominated by Nordic Seas Deep Water (e.g., Rudels et al., 2005).

Many data pairs between ca. 2,850 m and 3,015 m water depth are notable for positive temperature anomalies with ΔT up to 0.25°C compared to background temperatures (Fig. 5.3.3 bottom). These temperature increases in the water column were primarily observed at stations close to the sites of hydrothermal emissions (e.g., stations CTD-01, -02, -03, -07, -08, -09, -10, -11, -12, -13, -14-2, -22) and north of the emission sites (e.g., stations CTD-16, -17, -18) of the area a the Jøtul hydrothermal field. The SW-NE oriented water column section (Fig. 5.3.4) shows that temperature anomalies positioned in deepest waters were located directly above emission sites. As the distance to the northeast increases, temperature anomalies can be found in relatively shallower water layers.

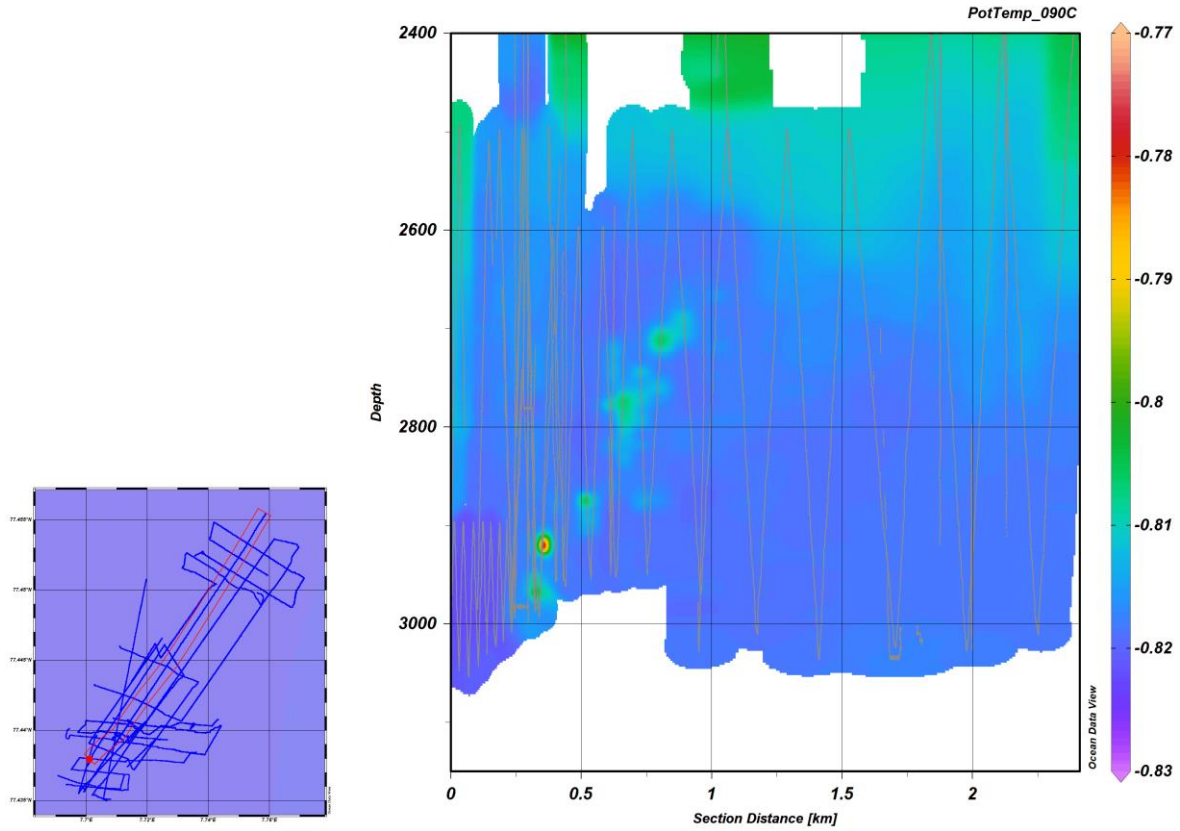

Fig. 5.3.4 SW-NE oriented water column section above the Jøtul hydrothermal field showing patchily distributed temperature anomalies

In contrast to submarine hydrothermal emissions in many other areas, the fluid releases from the Jøtul hydrothermal field did not result in a significant turbidity anomaly (mostly < 0.2 NTU, Nephelometric Turbidity Unit) in the water column (Fig. 5.3.5).

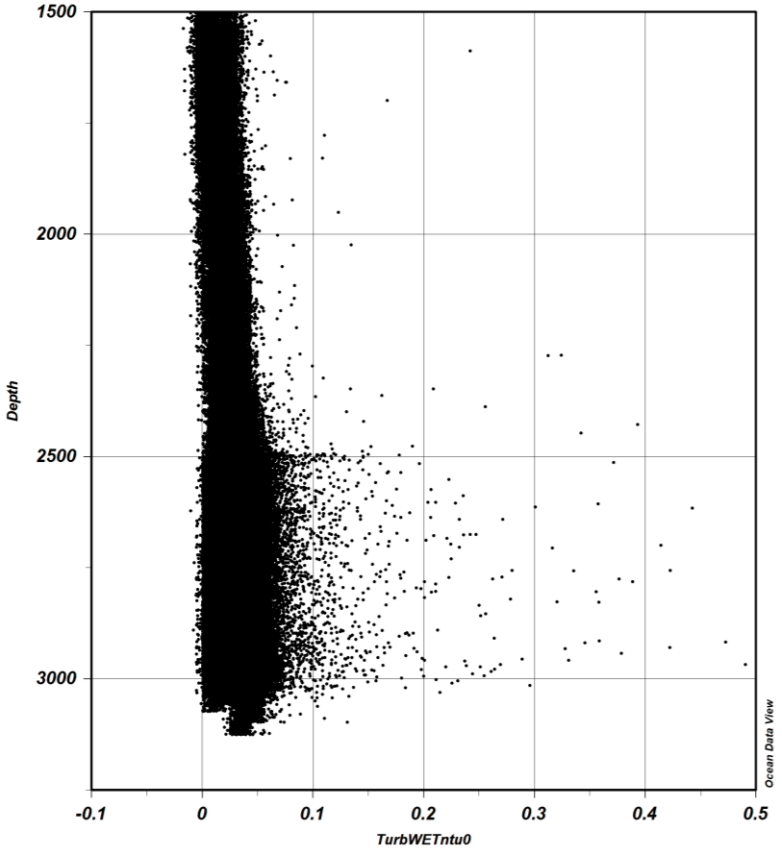

Fig. 5.3.5 Turbidity versus water depth for all data pairs below a water depth of 1500 m for all stations carried out at the Jøtul hydrothermal field. Note the small-scale range (0.6 NTU) for turbidity. A comparably high data density below approx. 2500 m is caused by the focus on this water depth during the Tow-Yo casts.

The high-resolution set of oceanographic data over the hydrothermal field obtained during cruise MSM131 will allow to characterize the spatial extent of the temperature plume in detail.

5.4 MAPR and ORP Sensor

(M. Römer, G. Feddersen)

The primary instrument in order to detect and map hydrothermal plumes during MSM131 cruise was the miniature autonomous plume recorder (MAPR) provided by the Pacific Marine Environmental Laboratory (PMEL) in Seattle (WA, USA). Main target area was the Jøtul hydrothermal vent field, but some deployments have also been conducted in the Molløy area. The Jøtul hydrothermal vent field has been detected during earlier cruises by ORP anomalies and were investigated using the same devices during MSM109 in 2021. During MSM131, the main objective was to investigate the plume distribution and variability in detail. By using a systematic mapping approach, it will be possible to extract the plume information through a 3D grid and document changes over time. The ORP and temperature anomalies were also used to guide the sampling strategy with the Niskin bottles attached to the CTD rosette.

Method and Work at Sea

The PMEL MAPR is a durable, self-contained instrument that records data from temperature, pressure, optical backscatter (LBSS, or "nephelometer") and oxidation-reduction potential (ORP) sensors located at one end of the instrument. Data are recorded internally, and cannot be accessed or viewed during deployment. For this reason, a further non-autonomous ORP sensor was installed on the shipboard CTD device in order to record live changes in water column ORP. A total of two MAPRs (serial numbers 74 and 64), and two non-autonomous ORP sensors (serial numbers 11 and 12) were provided, whereby only one of the latter (ORP-12) were used during MSM131.

Fig. 5.4.1A ORP sensor installation within the CTD rosette

Fig. 5.4.1B Close-up of the position of the ORP sensor attached to the frame of the CTD rosette.

The PMEL ORP sensor is equipped with a platinum working electrode and Ag/AgCl reference electrode located on a thermoplastic body. The platinum electrode is exposed to seawater during deployment. A porous barrier separating the seawater from the reference electrode is provided by a Teflon plug embedded in the cap of the reference cell. The ORP sensor determines the electric potential between the platinum and reference electrodes in the range of -500 to +500 millivolts (mV). The non-autonomous ORP sensor (CTD version) has an output scaled between 0 and 5 Volts as required for auxiliary analog sensors on a Seabird 9plus CTD. The ORP sensor was mounted directly to the CTD frame (Fig. 5.4.1A). The sensor was mounted facing downward on the CTD frame in a place where the unobstructed flow of seawater could be guaranteed during casts, and also to enable an easy and quick removal and replacement of the sensor cap (Fig. 5.4.1B). The sensor was coupled to the CTD with a pin-to-pin cable, and was identified by the Seasave Software Instrument Configuration. Both the MAPRs and the ORP sensors were washed and rinsed with fresh water after each deployment. The flexible vinyl sensor cap of the ORP sensors were initially filled with a potassium chloride solution for shipping, and filled with filtered seawater between casts to prevent the electrode from drying out.

While the ORP data from the non-autonomous ORP sensors are extracted with the raw data of the CTD, the MAPR data are read out using the MAPR-Terminal software package consisting

of the MAPR Terminal serial communication program, and an Excel workbook containing macros. The MAPR Terminal software is used to communicate and program the MAPR before deployment, and to read out data and additional information after deployment. MAPR runs with four 9V-batteries consisting of three Sensor batteries and one Logic battery. As MAPR performed continuously for almost every day during the entire cruise, batteries had changed several times when their voltage dropped below 6.5V by opening the bottom cap using a spanner wrench tool. The MAPR battery pack is secured by a black battery backer plate held by four screws, and separated from the bottom end cap by a foam spacer.

Because the ORP sensors do not reference the electric potential to the standard hydrogen electrode, the term E instead of Eh is used throughout. The ORP sensor values all showed a significant drift during deployment, mostly toward more positive values. The two main reasons for this drift are that ambient seawater during deployment is not at equilibrium, and the sensor continuously moves through it. It is therefore very rare for the sensor to have time to completely come to equilibrium with ambient seawater. A significant signal, such as a response to reduced species in hydrothermal plumes, is characterised by a decrease in voltage relative to the normal drift. This is usually followed by a slower recovery period with slowly increasing values. The ORP data recorded by the sensor in mV were normalised by the time differential (dE/dt or ΔE) to identify places where the sensor responded with more rapidly decreasing values. The logging interval of both MAPRs were set to 5 seconds during all deployments, and ΔE is calculated from recorded values, representing changes in ORP in mV over periods of 5 seconds throughout the time of deployment.

Fig.5.4.2A Position of the MAPR installed at bottom lower left side of ROV QUEST 4000m.

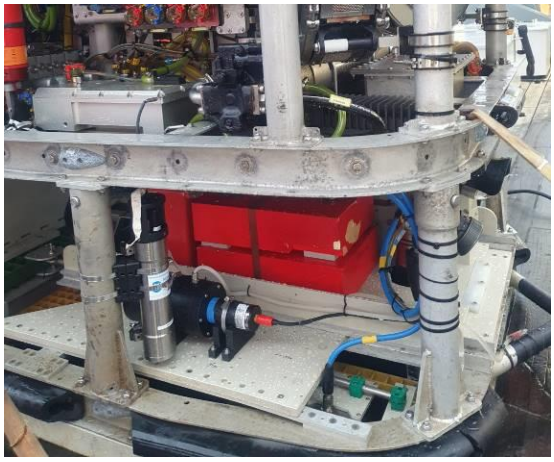

Fig. 5.4.2B Close-up of the MAPR installation within the ROV frame.

The MAPR is equipped with a strain gauge style pressure sensor that is not temperature compensated, so there is some inaccuracy in the measurements. Therefore, a depth correction of the raw data using an Excel macro was conducted in order to determine the atmospheric pressure (zero) value while on deck before deployment. These values were different for each MAPR, and were subject to change from day to day depending on weather conditions. These depth corrections rarely resulted in depth changes greater than 1 meter.

MAPR-62 and ORP-12 were exclusively used during CTD casts. MAPR-62 was additionally deployed during MIC stations, whereas MAPR-74 was only used for ROV dives. MAPR-62 was always installed 50 meters above the CTD or MIC, and attached to the wire using a clamp device

to which the MAPR was attached using metal clamps and one zip wire for additional safety. MAPR-74 was installed on the bottom lower left side of the ROV in a space allowing for seawater to continuously flow by the sensor during dives without obstruction by other devices from the vehicle. It was attached to the ROV frame using metal clamps.

Preliminary Results

MAPRs and non-autonomous ORP sensor were deployed in a total of 68 stations (4 without data records) during MSM131, and a complete list of these stations is given in Tab. App.1 (appendix). The MAPR has been attached to all 35 MIC deployments. However, during MIC-20 the data was not recorded (probably due to weak batteries) and during MIC-23 the cap of the ORP sensor was not taken off (hence, the ORP data are useless, but other sensors of the MAPR worked properly). Of these 33 MIC stations, ORP anomalies were detected during 18 deployments, in contrast to 15 deployments without any anomalies in the ORP records. The MIC stations were taken mainly within the Jøtul vent field and to the Northeast of it, since this is the prevailing current direction.

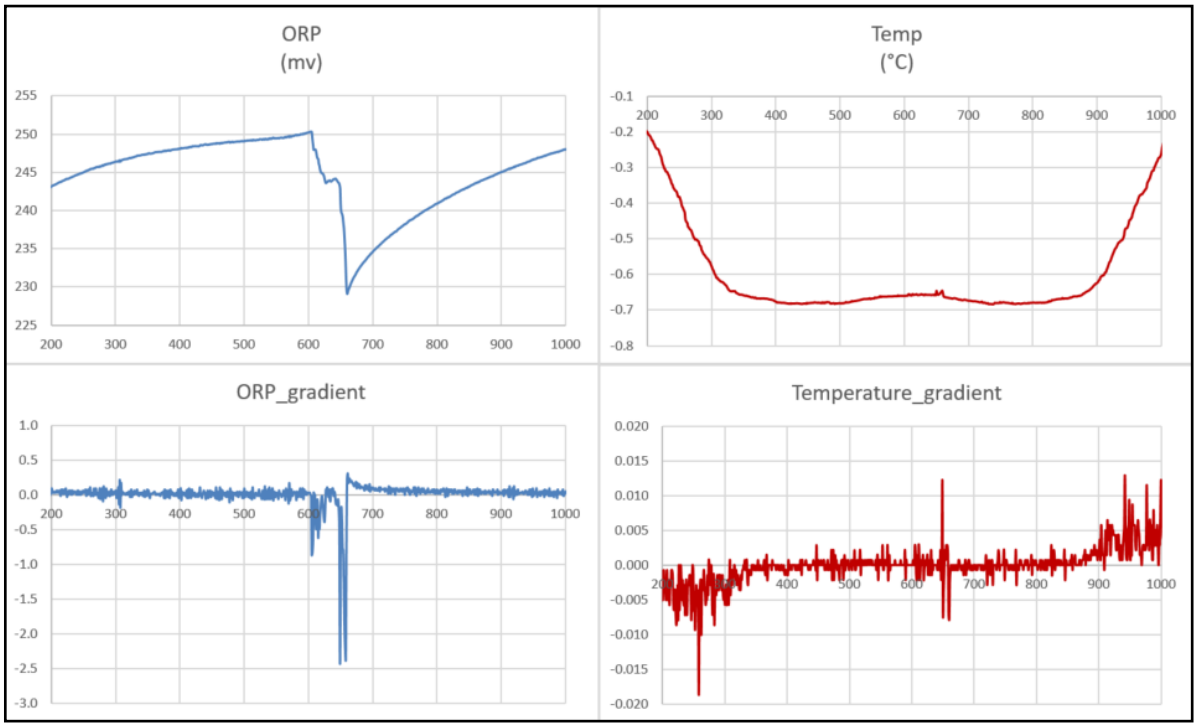

Fig.5.4.3 Graphs showing time-series records of MAPR installed at MIC-19. Besides clearly visible ORP anomalies close to the sea floor, also a temperature anomaly has been detected during this deployment.

The MAPR has been attached to the ROV during the ten successful deployments and also during the two dives that were aborted before reaching the sea floor (at ~800 m and 2600 m water depth). Only during the first ROV dive during MSM131 (ROV dive 481) the MAPR recording failed due to unknown reasons. Except ROV dive 482, all dives were located within the Jøtul vent field. ROV dive 482 was located at a seep site GFA in the Molløy area. ORP anomalies were detected during all dives (except the two aborted deployments).

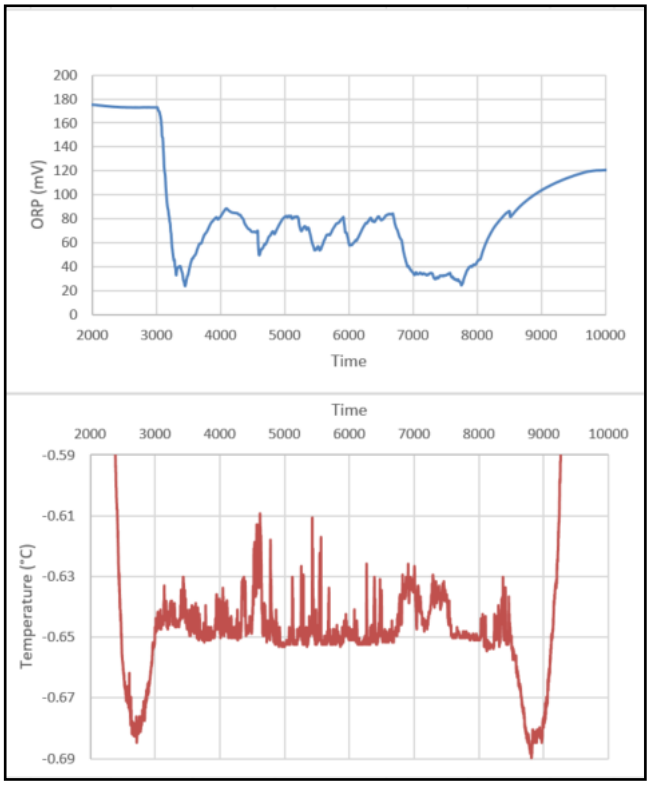

Fig. 5.4.4 Graphs showing time-series records of MAPR installed at ROV dive 488 conducted within the Jøtul hydrothermal vent field. Numerous ORP anomalies were detected during this deployment as well as slightly elevated temperatures in several areas.

23 CTD stations were conducted during MSM131. The ORP sensor was attached within the CTD frame during all deployments, and also the MAPR was attached to the wire in ~ 50 above the CTD during all deployments. Except CTD-04, CTD-05 and CTD-06 that were deployed in the Molløy area, all other deployments were conducted in the Jøtul vent field. Most CTD deployments were conducted as "Tow-Yo" CTD casts. Only the three deployments in the Molløy area as well as four CTD casts in the Jøtul vent field (CTD-01, CTD-03, CTD-07, and CTD-22) were deployed as simple down- and up-cast CTDs. CTD-14 was first aborted before reaching the maximum water depth and had to be recovered due to technical problems with the winch. The data are recorded and the casts was defined as Station CTD-14_1. Immediately after the failure, the CTD was deployed once more and conducted as a Tow-Yo CTD, defined as Station CTD-14_2. ORP anomalies were detected in most CTD casts; exceptions were the three deployments in the Molløy area and the aborted cast CTD-14_1.

An example for the records of a simple down- and up-cast CTD is shown in Fig. 5.4.5A and 5.4.5B. CTD-07 has been located close to the black smoker Fenris. Down- and up-casts have a spatial difference of less than 50 m, but the depths of detected ORP and temperature anomalies vary already within this small area.

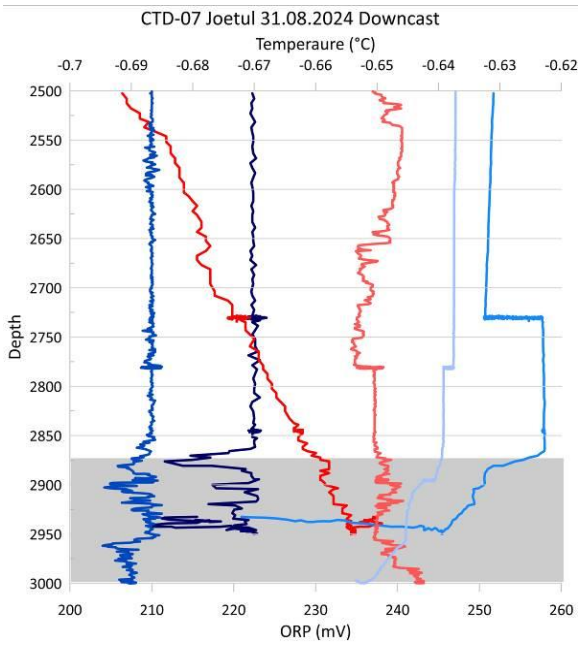

Fig. 5.4.5A Downcast of CTD-07. Shown are ORP raw values (light blue lines) as well as the delta ORP data (dark blues lines) and the temperature raw values (red lines) of both the MAPR and the ORP sensor.

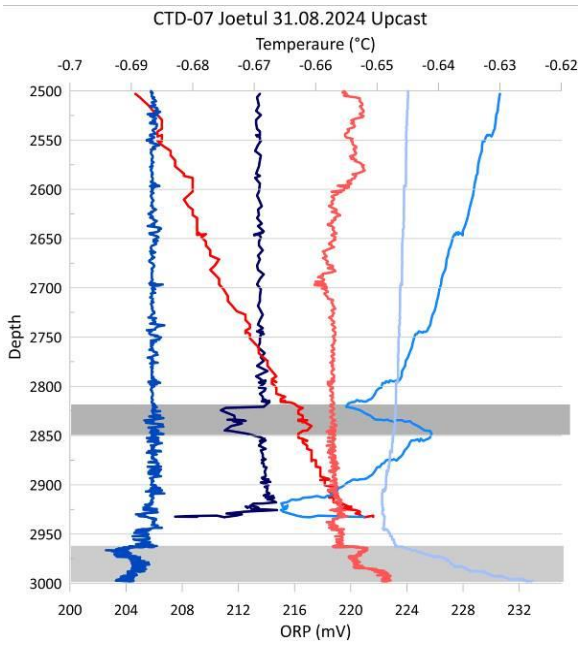

Fig. 5.4.5B Downcast of CTD-07. Shown are ORP raw values (light blue lines) as well as the delta ORP data (dark blue lines) and the temperature raw values (red lines) of both the MAPR and the ORP sensor.

As an example of a Tow-Yo CTD cast, the records of CTD-08 are shown in Fig. 5.4.6A and 5.4.6B. During the first part of the deployment, the CTD was towed from west to east between 2,500 m water depth and 10 m altitude. In both devices (MAPR installed 50 m above CTD and ORP sensor installed within the CTD frame) two ORP anomalies were detected indicating the crossing of a hydrothermal plume in about 50 to 100 m above the sea floor. The source of the plume could be the black smoker Gyme and/or Fenris assuming a water current in eastern direction.

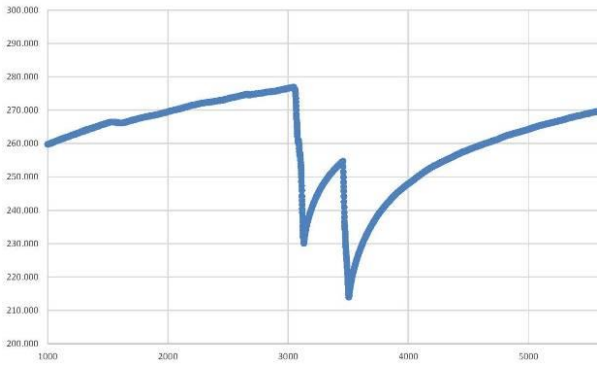

Fig. 5.4.6A Graph showing time-series records of the raw ORP data from the MAPR installed 50 m above the CTD rosette during CTD-08. Two major ORP anomalies were detected, clearly indicated by a sudden ORP decrease of ~50 mV each.

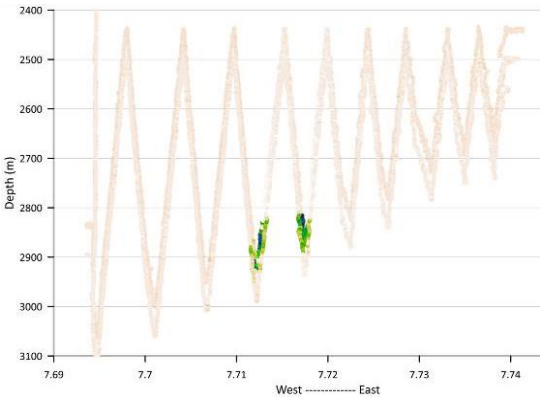

Fig. 5.4.6B Plot showing the delta ORP values of the two devices installed at the Tow-Yo CTD-08 on a W-E profile. The ORP anomalies were registered in both devices indicating a hydrothermal plume in about 50 to 100 m above sea floor.

5.5 Remotely Operated Vehicle (ROV) MARUM QUEST 4000

5.5.1 ROV Operations

(M. Bergenthal, H. Büttner, T. Kienitz, R. Rehage, C. Reuter, S. Schillai, M. Schröder, U. Spiesecke, T. von Wahl)

The scientific deepwater ROV (remotely operated vehicle) “MARUM ROV QUEST 4000” was used aboard RV MARIA S MERIAN during MSM131. The system is hosted at and operated by MARUM, Center for Marine Environmental Sciences at the University of Bremen, Germany. The ROV QUEST is based on a commercially available 4,000 m rated deepwater robotic vehicle designed and manufactured by Schilling Robotics, Davis, USA. Since its installation at MARUM in May 2003, it was set up as a mobile system specifically adapted to the requirements of scientific work aboard marine research vessels for worldwide operation. Today, ROV QUEST has a total record of 490 dives during 43 expeditions, including this cruise. During MSM131, ten dives were carried out with the system at depths ranging between 2,900 m and 3,555 m.

Dive tasks included rock and fluid sampling, geological as well as biological sampling, high quality still imaging, 4K video documentation and optical sea floor mapping. In addition, online in situ-measurements of fluid temperatures around hydrothermal vents were an important task. ROV QUEST was operated by a team of 8 pilots/technicians on a 12-hour basis. The weather conditions during the cruise restricted the available days for dives, whilst the cold temperatures posed a challenge to the ROV system. When diving, close cooperation between ROV team and ship’s crew through all departments allowed a safe and routinely performed handling, especially during deployment and recovery and an always clear and friendly communication prior to and during dives.

Fig. 5.5.1

ROV QUEST-setup for MSM131 Leg1

QUEST System Description

The total QUEST system weighs about 45 tons (including the vehicle, control van, workshop van, electrical winch, 5,000 m umbilical, Launch and Recovery System, and transportation vans) and is shipped in four standard ISO 20' vans. The electrical spooling winch hosts 5,000 m of 17.6 mm NSW umbilical. For the installation on RV Meteor, the launch and recovery frame (LARS) has to be installed on a traversal adapter structure in the A-Frame, providing mechanical mounts for the LARS and the sheave for the umbilical. The ships A-Frame hydraulic lift winch is needed to deploy and recover the ROV via a specialized Latch and Gimbal assembly.

The ROV QUEST uses a Doppler velocity log (DVL, 1200 kHz) to perform Stationkeep, Displacement, and other advanced auto control functions. The combination of 60-kW propulsion power with DVL-based auto control functions provides exceptional positioning capabilities at depth. Designed and operated as a free-flying vehicle, QUEST system exerts such precise control over the electric propulsion system that the vehicle could maintain relative positioning hold within decimeters. Absolute GPS-based positioning is provided by the shipboard Sonardyne Ranger USBL positioning system. The ROV QUEST control system provides transparent access to all Ethernet, serial data and video channels. The scientific data system used at MARUM feeds all ROV- and ship-based science and logging channels into a real-time database system based on the ROS2 (Robot Operating System) software framework. The ROS2 based data visualization and logging system is developed at MARUM and used on all our major robotic systems.

Due to the limited space in the Control Van of the ROV (2 pilots + 2 scientists), the ship's Universal Lab was prepared to allow scientists to follow all dives in real-time. Navigational information (Bathy-Map, Position and heading of ROV and ship), realized via the QGIS PlugIn Posiview (see below), CTD and high temperature measurements were displayed in the Lab together with a copy of the sonar screen. Furthermore, UHD video feeds from the Zeus camera and from the tiling screen with all relevant ROV cameras were streamed to the Lab. Using the Mumble VoIP software, a communication link between the control van and the Universal Lab was established allowing the scientists to coordinate their activities. A feed of the video tiling of the ROV cameras was streamed into the vessel´s intranet, allowing all other cruise participants to watch the dive as well.

Table 5.5.1 Scientific equipment used on board MARUM ROV QUEST 4000 (Fig. 5.5.1)

- ROV based standard tools, installed on vehicle:
  - 2 hydraulic manipulators for sampling and experiment handling
  - one fixed and one hydraulic drawer for probe and sample storage
  - toolskid center section setup for vertical mapping with cameras and lights
  - ROV starboard-side hydraulic basket frame for rock and fluid sampling
  - various nets and shovels with T-handles
  - Voyis Mapping camera

- MSM131 specific payloads, installed on vehicle:
  - MAPR autonomous sensor loggers
  - KIPS fluid sampler
  - high temperature probe with online data display
  - 8 Pushcores
  - offline low temperature probe (T-Stick)

- IGT fluid sampler

- MSM131 specific payloads, deployed at sea floor:
  - Homer Beacon, for specific site relocation between dives

Table 5.5.2 DIVE LOG Summary, Dates/Times UTC

No.	Dive No.	Date	Latitude	Longitude	Depth max (m)	Time Launch	Bottom hours	Total Dive hours
1	481	08/24/24	77°26.362'N	7°42.552'E	3050	11:45	**2.45**	**6.40**
2	482	08/28/24	79°36.840'N	3°39.600'E	3555	8:14	**6.08**	**11.90**
3	483	09/01/24	77°26.175'N	7°42.349'E	2998	6:22	**7.28**	**11.98**
4	484	09/03/24	77°26.161'N	7°42.447'E	3035	6:21	**7.38**	**11.80**
5	485	09/08/24	77°26.378'N	7°42.193'E	3048	4:04	**8.80**	**13.95**
6	486	09/13/24	77°26.173'N	7°42.276'E	3022	11:01	**4.83**	**9.58**
7	487	09/15/24	77°26.392'N	7°42.458'E	3022	8:56	**5.57**	**10.58**
8	488	09/16/24	77°26.355'N	7°42.461'E	3001	6:46	**6.83**	**12.15**
9	489	09/18/24	77°26.139'N	7°42.377'E	3018	6:32	**7.65**	**13.02**
10	490	09/19/24	77°26.376'N	7°42.243'E	3020	7:05	**5.47**	**9.87**
				Max. Dive Depth (m):	**3555**		**62.34**	**111.23**

New Developments Used During MSM131

We integrated a second UHD camera into the QUEST System. The DSPL Apex is a 4K UHD camera with 12x optical zoom and 6000m depth rating. Its relative small housing makes it easy to use on our lower pan tilt actuators. The high resolution of 3180x2160 pixel is more than we could capture with our former still camera at the same position and sixteen times the resolution of the former video camera that it replaces.

To improve science payload network capacity and multi camera UHD video distribution, we equipped the ROV QUEST 4000 system for the first time with a CWDM fiber bottle, already developed for its successor, ROV QUEST 5000. This allows up to six 1Gb/s Ethernet devices to be directly connected to the vehicle combined with a 10Gb/s fiber uplink to the control container and two video fiber channels with 12G video. During MSM131, the Voyis mapping camera and Zeus UHD video camera were connected to the Ethernet links, for real time image processing and high speed-video downloads. The Zeus and Apex UHD cameras were connected to the fiber video uplinks.

To improve live data processing and display, log entry, data logging and post dive data visualization, a set of new software components based on the open source software framework ROS2 was used for the first time. Similar software is used on several other systems operated by the MARUM Meerestechnik, allowing fast development and transfer between the vehicles.
Following thorough tests at MARUM, during MSM131 large portions of the software components were used during operation on ROV MARUM QUEST. Data from ship, winch, control container, ROV systems and scientific sensors connected to the ROV data interfaces is collected and processed by so-called ‚nodes', which run independently and exchange information via pre-defined interface called ‚topics'. In addition, manual input of text and pre-defined labels can be made in a scientific log and a pilot log. For each log entry, position and time stamp are added automatically and then data also shared via a topic.

During the dive, nodes of the ROS2 based system also make live data available through a diverse range of network and web interfaces, to provide position estimates to QGIS, an overlay to camera streams and custom data displays for pilots and scientists. The pilot displays combined ship and ROV information, enhanced by processed data e.g. to estimate the vertical velocity of the ROV, to aid tether management, or to estimate the time until the surface is reached after a dive. Additionally, a scientific display visualized CTD and the KIPS data both in the control container and the universal lab. All information exchanged through topics, as well as the timing of the exchange, is logged via the ROS2 logging system. With the newly deployed software, log data can be replayed, digitally processed, exported to human readable formats and enhanced with additional time-stamped data, e.g. frame grabs from the video recordings. Post-cruise data archival will be hosted by the World Data Center PANGAEA Data Publisher for Earth & Environmental Science (www.pangaea.de), which is operated on a long-term base in cooperation by MARUM in Bremen and the AWI in Bremerhaven.

5.5.2 Dive Reports

(M. Römer, K. Streuff, S.-M. Knutsen, G. Bohrmann, P. Ribeiro, A. Diehl)

ROV Dive 481 (GeoB26209, Station MSM131/09)
Area: Black Smoker of Jøtul Hydrothermal Field
Date: 24 August 2024
Start bottom: 15:02
End bottom: 15:50
Bottom time: 00:48
Start bottom (Lat/Long/Depth): 77° 26.411’N, 07° 42.506’E, 3016 m
End bottom (Lat/Long/Depth): 77° 26.411’N, 07° 42.243’E, 3041 m

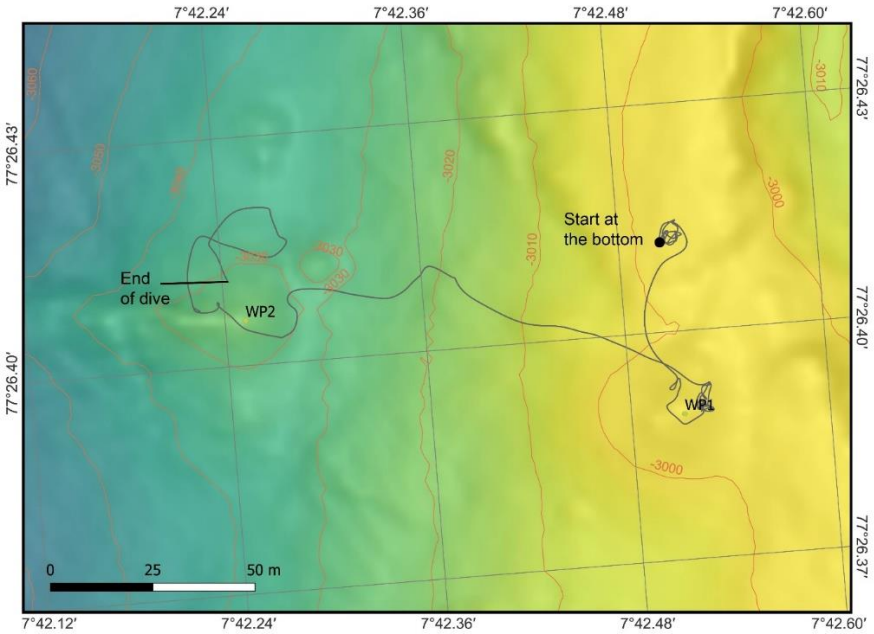

Fig.5.5.2 Map of ROV Dive 481 in the Blake Smoker area of the Jøtul hydrothermal field.

ROV dive visited the black smoker found during MSM109 of the Jøtul hydrothermal field. The black smoker had grown considerably in two years, changing its original tilted orientation to a

vertical growth and turning a large opening into several smaller fluid exits. The search for a second black smoker about 120 m to the West was unsuccessful during this dive, but bright microbial clusters continuously were observed on the way there.

Table 5.5.3: Handling of instrument and sampling during ROV Dive 481.

GeoB No	Instrument	UTC start	Latitude Longitude	Water Depth (m)	Comment
26209-2	Beacon	15:25	77° 26.389'N 7° 42.529'E	3010	Dropped for finding position in the future

Dive Description

Dive 481 was intended to locate the two known black smokers of the Jøtul field and, above all, to carry out a good photo documentation of the structures. The dive reached the sea floor about 40 m north of the active smoker, which was first described during the MSM109 expedition (Fig. 5.5.2). The landing point is at the southern end of a small rift-like depression structure, the edges of which are built up by pillow lavas and are partially covered or underlain by sediments. Small, patchy, bright white microbial mats can be seen on some edges, and examination of these in other places often revealed siliceous precipitation (Fig. 5.5.4b).

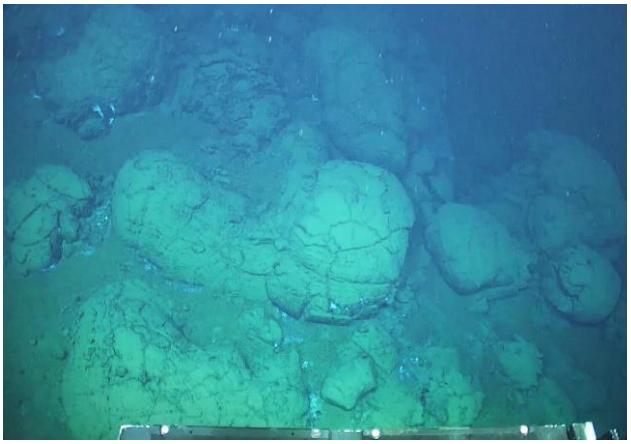

Fig. 5.5.3a Pillow basalt just north of the Black smoker with small microbial mats in some parts.

Fig. 5.5.4b Black Smoker at the southern corner of a hydrothermal mound covered by microbial mats and white precipitates.

The dive headed south, following the west side of a hydrothermal vent structure, and reached the smoker, which sits on a pedestal on the south side of a vent structure. Shortly before, characteristic very small white vent precipitates were observed, consisting of barite towers a few centimeters high and covered with filaments of the same color. The smoker showed very clearly that it has grown. While previously (in July 2022) it had a single outflow channel that was inclined diagonally to the cardinal direction (Fig. 5.5.2), the grown part of the channel has grown vertically in height and split into several tubes, which morphologically looks like a club structure (Figs. 5.5.5). A beacon was placed on the first plateau north of the smoker (Fig. 5.5.6), which will allow us to find the smoker more quickly in the future. The plateau-like elevation of vent precipitates shows rind-like structures indicating aborted smokers (Fig. 5.5.4b).

Fig. 5.5.5 Outflow area of the Black Smoker with several separate channels where black fluids emanate upwards. The view is approximately from south to north.

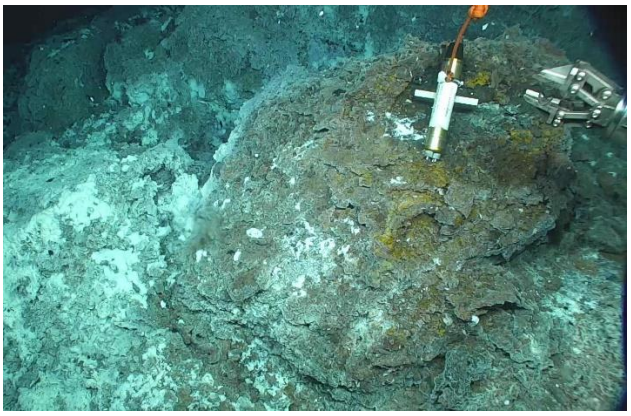

Fig 5.5.6 Detached beacon on a narrow plateau north of the Black Smoker. In the subsurface, ring structures on the brown-red break-off area indicate formerly active channels that have broken off.

The sea floor path was supposed to lead us to a second smoker, discovered about 120 m further west by colleagues from the Center for Deep Sea Research in Bergen on a cruise in 2022. Along this path, bacterial mats were repeatedly discovered between partially weathered hydrothermal precipitates, showing us that slight hydrothermal activity exists over a long stretch. We aimed for waypoint 2 (Fig. 5.5.2), which we set on a narrow west-east directed gradient. Due to excessive oil loss in ROV circuit 3, the dive had to be aborted without being able to find the second black smoker.

ROV Dive 482 (GeoB26222, Station MSM131/22)
Area: Molløy ridge at Flare GFA (Thorsnes et al. 2023)
Date: 28 August 2024
Start bottom: 11:43
End bottom: 17:33
Bottom time: 5 hours and 50 minutes
Start bottom (Lat/Long/Depth): 79° 36.847’ N, 03° 39.695’ E, 3554 m
End bottom (Lat/Long/Depth): 79° 36.862’ N, 03° 39.466’ E, 3552 m

Dive 482 (Fig. 5.5.7) targeted a seep location in the Molløy Ridge Area, that was discovered recently by colleagues from Tromsø University, and was based on work by Thorsnes et al. (2023), who originally observed gas flares in the area. We were kindly provided with a map of a previous ROV dive to the area, which outlined the location of potential carbonate sites, as well as the approximate location of two gas hydrate occurrences. Because of some initial problems with the ROV QUEST, we anticipated only about an hour of diving time, but the oil levels stabilized after about an hour, leading to a very successful dive with a bottom time of nearly 6 hours. Throughout dive 482 several outcrops of gas hydrates, two seepage sites of active bubble emission, as well as abundant chemosynthetic fauna were observed. The latter was composed of siglinoid tube worms, arthropods, snails and clams. Several samples were obtained, including a shovel sample of tube worms and potential authigenic carbonates, and three water samples from close to/on top of the bubble emission site (Tab. 5.5.4, Fig. 5.5.7).

Table 5.5.4 Samples recovered during ROV Dive 482

GeoB No	Instrument	UTC start	Latitude Longitude	Water Depth (m)	Comment
26222-2	Niskin	12:51	79°36.861 3°39.451	3555	# 3 green
26222-3	Niskin	12:56	79°36.861 3°39.481	3550	# 2 yellow
26222-4	shovel	13:14	79°36.862 3°39.471	3554	Portside box, compartment 1
26222-5	Niskin	17:24	79°36.862 3°39.427	3554	# 1 white

Dive Description

Dive 482 started in the morning of 28 August 2024, with ROV QUEST going into the water at 08:14 UTC. Thanks to the map, the ROV QUEST reached the sea floor about 40 m east of the target location at 11:20 UTC, and began moving towards the target area at 11:43. Along the way some sediment structures, patches of bacterial mats, and the presence of ROV tracks from previous dives revealed this an interesting location. Thanks to the map provided by our colleagues, we managed to find the first outcrops of gas hydrate within only 17 minutes (Fig. 5.5.8A).

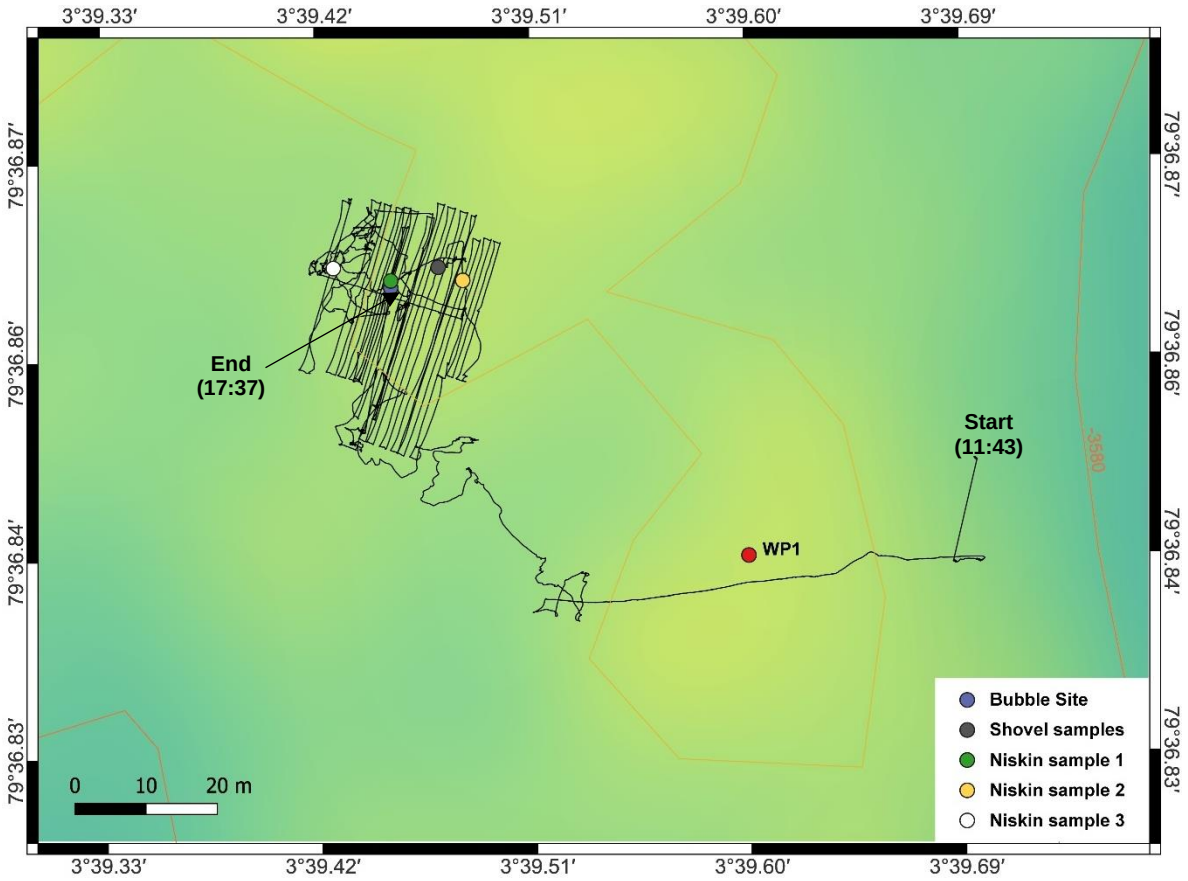

Fig. 5.5.7 Map showing the combined USBL and DVL navigation tracks of ROV QUEST Dive 482 to the Molløy Deep. Waypoint 1 (WP 1) was used for initial navigation. Samples, as well as the site of bubble emissions, are shown as colored dots.

The gas hydrates occurred as smaller mounds on the sea floor, which appeared to be heavily sediment-covered at first glance (Fig. 5.5.8A). After taking the time to observe the gas hydrate

outcrop and to take some 4k-resolution videos, zooming in on different parts of the structures, it became clear, that the "sediment-like overgrowth" consisted mainly of tube worms, interspersed with some small snails, and potentially some authigenic carbonate (Fig. 5.5.2.6F).

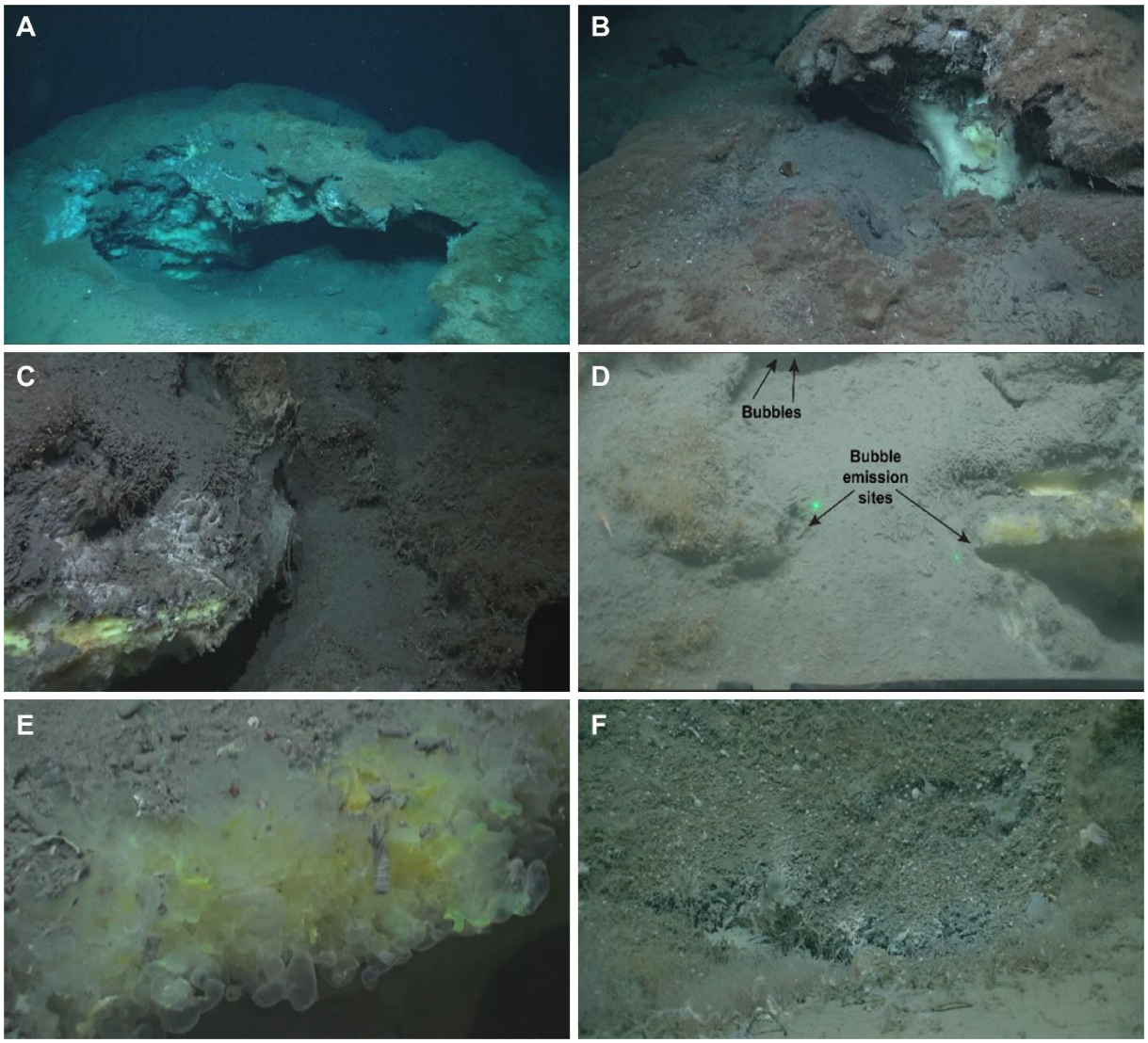

Fig. 5.5.8 Observations during the dive. A), B) Examples of gas hydrate outcrops with the sediment-like overgrowth clearly visible. C) Characteristical yellow color of oil-stained gas hydrates. Some white bacterial mats and numerous tube worms are also visible. D) Location of the two gas emission sites (labelled). Distance between the two green laser points is 20 cm. E) Hydrate-coated bubbles of free gas stick to the margins of the yellow-stained older hydrate structure. F) Example of the abundant fauna found at the seep site with sea anemones, different species of tube worms, and many small snails.

The distinct yellow color of some areas of the gas hydrate further indicated that the area might have been affected by oil seepage. Although we did not find any oil bubble release, the yellow color continued to be present throughout the gas hydrate structures, showing that several regions of the gas hydrates were stained by oil (Fig. 5.5.2.6C).

Close to the first hydrate structure, ROV QUEST's sonar also showed a bright echo indicating active bubble seepage, and, using the sonar for navigation, we observed the first bubbles in the water column at 12:15. Two sites of active bubble release were encountered in very close proximity, one along the edge of a second gas hydrate outcrop, the other from underneath the

"sediment-like overgrowth" next to it (Fig. 5.5.8D). Two Niskin bottles were used to acquire water samples, one from close to the bubble emission site, the second from directly on top of it (Tab. 5.5.4), to be measured for methane concentrations after the dive. Samples of the "sediment cover" were also taken for further investigations, using the ROV's shovel (Tab. 5.5.4, Fig. 5.5.7), which broke or scraped off several pieces of the mounds. Further moving around the dive area revealed several more gas hydrate outcrops, some of which showed the adhesion of methane-hydrate-covered free-gas bubbles (Fig. 5.5.8E).

As the oil levels of the ROV QUEST had stabilized at this time, a survey of the gas hydrate structures became feasible, and the ROV started mapping a grid of ~35 x 20 m (Fig. 5.5.7). The survey took two hours and used the integrated VOYIS camera for high-resolution imaging, which will provide great footage for the compilation of a 3D mosaic. After the survey, some time was left for additional observations, revealing more abundant chemosynthetic fauna in the form of several species of tubeworms, some clam shells, arthropods, and a lot of snails (Fig. 5.5.9F). Just prior to starting its ascend, the ROV moved back over the bubble emission site to take another Niskin bottle water sample (Tab. 5.5.4). All sampling activities stopped at 17:33 UTC and ROV QUEST began its ascend at 17:37 UTC.

ROV Dive 483 (GeoB26228, Station MSM131/28)
Area: Yggdrasil and Nidhogg hydrothermal mounds
Date: Sunday 1 August 2024
Start bottom: 08:49
End bottom: 16:07
Bottom time: 6 hours and 18 minutes
Start bottom (Lat/Long/Depth): 77° 26.201' N, 07° 42.460' E, 2965 m
End bottom (Lat/Long/Depth): 77° 26.204' N, 07° 42.227' E, 2992 m

Dive 483 (Fig. 5.5.9) was designed to re-visit the areas of the Yggdrasil and the Nidhogg hydrothermal mounds and vent sites positioned on the southern parts of the Jøtul hydrothermal field. Both vent sites were located during the dive. The well-developed chimneys and flange structures at the Yggdrasil vent site was investigated, with numerous outlets and including apparent mirroring-effects of high-temperature waters below several of the flanges. The Nidhogg site has less venting than the Yggdrasil but is characterized by several fossil vents and chimneys, and with frequent hydrothermal precipitation. The Yggdrasil vent area is characterized by bacterial mats whereas the Nidhogg mound has many areas dominated by amphipods and snails. Three samples were taken from the Yggdrasil and one from the Nidhogg, in addition to three Niskin-bottles filled at, and in two steps at each approximately five meters from an active vent at the Nidhogg hydrothermal mound (Fig. 5.5.9 and Tab. 5.5.5). A photo-mosaic composed of 17 vertical profiles which in steps circling the Yggdrasil mound was acquired. For the Nidhogg mound it was acquired three parallel lines and one cross-line horizontally over the structure.

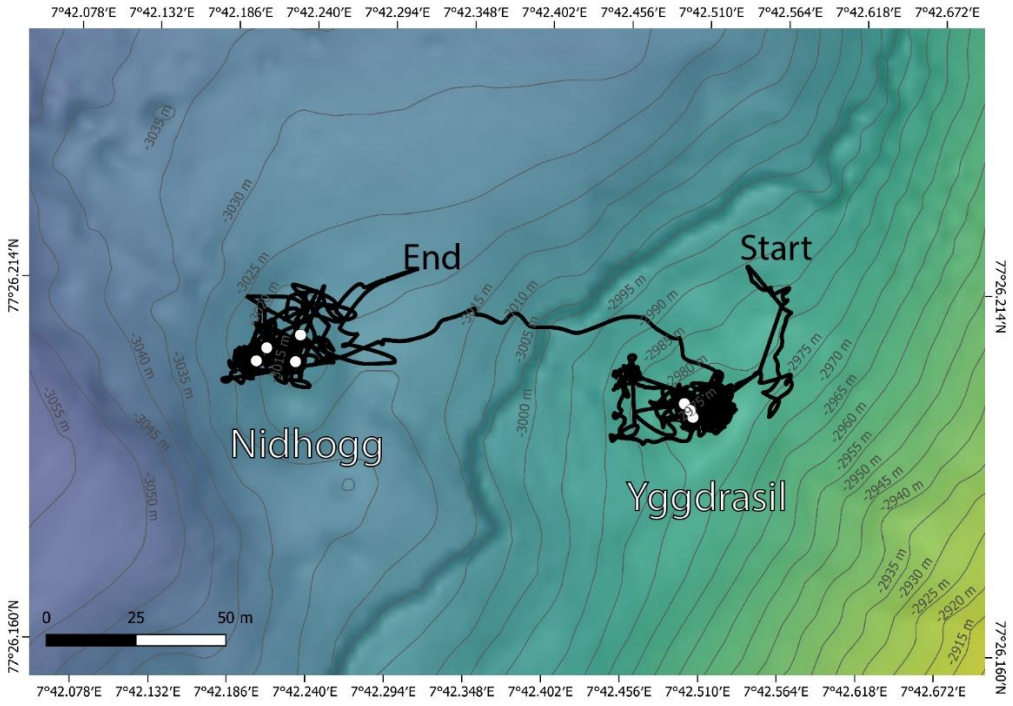

Fig. 5.5.9 Map showing navigation tracks of ROV QUEST Dive 483 to the Yggdrasil and Nidhogg vent sites, and the bathymetry of the area. Location of samples are shown as white dots.

Table 5.5.5 Samples recovered during ROV Dive 483

GeoB No	Instrument	UTC start	Latitude Longitude	Water Depth (m)	Comment
262228-2	shovel	12:45	77° 26.197' 07° 42.497'	2955	Flange piece Yggdrasil
262228-3	Man	13:13	77° 26.195' 07° 42.503'	2950	Flange piece Yggdrasil
262228-4	Man	13:29	77° 26.196' 07° 42.501'	2951	Precipitate Yggdrasil
262228-5	Man	15:03	77° 26.202' 07° 42.202'	2990	Precipitate Nidhogg
262228-6	Niskin	16:04	77° 26.204' 07° 42.209'	2989	3 (green)
262228-7	Niskin	16:05	77° 26.202' 07° 42.229'	2990	1 (white)
262228-8	Niskin	16:07	77° 26.206' 07° 42.232'	2992	2 (yellow)

Dive Description

Dive 483 started in the morning 1 August 2024 and the ROV QUEST 4000 reached the sea floor at 08:49 UTC and approximately 50 meters north of the Yggdrasil vent site (Waypoint – WP – 1). When moving southwards we observed white precipitates, bacterial mats and hints of shimmering water on the sea floor. The Yggdrasil hydrothermal mound was reached after approximately 35 minutes. The well-defined flange-structures, largest at the base and decreasing upwards often appeared to be almost completely covered with dominantly white bacterial material with a "fluffy" expression. Between and under/over the many flange-structures chimneys were observed (Fig. 5.5.10). High temperature water was observed shimmering out from chimneys as well as below the flanges, some showing nice mirror-like effects. Areas with amphipods and snails could be seen,

as well as an eel pout (small fish). At 10:10 UTC we initiated acquisition of vertical profiles circling the mound structure – a total of 17 profiles were completed by 12:07 UTC. Collected three samples: first large piece of flange picked up using the shovel, second sample of flange further up on structure and third sample with potential precipitation high up on structure. When collecting samples (breaking of pieces) shimmering water immediately starts pouring out from the flange where sample was collected. Repositioned towards the Nidhogg structure, located approximately 140 meters west-northwest for Yggdrasil – arrived at 14:00 UTC.

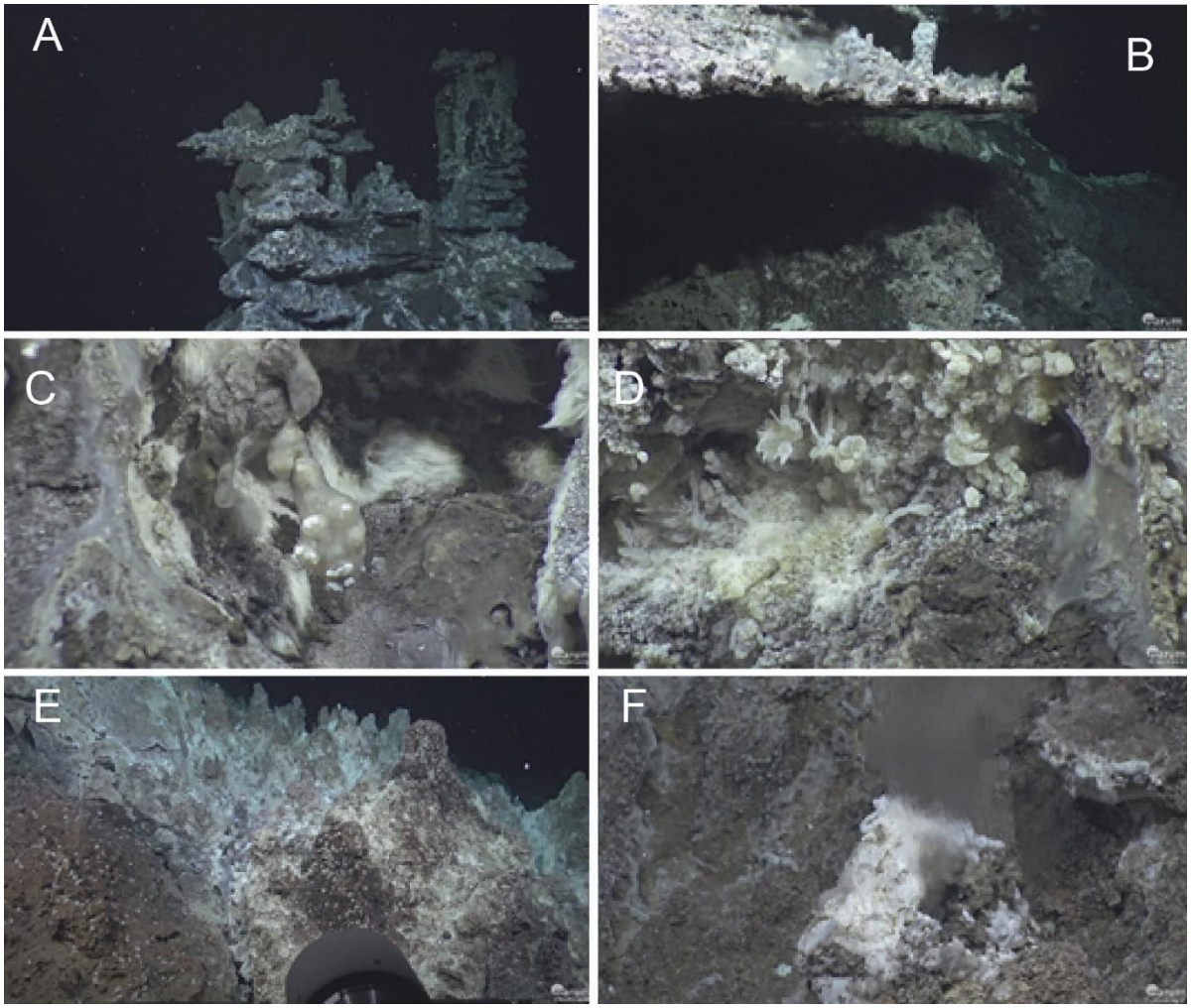

Fig. 5.5.10 Observations during the dive. A) The Yggdrasil hydrothermal vent system, B) One of the flanges at Yggdrasil with hot shimmering water under appearing as mirror effect under flange, Examples of gas hydrate outcrops with the sediment-like overgrowth clearly visible. C),D) Close-up of bacterial growth and snails at Yggdrasil, E) Nidhogg vent system with fossil chimneys and frequent occurring amphipods observed as white coloring the dominant darker surroundings (ROV-camera in foreground), D) Close-up of one active vent at Nidhogg.

The Nidhogg hydrothermal mound was characterized by fossil/collapsed chimneys, ragged and fractured terrain and frequent areas with almost covered with mainly white amphipods as well as numerous snails apparently feeding on bacterial mats. Took one sample of the precipitate. At 15:20 UTC started sampling five lines flying over structure. Few active vents were observed, but after the profiles/lines for photo-mosaic we sampled three Niskin-bottles at one vent, and then two more each with attempted approximately 5 meters step-out from the vent. Dive ended 16:08 UTC.

ROV Dive 484 (GeoB26235, Station MSM131/35)
Area: Yggdrasil and Nidhogg hydrothermal mounds
Date: 03. September 2024
Start bottom: 08:34
End bottom: 16:00
Bottom time: 7 hours and 26 minutes
Start bottom (Lat/Long/Depth): 77° 26.217’ N, 07° 42.484’ E, 2973 m
End bottom (Lat/Long/Depth): 77° 26.192’ N, 07° 42.208’ E, 2998 m

The dive was primarily used to sample hydrothermal fluids using KIPS, IGTs and Niskin bottles at the two hydrothermal structures Nidhogg and Yggdrasil. Using KIPS and IGT, a fluid could be sampled directly under a flange, where temperatures of up to 289°C occur. A second sampling at an exciting chimney at the top of the structure also showed temperatures of up to 289°C. These temperature measurements hardly differ from those measured 2 years ago during MSM109. At Nidhogg hydrothermal mound, an exit point with a fluid of 152°C was sampled, which was significantly warmer than measured two years ago.

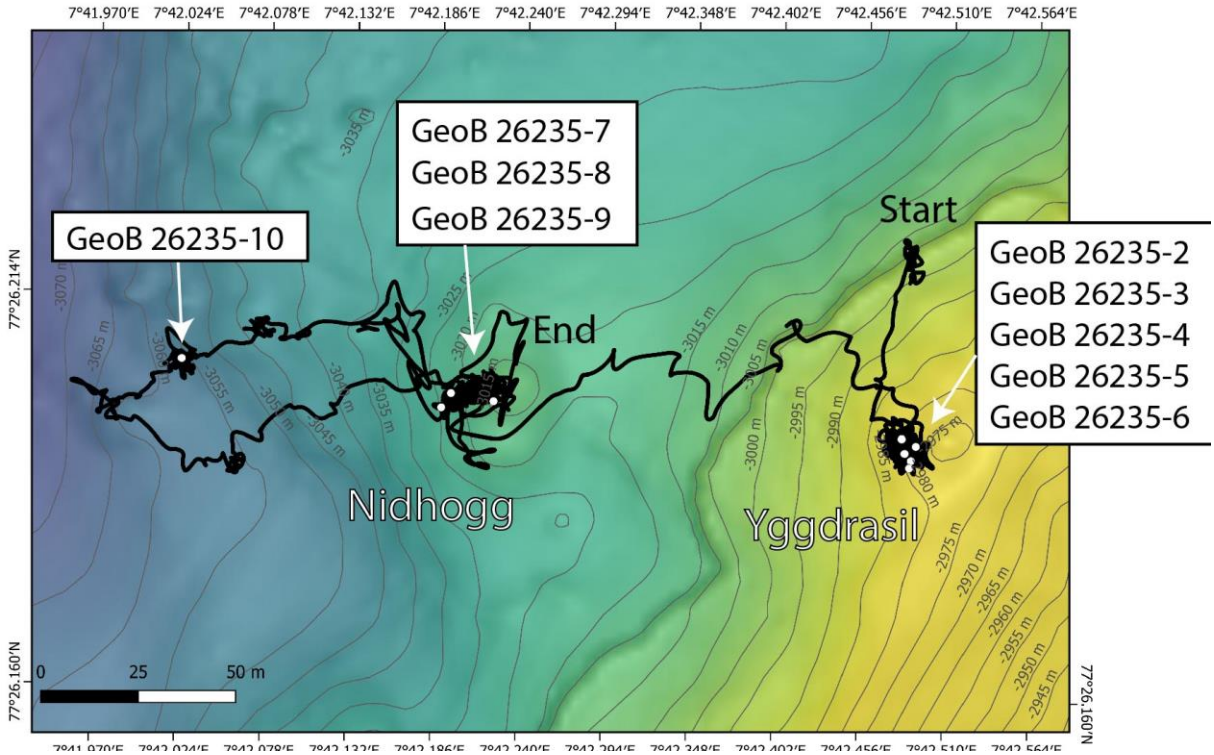

Fig.5.5.11 Map of ROV Dive 484, covering Yggdrasil and Nidhogg hydrothermal mounds and some areas to the West.

Dive Description

The dive was primarily planned to use the various systems for fluid sampling in the Nidhogg and Yggdrasil areas and to explore unknown structures on the sea floor during the remaining dive time (Fig. 5.5.11; Tab. 5.5.6). ROV QUEST 4000 landed about 50 m north of Yggdrasil and began to move towards the hydrothermal mound after all systems on the sea floor were working stably (Fig. 5.5.11). The upper structures of Yggdrasil, which consist of flanges of different sizes, were circled during the dive anti-clockwise to select a suitable fluid outlet structure. An initial sampling was carried out on the east side under a flange that could be reached at about mid-height (Fig. 5.5.12). The temperature sensor of the KIPS sampler showed an average temperature of 279°C over the suction time into the sample vessel (KIPS A), with maximum values of up to 286°C being reached. The subsequent IGT sampler recorded maximum temperatures of up to 289°C. A similar high temperature of 272°C was measured 2 years ago during MSM109 (Bohrmann et al. 2024) and this confirms constant hydrothermal activity with the release of shimmering fluids.

Table 5.5.6 Samples recovered during ROV Dive 484

GeoB No 26235-1	Instrument	UTC start	Latitude Longitude	Water Depth (m)	Comment
26235-2	KIPS A	09:55	77° 26.193’ 07° 42.487’	2953	Outflow flange Yggdrasil
26235-3	IGT 7	10:24	77° 26.195’ 07° 42.490’	2954	Outflow flange Yggdrasil
26235-4	KIPS B	11:40	77° 26.196’ 07° 42.481’	2950	Outflow top Yggdrasil
26235-5	MAN	12:04	77° 26.194’ 07° 42.483’	2950	Outflow top Yggdrasil, precipitate
26235-6	Niskin 3, green	12:15	77° 26.192’ 07° 42.486’	2948	1 m above outflow top Yggdrasil
26235-7	KIPS C	13:37	77° 26.200’ 07° 42.222’	2992	Nidhogg vent
26235-8	IGT 8	13:58	77° 26.199’ 07° 42.189’	2992	Nidhogg vent
26235-9	Niskin 2 yellow	14:10	77° 26.201’ 07° 42.195’	2992	1,5 m above Nidhogg vent
26235-10	Net	15:07	77° 26.205’ 07° 42.024’	3024	Hydrothermal precipitates

After the flange had been sampled, another fluid outlet point was sought in the summit area of the mound, as outlets from small chimneys had been observed there during a previous dive. A chimney that was accessible from the southern side was initially selected, but had to be discarded because the chimney opening had a diameter that was too small for the KIPS intake nozzle (Fig. 5.5.13), so that suction could not be constant and the temperature measurement also fluctuated greatly. A new attempt focused on an outlet point between the two summit peaks, which could be reached from the northwest with a ROV heading of 126-135°. A fluid sample (KIPS B) was taken at a temperature of 282°C. A precipitate sample from this point was recovered with the QUEST manipulator arm and the ambient water about 1m directly above the outlet point was sampled with a Niskin bottle.

ROV QUEST then dived westwards with the intention of exploring some of the mounds that can be seen on the AUV map in the remaining 1.5 hours.

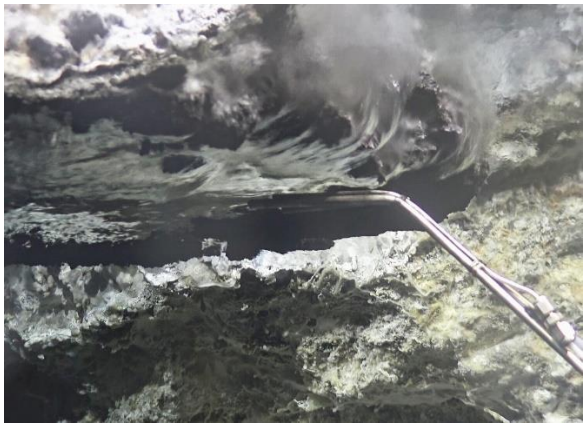

Fig. 5.5.12 Fluid sampling with the KIPS sampler under a flange at the Yggdrasil hydrothermal mound. Due to its lower density, the hot fluid flows upwards over the edge of the flange.

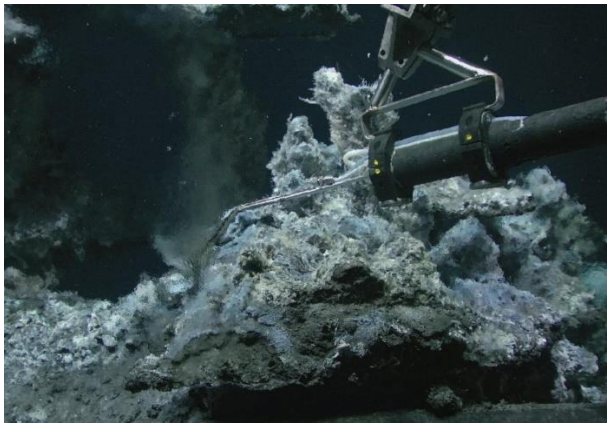

Fig 5.5.13 Attempt to take fluid samples with KIPS on the southern upper edge of Yggdrasil, but this could not be carried out in full due to the small diameter of the fluid outlet point.

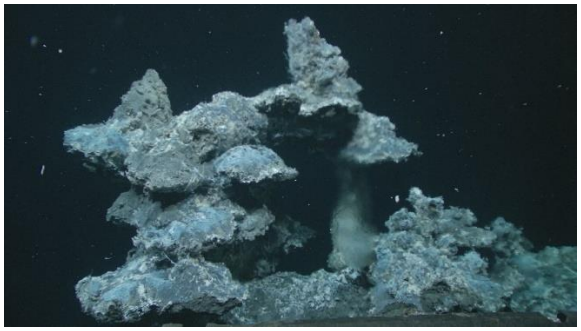

Fig. 5.5.14 Attempt to take fluid samples with KIPS on the southern upper edge of Yggdrasil, but this could not be carried out in full due to the small diameter of the fluid outlet point.

Fig. 5.5.15 Fluid outlet point in the summit area of Yggdrasil visible through a shimmering water column under a flange. The hydrothermal mound is characterized at its highest point by many small flanges and chimneys.

Fig. 5.5.16 Collections of amphipods are often found in the vicinity of hot fluids, as here at the Nidhogg hydrothermal mound.

Fig. 5.5.17 Fissure or crevice fillings made of barite and other hydrothermal minerals that have weathered out on the sea floor.

Due to the unfavorable position of the ship to the ROV, the vehicle could not initially move forwards but had to traverse sideways. At a water depth of about 3060 m at the western end of the dive (Fig. 1), further hydrothermal activity was detected, evidenced by bacterial mats. Along the sea floor, heavily weathered hydrothermal deposits were also visible, which differed significantly from the normal sea floor covered with hemipelagic sediments. On an easterly course, large blocks of solid rocks were observed that were exposed on the sea floor. As we continued to ascend towards Nidhogg, weathered sediments were observed with parallel fracture fillings exposed (Fig. 5.5.17). A sample that we recovered with one of the nets (Tab. 5.5.6) contained dark brown fine-grained precipitates and very clearly light-colored barite, which, according to the optical impression, is more widespread in specific locations on the sea floor. During the further dive to the east and finally to the South, the Nidhogg hydrothermal mound was reached again, where the dive was terminated.

ROV Dive 485 (GeoB26252, Station MSM131/52)
Area: Jøtul Field, Black Smoker area
Date: 08 September 2024
Start bottom: 06:29
End bottom: 15:26
Bottom time: 08:57
Start bottom (Lat/Long/Depth): 77° 26.414’ N, 07° 42.265’ E, 3000 m
End bottom (Lat/Long/Depth): 77° 26.377’ N, 07° 42.426’ E, 3000 m

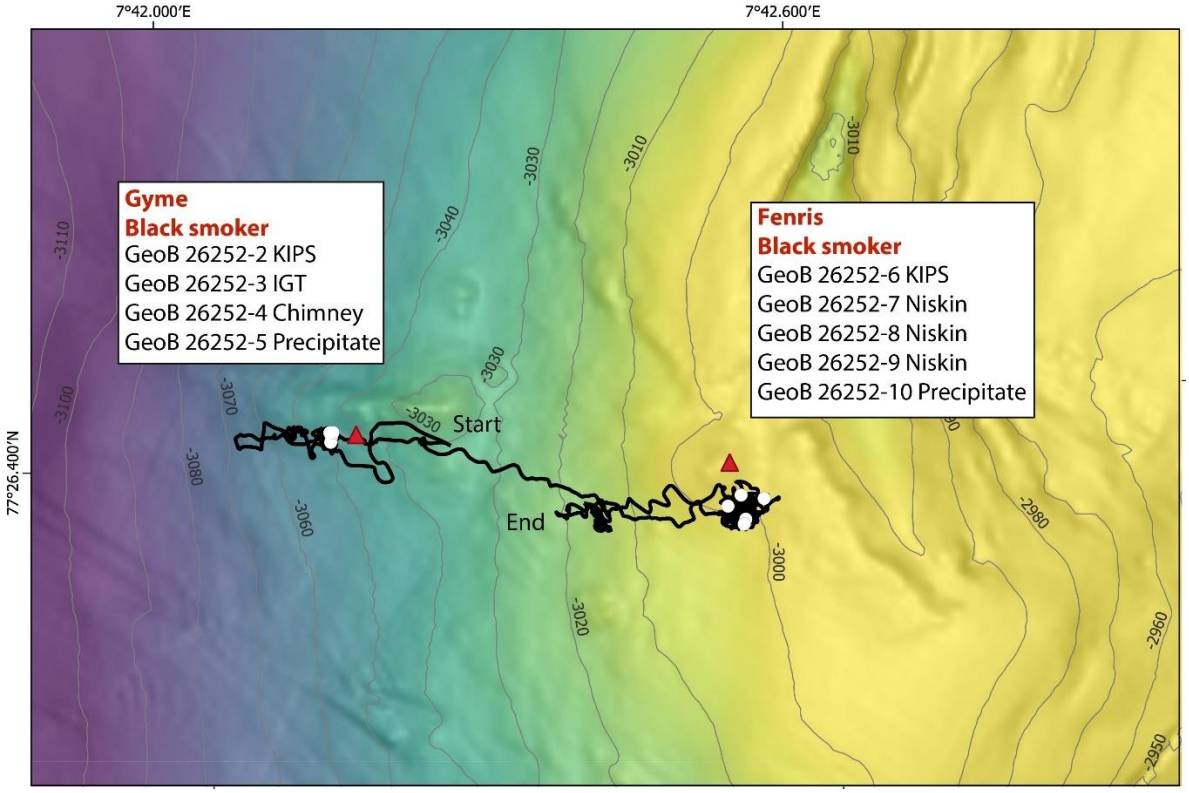

Fig. 5.5.18 Map of ROV Dive 485The ROV’s USBL positioning showed an estimated positive latitudinal deviation of approximately 30 m in relation to the map during most of the dive. The deviation was then shifted southward after the vessel reversed its heading to withstand the strong swell. This shift in the ROV’s USBL positioning is noticeable as an (apparent) U-turn of the ROV track around Fenris during the ship’s maneuver.

Dive 485 of ROV QUEST 4000 targeted Jøtul's two known black smokers, now baptised as Gyme and Fenris by the Norwegian Offshore Directorate. Main objectives were to (1) collect hydrothermal fluids for geochemical analysis using KIPS, IGTs and Niskin bottles, (2) acquire image mosaics of the chimney structures, (3) explore some target structures in the vicinity of Fenris in the remaining dive time. At Gyme, KIPS sampling (A + B) was performed at a fluid exit point near the base of the collapsed chimney registering 287°C. Fluid sampling with IGT7 at the same exit point recorded a maximum temperature of 296°C. At Fenris, KIPS sampling (C + D) was performed at a fluid outlet registering 313°C. IGT sampling was not successful due to equipment failure when fluid temperature was recording 324°C. Three Niskin bottles were closed at 1, 3, and 5 m above the plume exit.

Table 5.5.7 Samples recovered during ROV Dive 485.

GeoB No. 26252-1	Instrument	UTC start	Latitude Longitude	Water Depth (m)	Comment
26252-2	KIPS A + B	08:14	77° 26.415' 07° 42.172'	3020	Black Sm. West, max. T = 287°C
26252-3	IGT-7	08:54	77° 26.414' 07° 42.171'	3021	Black Sm. West, max. T = 296°C
26252-4	Net, white	09:21	77° 26.416' 07° 42.174'	3021	Chimney sample
26252-5	Same Net	09:25	77° 26.416' 07° 42.171'	3021	precipitate
26252-6	KIPS C + D	11:09	77° 26.395' 07° 42.547'	2971	Black Sm. East max. T = 313°C
26252-7	Niskin, green	12:53	77° 26.380' 07° 42.582'	2969	1 m above B.S.
26252-8	Niskin, yellow	12:55	77° 26.376' 07° 42.563'	2967	3 m above B.S.
26252-9	Niskin, white	12:57	77° 26.375' 07° 42.561'	2966	5 m above B.S.
26252-10	MAN	14:32	77° 26.379' 07° 42.547'	2975	Rock precipitate

Dive Description

NOTE: Due to technical error, significant parts of the first six hours of dive were not video recorded, or only recorded with some of the cameras. The first three hours of the pilot screen video are also missing.

ROV QUEST 4000 was deployed at 04:00 UTC on 8 September 2024, reaching the sea floor at 3,000 m depth at 06:29 UTC. We landed about 30 m northeast of the presumed position of the Gyme black smoker, which was originally discovered in 2022 during a research cruise led by the University of Bergen. After a brief search along the sea floor the smoker was located. This initial part of the dive was not video recorded.

Gyme was standing on top of a narrow ridge at 3020 m depth, the surrounding hydrothermal areas covered with bright microbial mats and precipitates. The smoker was approximately 1 meter tall (lack of parallel laser pointers did not enable a precise measurement) and composed of several individual active chimneys growing vertically and exhibiting a porous beehive structure (Fig. 5.5.19). A large part of the chimneys surface, particularly at the base and mid-section, was covered with microbial mats, and a few vent-associated amphipods were also observed. The first activity conducted at this site was a vertical video survey around the vent using the forward-facing cameras, to generate a 3D-photomosaic of the entire structure. A horizontal photomosaic survey

was attempted with the downward-facing Voyis camera system, but without success due to technical malfunction detected during the dive. Next, we maneuvered the ROV to find a suitable position for hydrothermal fluid sampling. In this process, the ROV collided against the smoker causing its collapse down to the base (video accidentally not recorded) and exposing five strong fluid outflow points (Fig. 5.5.20). Two KIPS bottles were filled at one of the exit points reaching a maximum fluid temperature of 287°C. One IGT fluid sample was also taken at the same exit point (IGT7) while recording a maximum temperature of 296°C. The last activity at this site was to collect one of the fallen chimney pieces (Fig. 5.5.21).

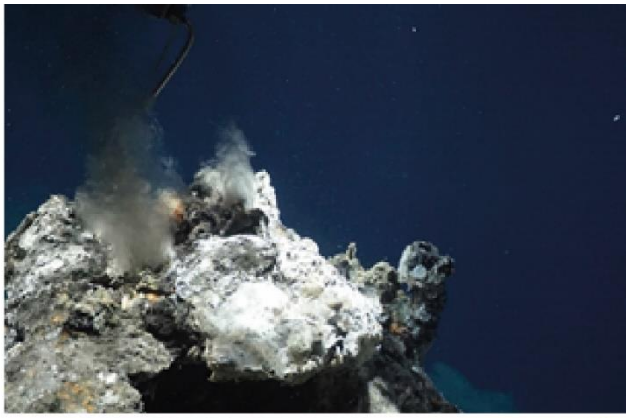

Fig. 5.5.19 (left) Photographic composite of the Gyme black smoker.; **Fig. 5.5.20 (right top):** Base of the smoker after the chimney structure collapsed, showing several active fluid outflow points; **Fig. 5.5.21 (right bottom)** Chimney piece collected from Gyme.

Our next target was the Fenris black smoker, located approximately 120 m east of Gyme. For more precise navigation during the flight towards Fenris we followed a beacon that had been deployed in its vicinity on dive 481. Deploying this beacon proved to be a very good decision, given that the smoker had spontaneously collapsed since our last dive at this site and only the base remained. We picked up the beacon and successfully sampled hydrothermal fluids with KIPS (2 bottles, maximum temperature 313°C). Fluid sampling with the IGT failed due to equipment malfunction during operation, most likely caused by exposure of its battery to very high temperature (maximum fluid temperature recorded before failure was 324°C). Continuing with the dive plan, three Niskin bottles were closed at 1, 3, and 5 m above the hydrothermal plume exit. Before leaving the site, we performed a vertical video survey with the forward-facing cameras to generate a 3D photomosaic of the structure, and picked a fragment of a fallen chimney with the Orion manipulator (Fig. 5.5.23).

The last 45 minutes of the dive were spent exploring a sediment-covered area west of the Fenris hydrothermal mound. We found several small diffuse venting areas inhabited by microbial mats, tube worms and other associated fauna. High-quality close-up imagery was recorded at one of these areas (Fig. 5.5.24). The ROV initiated its ascent back to the surface at 15:26 UTC and was on deck at 18:00 UTC.

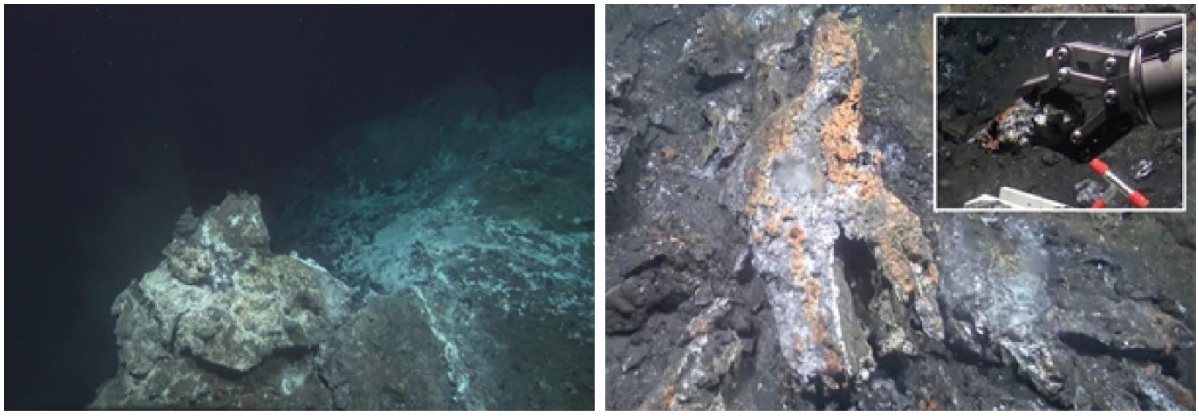

Fig. 5.5.22 (left): Fenris black smoker as it was first sighted on dive 485. Most of the vertical structure documented on dive 481 had spontaneously collapsed. **Fig. 5.5.23 (right)**: Recently collapsed Fenris chimney, from which a small piece was collected with the ROV.

Fig. 5.5.24 Diffuse venting area west of the Fenris mound. Inset: close-up picture of the biological community inhabiting the diffuse venting patch.

ROV Dive 486 (GeoB26269, Station MSM131/69)
Area: Jøtul Field
Date: 13 September 2024
Start bottom: 13:59
End bottom: 18:23
Bottom time: 4hours and 24 minutes (04:24)
Start bottom (Lat/Long/Depth): 77° 26.197' N, 07° 42.193' E, 2989 m

End bottom (Lat/Long/Depth): 77° 26.404' N, 07° 42.143' E, 3016 m

Goal of the dive was sampling of hydrothermal fluids via isobaric-gas tight (IGT) and KIPS samplers and to recover a set of KIPS and Niskin samples at a single vent to trace processes associated with increasing of dilution of vent fluids. The dive started at the Nidhogg vent site where we successfully retrieved one IGT and one KIPS sample. A maximum temperature of 214°C was measured here. This temperature exceeded the one measured during dive 484 by around 60°C. Subsequently the ROV transited to the Fenris vent where another pair of high quality IGT and KIPS samples were recovered. Here similar temperatures (T_{max}= 314°C) were measured as compared to dive 485. During the last part of the dive we revisited the Gyme vent to sample fluids via KIPS and to recover a profile of rising plume samples with the three Niskin bottles. All operations were conducted successfully.

Table 5.5.8 Samples recovered during ROV Dive 486

GeoB No. 26269-1	Instrument	UTC start	Latitude Longitude	Water Depth (m)	Comment
26269-2	IGT	14:03	77° 26.195' 07° 42.199'	2992	IGT 6, max. T = 214°C Nidhogg
26269-3	KIPS	14:26	77° 26.192' 07° 42.192'	2992	Kips A, max. T = 210°C Nidhogg
26269-4	IGT	15:58	77° 26.384' 07° 42.514'	2972	IGT 7, max. T =313°C Fenris
26269-5	KIPS	16:12	77° 26.385' 07° 42.518'	2972	KIPS B, max. T = 309°C Fenris
26269-6	KIPS	17:48	77° 26.406' 07° 42.151'	3021	KIPS C, max. T = 301°C Gyme
26269-7	Niskin	18:05	77° 26.404' 07° 42.142'	3020	Niskin 3, green, 1m above Gyme
26269-8	Niskin	18:18	77° 26.406' 07° 42.148'	3018	Niskin 1, white, 3m above Gyme
26269-9	Niskin	18:23	77° 26.404' 07° 42.145'	3015	Niskin 2, yellow, 5 m above Gyme

Dive Description

ROV QUEST dive 486 was limited by a narrow weather window and was hence dedicated to close gaps in our fluid sample collection. The prioritized target was sampling of IGT fluid samples from Nidhogg and Fenris, which failed during dives 484 and 485, respectively, due to technical reasons. Another target was to collect KIPS and Niskin samples and specifically to recover another vent fluid in conjunction with a profile of the rising plume over the first 5m of the orifice. ROV QUEST spent 4 and a half hours at the ocean floor and successfully investigated the vents Nidhogg, Fenris and Gyme.

The ROV landed right at the foot of the eastern flank of the structure called Nidhogg and a discrete patch of white microbial mats was quickly recognized. In the center of the white patch an orifice that quiet vigorously, emitted clear vent fluids was identified as the exact same orifice that was sampled during dive 484. The orifice was sampled with IGT6 and KIPS A and while, in the prior dive it was hard to enter the orifice with the samplers snorkel, this time the sampling worked effortless (Fig. 5.5.26). The maximum temperature measured, which equals the sample temperature, was 214°C and is around 60°C higher than the temperature measurement from dive

484 suggested. This measurement shows that fluids at Nidhogg are hotter and less diluted than expected before.

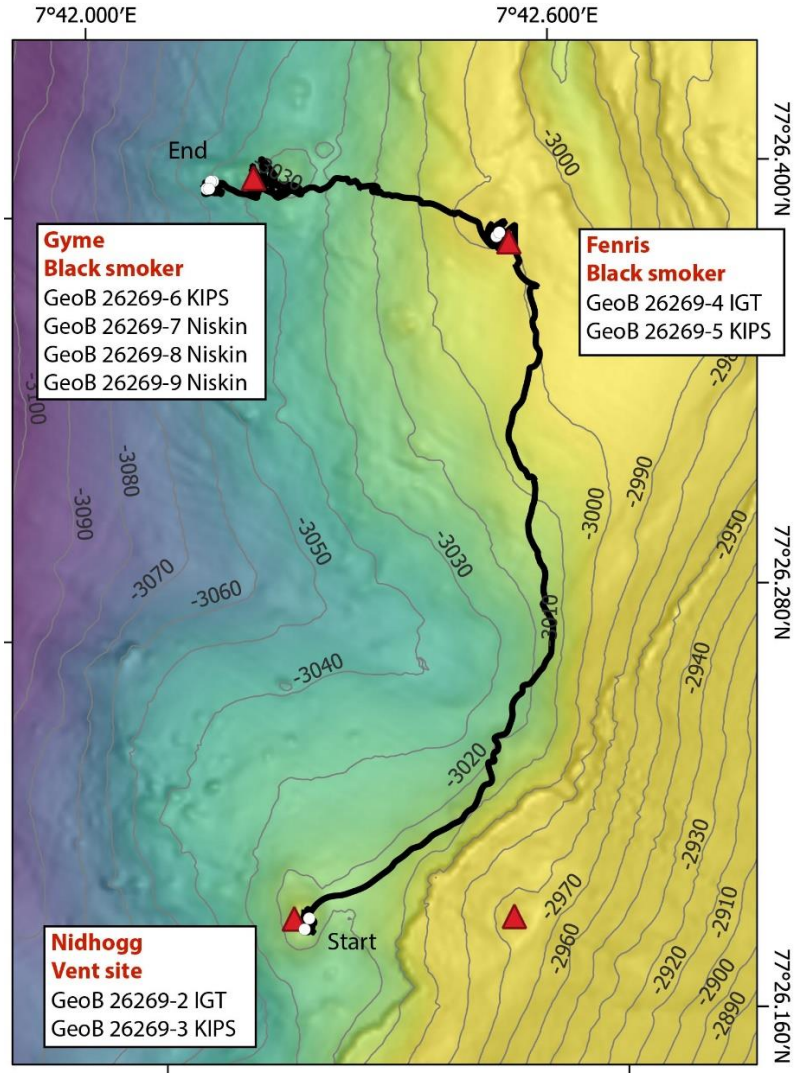

Fig. 5.5.25 Map of ROV Dive 486. From south to north the three studied vents are shown: Nidhogg, Fenris, Gyme. Retrieved fluid samples for each vent are denoted in the inset.

After the sampling ROV QUEST transited to Fenris and stayed near the ground to be able to make sea floor observations. First we transited around 100m in north-east direction and then turned northwards to roughly follow the -3,200 m elevation isoline. During the transit, the ocean floor consisted mainly of undisturbed sediments, but just before reaching the southern flank of the mound that hosts Fenris, a few basaltic pillows cropped out of these sediments. Fenris was located on the crest on the top of the mount (Fig. 5.5.25) and samples IGT7 (Fig. 5.5.26) and KIPS-B were retrieved from this vigorously venting black smoker. The temperature of Fenris was measured as 314°C (Fig. 5.5.27) similar to the measurements of dive 485 (KIPS:313°C and IGT 324°C). After the sampling the ROV headed to Gyme.

During the transit in to Gyme, the sea floor was more rubbly and the sediment are here presumably intermingled with sulfide debris. Multiple patches of white precipitates/bacterial mats were observed that appeared to be aligned in lineaments. No active outflow was observed but such an outflow cannot be excluded. However, the patches suggest at least diffuse hydrothermal activity in the past. When approaching WP Gyme could not be located.

Fig. 5.5.26 IGT sampling of clear vent fluids at Nidhogg. The area is covered in densely populated bacterial mats.

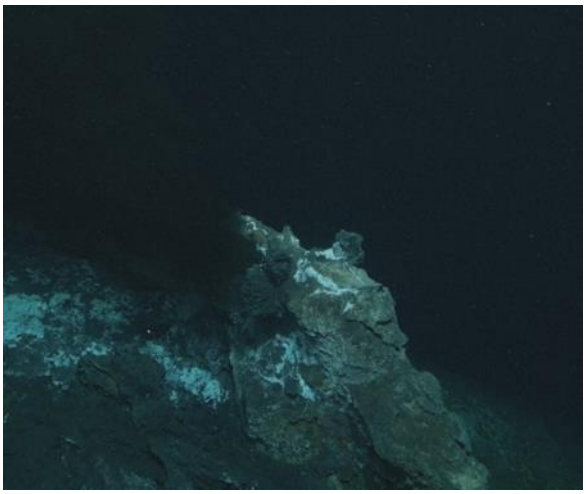

Fig. 5.5.27 View on the black smoker Fenris. In contrast to the Nidhogg site, the hydrothermal fluids here form a particle-laden plume.

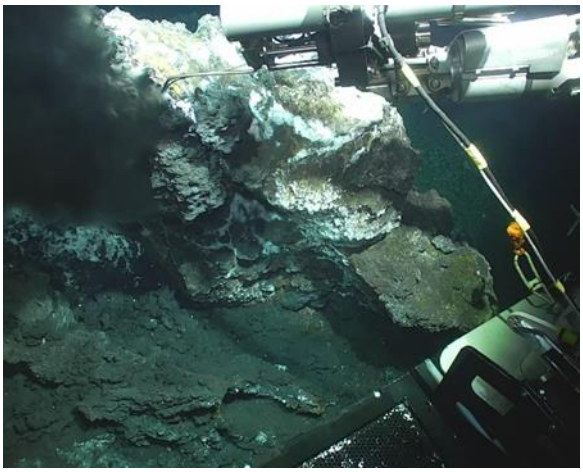

Fig.5.5.28 IGT sampling of black-smoker fluids at Fenris. The beehive structures in the vicinity to the samplers snorkel have likely grown since the last sampling.

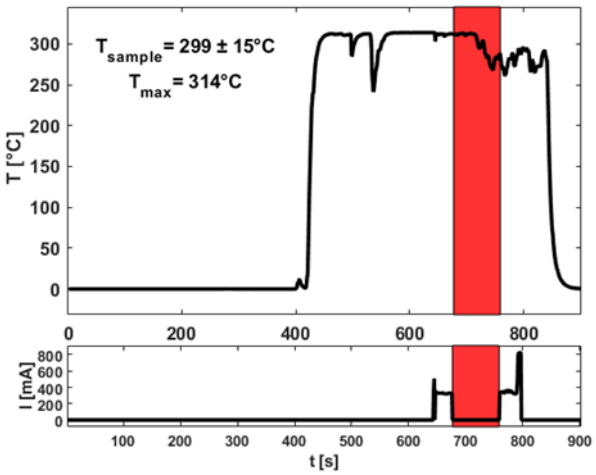

Fig. 5.5.29 Temperature log during IGT sampling at Fenris. The average temperature during sample intake is 299°C. Maximum measured temperature was 314°C.

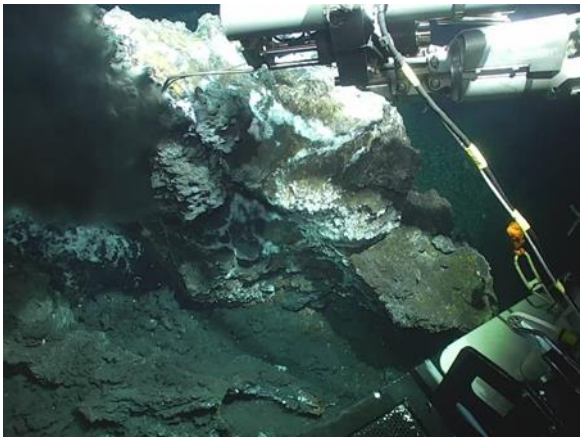

Fig.5.5.30 KIPS sampling at Gyme vent. In contrast to Fenris visible particle formation due to seawater entrainment is less pronounced.

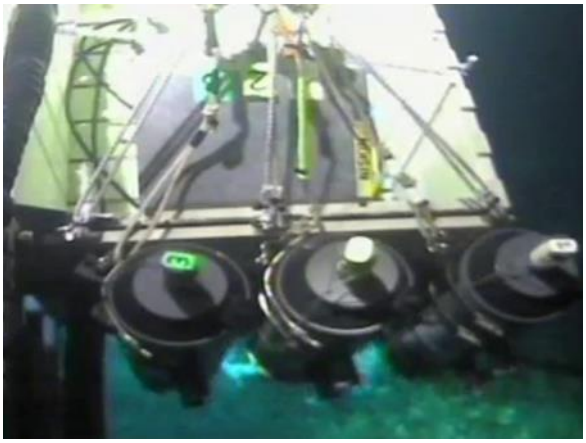

Fig. 5.5.31 View on the Gyme vent site through the toolbox camera. Niskin bottles were just fired, upon which the dive was terminated.

The ROV circled the structure with hydrothermal activity lacking. After the decision to continue to explore west of the waypoint (red triangle) Gyme was located around 40m west to the waypoint. The vent was sampled via the KIPS sampling system and sample KIPS-C was recovered (Fig. 5.5.30). The maximum temperature was detected as 301°C. Subsequently all three Niskin bottles (Niskin 1-3) were fired to sample a profile of the rising buoyant fluid emitted by Gyme (Fig.5.5.31). Due to the unfavorable weather conditions, no exploration of the surrounding area could follow and the ROV was prepared to ascend.

ROV Dive 487 (GeoB26272-1, Station MSM131/72)
Area: Jøtul Field
Date: 15. September 2024
Start bottom: 11:34
End bottom: 17:03
Bottom time: 05:29
Start bottom (Lat/Long/Depth): 77° 26.389’ N, 07° 42.515’ E, 2976 m
End bottom (Lat/Long/Depth): 77° 26.478’ N, 07° 42.712’ E, 2970 m

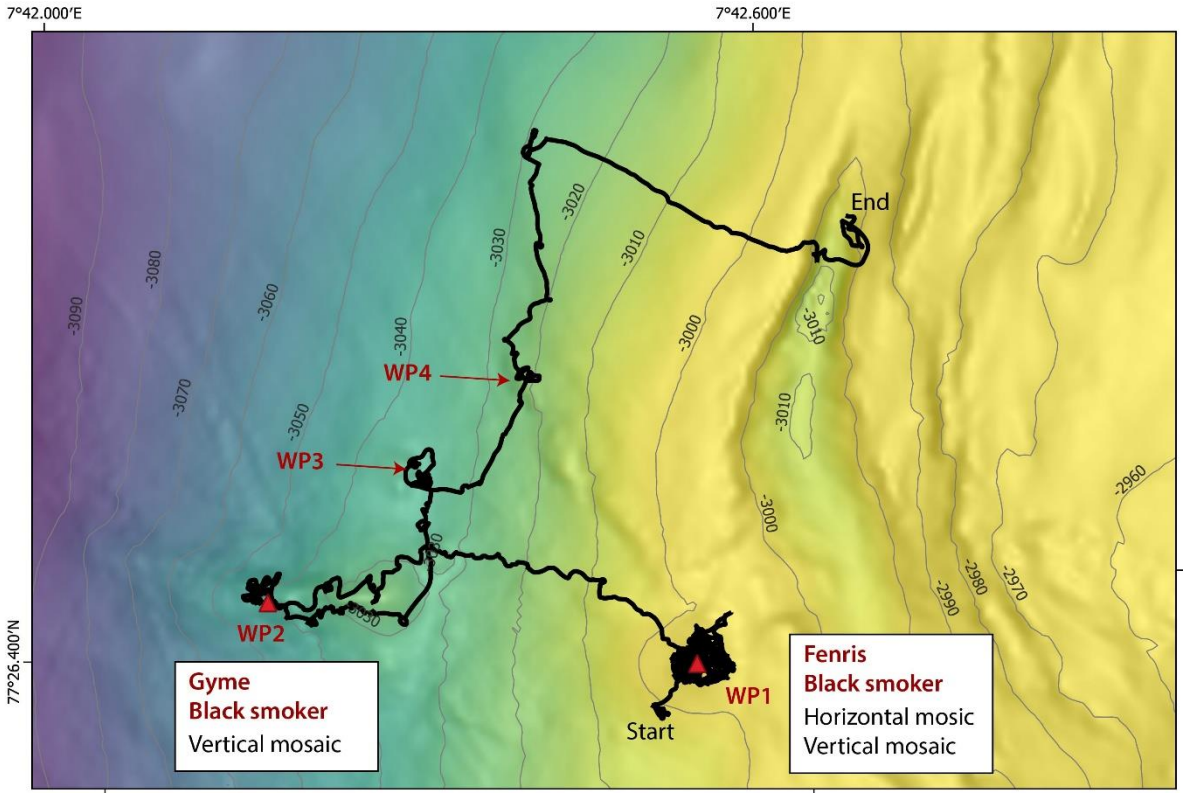

Fig. 5.5.32 Map of ROV Dive 487. USBL track line has been shifted to match the known morphological structures visited and was visually observed during the dive.

The two black smokers (Fenris and Gyme) have been revisited after two days and changes at the vent outlets were documented by high-resolution video footage. New precipitates in cm to decimeter size were already growing both at the lower part of the outlet as well as on top of the Fenris. A horizontal mosaic was recorded from the entire mound structure. Black smoker Gyme

showed an even larger growth of the chimney that was still standing after the last visit. Exploration during the last part of the dive revealed an extinct hydrothermal mound north of Gyme with some signs of minor fluid release in its center.

Dive Description

ROV dive 487 started at black smoker Fenris (Fig. 5.5.32), which was found only a view minutes after reaching the sea floor at 11:41 UTC. The outflow area of the smoker showed some newly precipitated parts (Fig. 5.5.32) that should be documented in more detail after a vertical mosaic has been recorded. The vertical mosaic was recorded with the Zeus high-resolution in 6K. It took about 16 minutes to finish several lines moving up and down around the chimney. Visual inspection of the outflow area from different sides and using the laser points for scaling revealed that some new precipitates were already grown since our last visit two days ago. A small new chimney evolved on top of the structure, of about 5 cm in size. And at the lower part of the outflow area, dark appearing new precipitates in decimeter scale appear to be new. A horizontal mosaic was then recorded to get a better overview of the entire mound using the downward looking Voyis camera. The altitude had to be increased to 4 m due to the steep terrain. The first 11 lines were orientated SE-NW with a line spacing of 1 m and length between 8 to 13 m. Due to smoke and increasing temperatures when coming closer to the smoker, the line orientation was changed to SW-NE almost perpendicular and covering the mound area east of the smoker. The last two lines were running west and just above the smoker, however, after finishing the last crossing, the pilots noticed that the Voyis camera stopped working and could not be reconnected. These final two lines were not recorded anymore with the Voyis camera. The program at Fenris was then finished at 14:20 UTC.

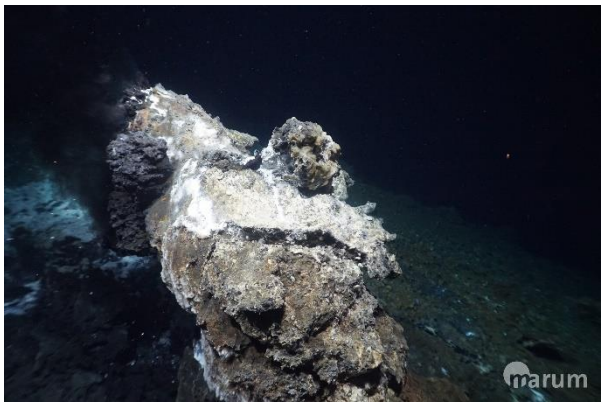

Fig. 5.5.33 Black smoker Fenris (WP 1)

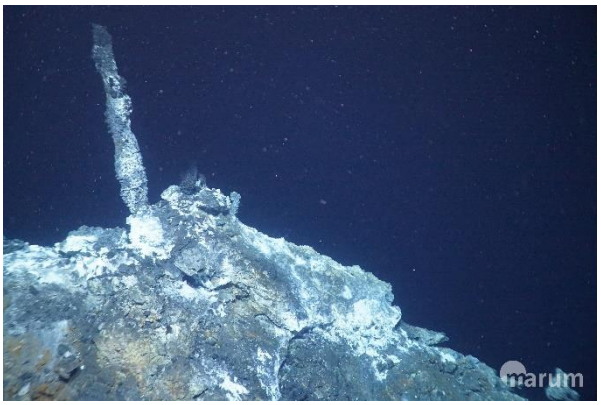

Fig. 5.5.34 Black smoker Gyme (WP2)

The next target of dive 489 was black smoker Gyme, which was reached at 14:50 UTC. A first inspection surrounding slowly the smoker was very useful to document changes of the chimney structure since our last visit two days ago (Fig. 5.5.34). The chimney was still in place and seems to have even grown several decimeters. The whitish appearing cover also increased since the last visit. A vertical mosaic was then recorded using the Zeus 6K high resolution camera. Nine lines up and down surrounding the smoker were performed. Finalization of the mosaic took about 19 minutes. The smoker location was left at 15:35 UTC.

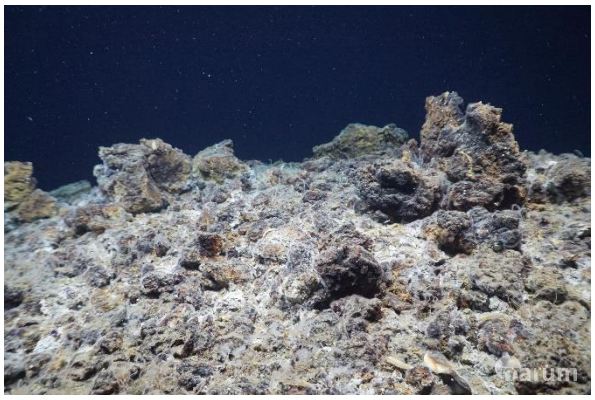

Fig. 5.5.35 Central part of the mound structure inspected at WP3.

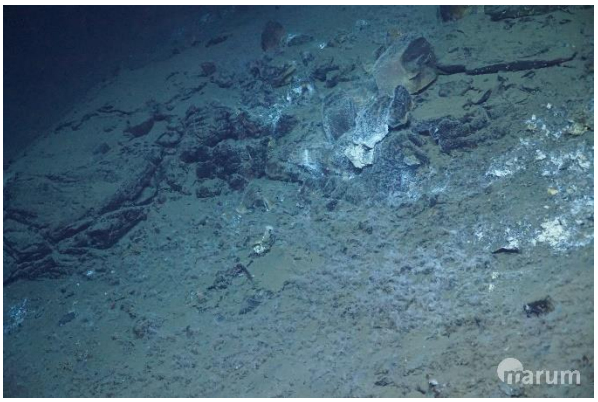

Fig. 5.5.36 Whitish staining of magmatic rocks indicate fluid venting activity seen close to WP4.

As a discussion about a potential second smoker at this ridge evolved since the last dive, it was decided to have a short inspection along this ridge in eastern direction until reaching the top, where an extinct hydrothermal site with still intact small chimneys was found. This area has been seen already during earlier dives and was not inspected in more detail. At 16:00 UTC, the ROV was moved northward towards WP3, a bathymetric mound structure visible in the high-resolution AUV map. The mound was found and inspected visually for potential hydrothermal activity. The mound appears to consist of hydrothermal material and still showed some minor signs of activity in its center (Fig. 5.5.35). Zooming in with the cameras documented the abundant organisms colonizing this area. Before leaving this site, the mound was encircled to ensure not having overlooked a site of hydrothermal activity. But the mound seems to be almost extinct, with a remaining minor activity only in its center.

At 16:20 UTC the ROV headed towards WP4, which is another morphological structure visible in the high-resolution AUV map, but in contrast to WP3 more an elongated ridge structure than a circular mound. It was reached 16:30 UTC and found it to be of magmatic material, an outcropping wall of pillow lava. Some indications for fluid venting activity could be seen along that ridge (Fig. 5.5.36). The remaining time of the dive was used for exploration of an unknown area to the North. In that part, we observed a smooth and sediment covered sea floor. After about 100 m without any change, it was decided to change course to SE, to reach the depression structure that was already known to show pillow lava. This was reached and confirmed before ending the dive.

ROV Dive 488 (GeoB26274, Station MSM131/74)
Area: Jøtul hydrothermal field
Date: 16 September 2024
Start bottom: 08:55
End bottom: 16:26
Bottom time: 07:31
Start bottom (Lat/Long/Depth): 77° 26.351' N, 07° 42.379' E, 2993 m
End bottom (Lat/Long/Depth): 77° 26.410' N, 07° 43.219' E, 2924 m
The dive from west to east began in a morphologically striking area south of the Fenris Smoker, crossed the small rift area in the South and explored a seep area in 2,935 m water depth. A photo

mosaic of 25 m x 25 m recorded the different habitats of the seepage area. The dive ended in the east at a rock outcrop.

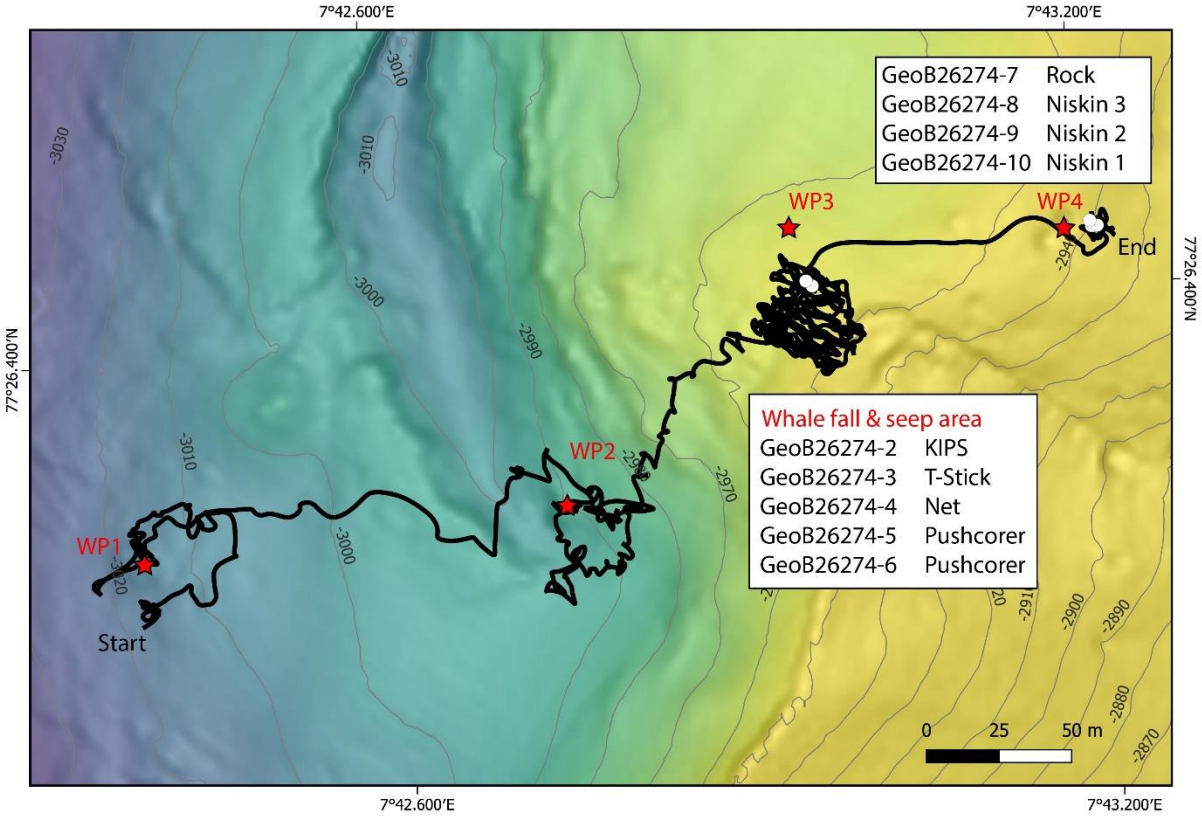

Fig. 5.5.37 Map of ROV Dive 488 track and sample locations.

Table 5.5.9 Samples recovered during ROV Dive 488

GeoB No	Instrument	UTC start	Latitude Longitude	Water Depth (m)	Comment
26274-02	KIPS	14:59	77° 26.404' 77° 26.404'	2935	KIPS-A, - 0.7°C
26274-03	T-stick	15:27	77° 26.405' 07° 42.964'	2935	Vent area
26274-04	Net	15:31	77° 26.404' 07° 42.969'	2935	Vent area
26274-05	Push core	15:36	77° 26.405' 07° 42.964'	2935	Push core 12, center
26274-06	Push core	15:36	77° 26.405' 07° 42.964'	2935	Push core 11, rim
26274-07	MAN	16:15	77° 26.411' 07° 43.210'	2916	Piece of rock
26274-08	Niskin	16:10	77° 26.411' 07° 43.212'	2924	1m above sf green No 3
26274-09	Niskin	16:12	77° 26.411' 07° 43.215'	2919	5 m above, yellow No 2
26274-10	Niskin	16:14	77° 26.412' 07° 43.209'	2914	10 m above, white No 1

Dive Description

The dive started about 80 m southwest of the Fenris smoker, where a striking morphological elevation exists (Fig. 5.5.37). Individual areas with hydrothermal rocks can be found there and these former precipitates are usually marked by bright areas in which microbes very probably exist, which indicate the existence of diffuse venting. On the way east, hemipelagic-covered deep sea

floor is encountered. In the vicinity of the small rift, magmatic rocks are encountered, some of which have flowed out as pillows or some of which have been broken down into small pieces of rock along cooling cracks. Waypoint 2 (star in the middle of the map track Fig. 5.5.37) should be on a small elevation, which an attempt was made to find during the dive. Due to discrepancies between the map and the underwater navigation, a circle of 30-40 m was traveled with ROV QUEST.

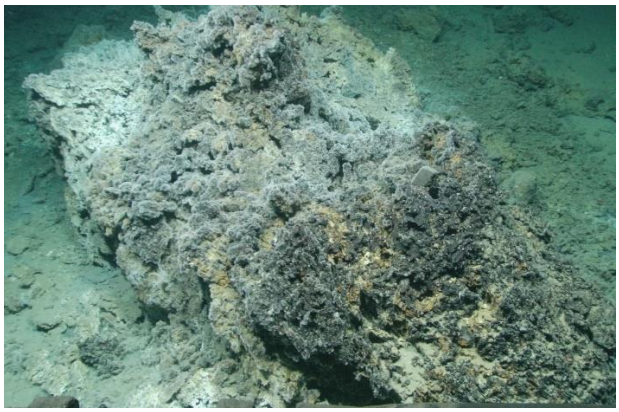

Fig. 5.5.38 Hydrothermal rocks, in some parts covered by microbial organic material.

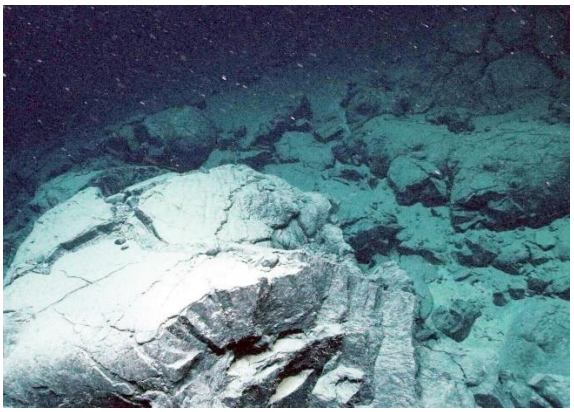

Fig. 5.5.39 Pillow basalt on the sea floor imaged close to the small rift structure.

Basalts are also found in parts of the eastern rift shoulder (Fig. 5.5.39), which changed into deep-sea sediments after 10:46 (UTC) and patterns of seep habitats appear. At 10:57, remains of what are probably whale bones are identified on the bottom, which are also partly associated with bacterial mats. Since various habitats with clear seep areas occur in the region, it was decided to fly a larger photo mosaic of 25 x 25 m, which was taken at a height of 2.5 m with the Voyis camera (from 11:43 - 14:02 UTC, Fig. 5.5.37). The distance between the lines flown in a NW-SE direction was 1m and 2 transverse lines were flown at the end.

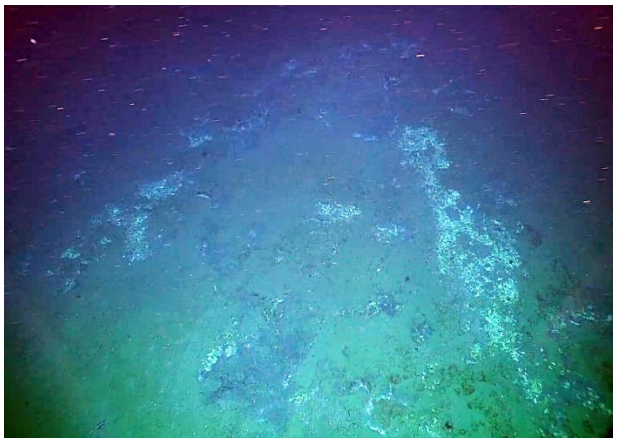

Fig. 5.5.40 Overview picture of the seepage area showing different habitats

Fig. 5.5.41 Close-up from the surface of the area showing a crumbly structure and a tubeworm.

Afterwards, we placed ROV QUEST on the sea floor to take a closer look at the habitat with the crumbly surface structure with the Zeus camera (Fig. 5.5.40). Numerous small animals, such as amphipods and snails and tubeworms (Fig. 5.5.241) could be observed. At about 14:28 UTC, a slight shimmer was observed, which led to a sample being taken with the KIPS sampler (Tab.

5.5.9). However, the bottom water temperature of -0.7°C showed no temperature increase in front of a supposed outflow opening. The methane content measured afterwards in the sampler unfortunately showed no increase either. Sampling was completed with a T-stick measurement (Fig. 5.5.42), a net (Tab. 5.5.9) and two push cores (Fig. 5.5.43).

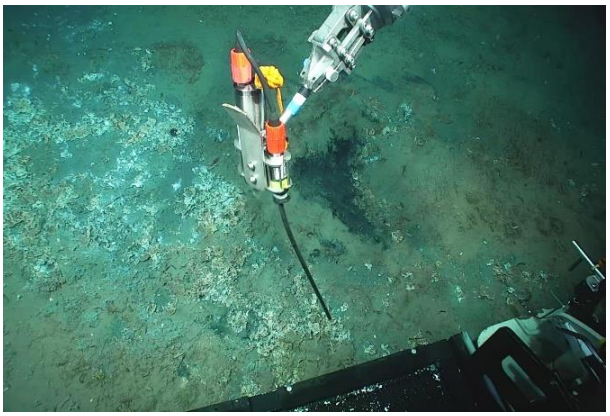

Fig. 5.5.42 T-stick measurement in the seep area.

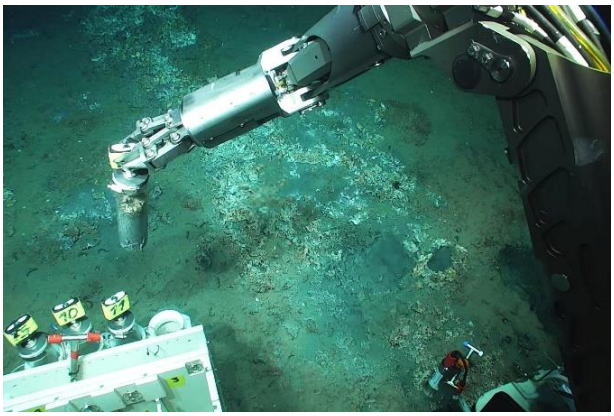

Fig. 5.5.43 Push coring in the same area.

The final part of the dive led about 100 m to the East to waypoint 4, which also represents a raised area of the sea floor on the map. An outcrop of solid rock was found there, although it was not pillow basalt. A relatively large piece of rock was collected, but it was too heavy for the vehicle to lift, so it was unloaded and a smaller rock sample (Tab. 5.5.9) was collected. On surfacing, the 3 Niskin bottles were closed at 1 m, 5 m and 10 m from the sea floor in order to determine near-bottom methane levels. The dive ended at 16:26 UTC.

ROV Dive 489 (GeoB26280, Station MSM131/80)

Area:	Oceanic Core complex east of Jøtul hydrothermal field
Date:	18 September 2024
Start bottom:	10:33
End bottom:	17:24
Bottom time:	06:51
Start bottom (Lat/Long/Depth):	77° 26.197' N, 07° 42.490' E, 2950 m
End bottom (Lat/Long/Depth):	77° 26.048' N, 07° 43.815' E, 2552 m

Dive 489 (Fig. 5.5.44) was designed to re-visit the Yggdrasil structure, and to investigate a shallowing-up profile along the eastern boundary fault of the rift graben. The dive successfully made IGT-samples from the fluids emerging below the pronounced flange-structures at Yggdrasil. High-resolution images of the "mirror-effect" made by the hot fluids below the flanges were taken. Moving away from the Yggdrasil vent site a base-line water-sample with Niskin bottle was acquired. The shallowing-up profile along the east boundary was designed to overlap and calibrate with Dive #462 made during MSM109 in 2022. This was successful and observations from two MSM109 were confirmed through Dive 489. As the dive continued east and shallowing upwards several rock-samples were acquired (Fig. 5.5.44 and Tab. 5.5.10) to make systematic analysis of possible changes in composition and origin of the rocks with the purpose of possibly defining the presence of a core complex along the delimitating fault to the East.

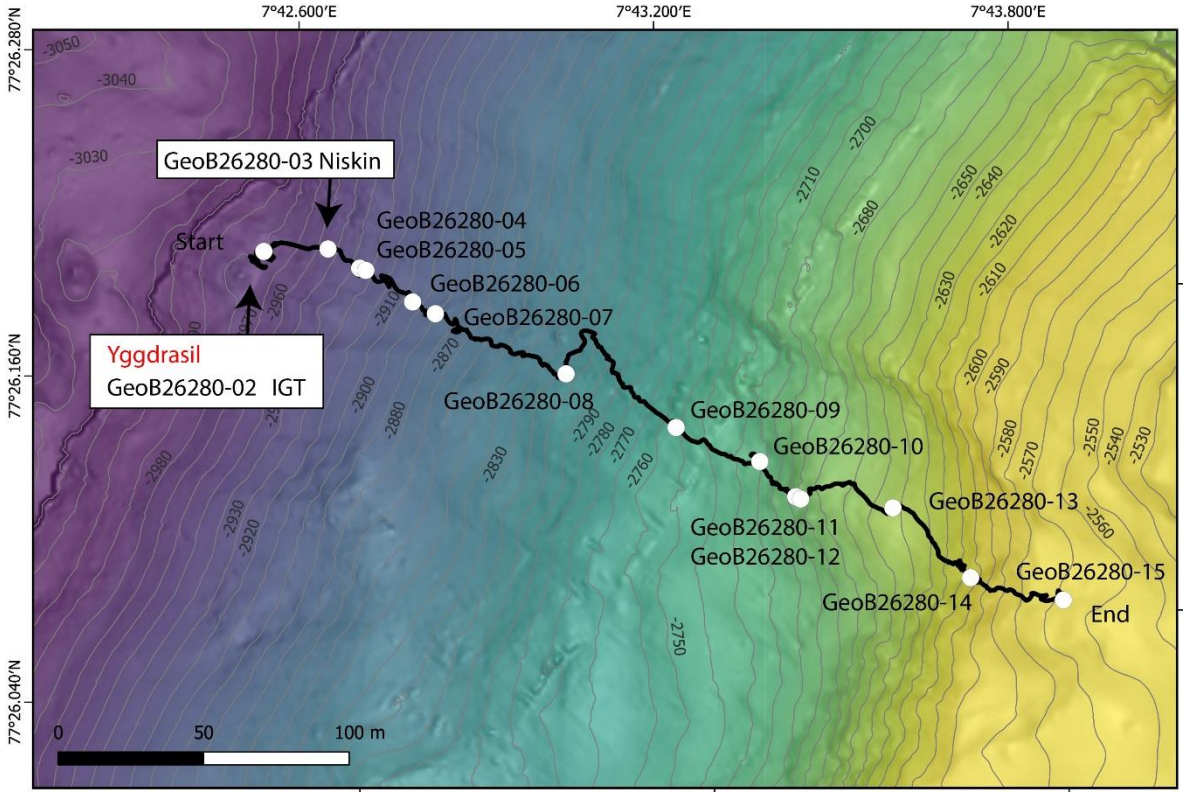

Fig. 5.5.44 Map of ROV Dive 489. Map showing navigation tracks of ROV QUEST Dive 489 and the bathymetry of the Yggdrasil site and the eastern boundary (fault) of the Jøtul field area. Samples are annotated and shown as white dots

Observing the seabed along the profile illustrated how the sedimentation changed from fine grained hemipelagic material to rocks, boulders, possible gravity deposits and large outcrops. The sedimentation mirrored the changing gradient along the profile, with the largest rocks and most significant outcrops without hemipelagic material along the steepest areas. The biological characteristics also changed; from bacterial mats and tubeworms in the deeper and fine-grained sedimentary areas, to large and well-developed different types of sponges in the shallower and steeper areas dominated by boulders and rocky outcrops.

Dive Description

Dive 489 started in the morning 18 September 2024 and the ROV QUEST 4000 reached the sea floor at 10:33 UTC at the Yggdrasil vent site (Waypoint – WP – 1). Circled around the structure to find a suitable flange with hot-water outflow to sample the IGT and decided on a lower large flange (approximately 2 m horizontally). Acquired high resolution (4K and 6K) photos of nice "mirror" below flange and sampled flowing waters with a temperature of 280°C (Fig. 5.5.45A). When backing off and approximately 12 m away from the vent site a Niskin bottle was sampled and closed for background/base-line water-composition. Started moving towards east-southeast at 11:40 UTC and gradually moved to shallower areas along the planned profile. Sediments along the seabed changed from fine-grained assumed hemipelagic material to very unsorted possible gravity driven deposits. First rock sample (GeoB No 26280-04) were taken from this. Continuing patches of white precipitates and tubeworms were observed between or below possible gravity-deposits.

Table 5.5.10 Samples recovered during ROV Dive 489

GeoB No 26280-1	Instrument	UTC start	Latitude Longitude	Water Depth (m)	Comment
26280-02	IGT 6	11:26	77° 26.199' 07° 42.510'	2953	Yggdrasil flanch 280°C
26280-03	Niskin	11:41	77° 26.198' 07° 42.619'	2941	Green, no 3
26280-04	MAN	12:00	77° 26.190' 07° 42.670'	2924	rock
26280-05	MAN	12:12	77° 26.189' 07° 42.680'	2923	rock
26280-06	MAN	12:34	77° 26.176' 07° 42.755'	2893	rock
26280-07	MAN	12:59	77° 26.171' 07° 42.792'	2878	rock
26280-08	MAN	13:39	77° 26.145' 07° 43.005'	2805	rock
26280-09	MAN	14:19	77° 26.122' 07° 43.184'	2747	rock
26280-10	MAN	14:43	77° 26.107' 07° 43.321'	2709	rock
26280-11	MAN	15:10	77° 26.093' 07° 43.377'	2689	rock
26280-12	MAN	15:43	77° 26.086' 07° 43.540'	2683	rock
26280-13	MAN	16:23	77° 26.092' 07° 43.385'	2680	Two rocks
26280-14	MAN	16:47	77° 26.058' 07° 43.662'	2604	rock
26280-15	MAN	17:16	77° 26.047' 07° 43.816'	2552	Two rocks

A rock-sample was taken (GeoB No 26280-05, Figures 2B, C below). When moving onwards to WP2 black blocky terrain possibly downfall occurring from areas further up occurred (Fig. 5.5.45D); sample GeoB No 26280-08 was collected, and at 13:27 UTC WP2 was reached – same area that was mapped and investigated during MSM109 (Dive 462). Larger dark blocks, some partly rounded others more sharp-edged and with increasing sponge communities became more frequent as moving upwards (Fig. 5.5.45E) Samples GeoB No 26280-09 and 10 was sampled from these environments. At 15:03 UTC WP3 was reached and rock sample GeoB No 26280-11 was taken. When continuing towards WP4 increased gravels were observed at seabed, and at 15:28 a very steep slope dominated by rocky unsorted material, and frequent sponges, was encountered (Fig. 5.5.45F). Sample GeoB No 26280-12 collected. Seabed mainly dominated by black rocks with numerous sponges when continuing towards WP4, sampled GeoB No 26280-13 and 14 as moving upwards. Parts of the outcrops looks slightly lighter in color than the very dark and otherwise prevailing rocks, and possible fractured (layering) might be indicated. The gradient along the slope decreased and WP4 was reached at 17:20 UTC. An elongated small “ridge” of darker rocks was observed in an otherwise light fine-grained dominated area of the seabed. The rockier, possible ridge area, continued upwards to the east-southeast, uncertain if it was in situ or represented gravity-driven deposits. Sample GeoB No 26280-15 was acquired. Dive ended 17:24 UTC.

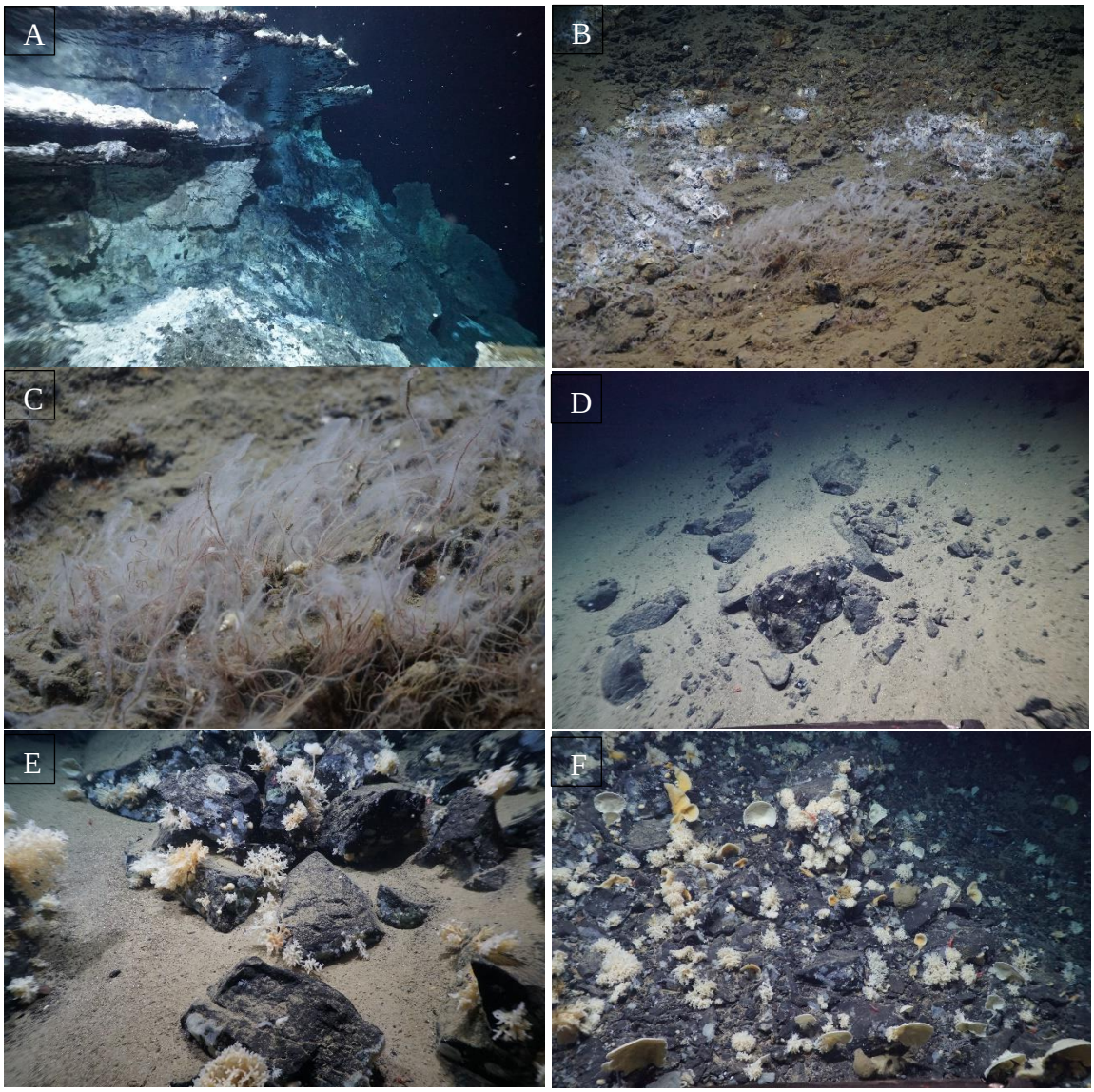

Fig. 5.5.45 Observations during the dive. A) Flange-structure with "mirror" below at Yggdrasil; B) and C) area with white precipitation and tubeworms; D) Black partly rounded blocks possibly originating from shallower areas, E) Gravity driven less rounded black rocks with sponges; F) Black rocky material at steep slope between WP3 and WP4.

ROV Dive 490 (GeoB26282, Station MSM131/82)
Area: Jøtul field, Gyme and Fenris Smoker and seepage area
Date: 19 September 2024
Start bottom: 08:57
End bottom: 14:25
Bottom time: 05:28
Start bottom (Lat/Long/Depth): 77° 26.414' N, 07° 42.274' E, 3002 m
End bottom (Lat/Long/Depth): 77° 26.453' N, 07° 43.005' E, 2937 m

The most important result of the dive is the successful sampling of four different habitats in the seep area east of the small rift in the Jøtul hydrothermal field using pushcores and a temperature

gradient measurement in each case. Different methane contents and profiles as well as different temperature gradients show the dynamics of the seep area.

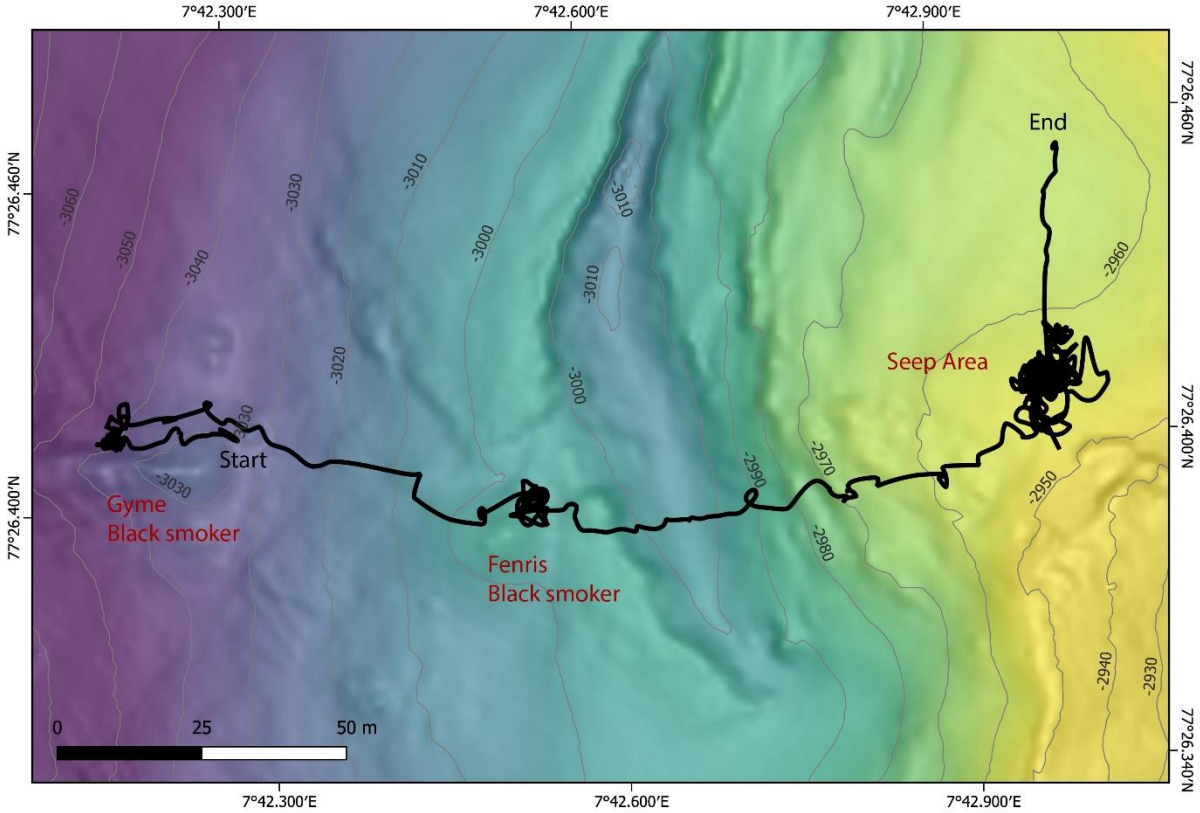

Fig. 5.5.46 Map of ROV Dive 490

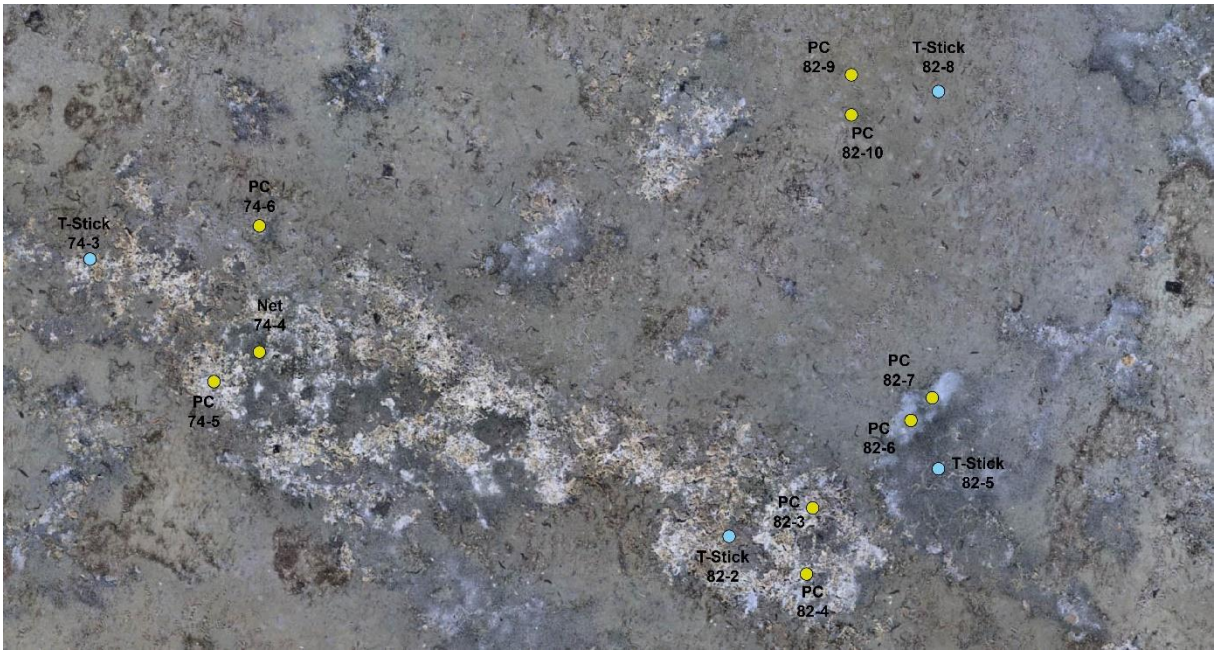

Fig. 5.5.47 Part of the photo mosaic from the seepage area with locations of push cores and T-stick measurements in the different habitat patches.

Dive Description

The ROV reached the sea floor on the small hydrothermal ridge, with an offset of about 10-15 m to the North from the map (Fig. 5.5.47). By searching along the ridge to the West, the Gyme smoker was discovered after just 7 minutes and circled for photo and video documentation without the vehicle being put down. The isolated chimney has grown since the last visit and has become wider in the upper area. Its outflow is diverse and has led to the formation of a beehive structure. West of the chimney are 3-5 outflow openings from which massive amounts of fluid flow out. The dive then continued west along the ridge over numerous diffuse fluid outlets and hydrothermal rocks on the bottom. After about 70 m we reached the Fenris Smoker, which, like last time, is known for its large, slanted outflow opening. However, precipitate thickenings are already visible on the edge, which will probably lead to a vertical precipitate build-up in the foreseeable future, as seen at the beginning of the trip in dive 481.

Table 5.5.11 Samples recovered during ROV Dive 490.

GeoB No 26282-1	Instrument	UTC start	Latitude Longitude	Water Depth (m)	Comment
26282-2	T-stick	12:18	77°26.40'N 07°42.95'E	2954	
26282-3	Push core	12:23	77°26.40'N 07°42.95'E	2954	R1, white
26282-4	Push core	12:27	77°26.40'N 07°42.95'E	2954	9, yellow
26282-5	T-stick	12:45	77°26.40'N 07°42.95'E	2954	
26282-6	Push core	12:49	77°26.40'N 07°42.95'E	2954	R2, white
26282-7	Push core	12:57	77°26.40'N 07°42.95'E	2954	10, yellow
26282-8	T-stick	13:14	77°26.40'N 07°42.95'E	2954	
26282-9	Push core	13:16	77°26.40'N 07°42.95'E	2954	R3, white
26282-10	Push core	13:18	77°26.40'N 07°42.95'E	2954	5, yellow
26282-11	T-stick	13:31	77°26.40'N 07°42.95'E	2954	
26282-12	Push core	13:34	77°26.40'N 07°42.95'E	2954	R4, white
26282-13	Push core	13:36	77°26.40'N 07°42.95'E	2954	8, yellow
26282-14	Net	14:15	77°26.40'N 07°42.95'E	2954	Surface sample

The further dive to the East led over the rift area again and at 10:24 reached an area with layered lava, which in some places had broken down into individual blocks. Bacterial mats can also be found in this layered lava at times. This is followed by the sediment area, where 488 clear seep signals were found during dive 488 and a large-scale photo mosaic was carried out. In the large mosaic, we chose an area with the largest seep and carried out another higher-resolution photo mosaic at a distance of 1 m and a size of 6 x 6 m. 13 lines at a distance of half a meter were flown 6 m long and provided with 2 cross lines. Then the sampling program of 4 different habitats began (Figs. 5.5.48 to 5.5.51), each with 2 push cores and a T-stick measurement. First the temperature lance was placed and after the push cores were taken, the T-stick was recovered again. This

ensured that the temperature lance had a service life of at least 10 minutes to allow it to adjust to the ambient temperature over time after heating up due to friction during penetration.

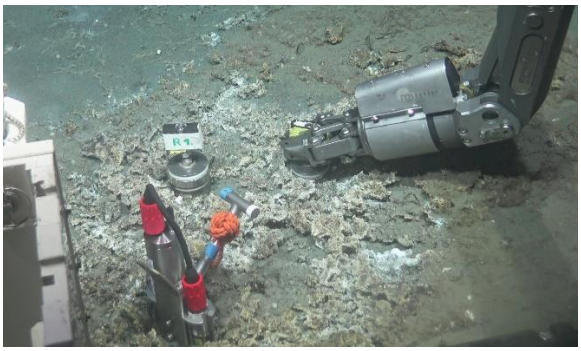

Fig. 5.5.48 Push core set and T-stick in the crumbly habitat, with possibly carbonates.

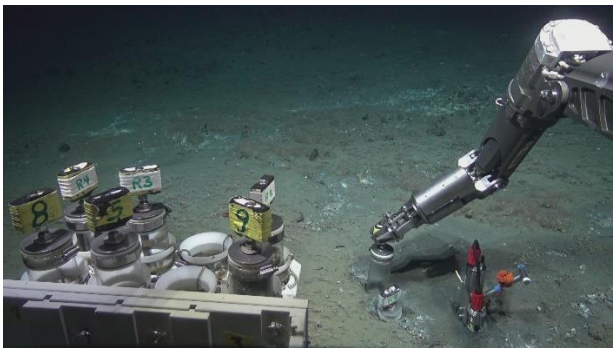

Fig. 5.5.49 Push core set and T-stick in area of bacterial mats on the surface

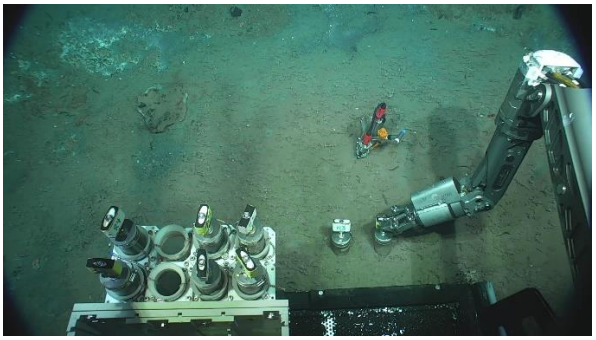

Fig. 5.5.50 Push core set and T-stick in the area of scattered tubeworms.

Fig. 5.5.51 Push core set and T-stick of homogenous sea floor area.

5.5.3 Optical Seabed Surveys and Photo-Mosaicking

(M. Römer, Y. Marcon)

During the MSM131 cruise, a comprehensive program of seabed mosaicking surveys was executed, encompassing a total of seven dives conducted by the ROV QUEST (Tab. 5.5.12). Two primary methodologies were employed to capture detailed imagery of the underwater environment: horizontal lawn-mower mapping and vertical imaging. Horizontal mapping surveys used the downward-looking 12MP Voyis camera mounted on the ROV QUEST to create extensive photo-mosaics of the sea floor. This technique was particularly effective in surveying larger areas with relatively low to moderate relief. By maintaining a consistent altitude of 1.5 to 3.5 meters above the seabed, depending on visibility conditions, the ROV captured high-resolution images that were subsequently processed into detailed mosaics. In contrast, vertical imaging surveys utilized the forward-looking Zeus (6K) and Apex (4K) video cameras to capture three-dimensional views of underwater structures, such as hydrothermal chimneys. This approach provided a comprehensive perspective of these features from all sides, enabling a more thorough understanding of their morphology and geological context.

Table 5.5.12 List of mosaics recorded during MSM131

ROV dive	Structure recorded	Mosaic type	Camera/s used
482	Molløy Flare GFA	horizontal	Voyis (plus Zeus)
483	Yggdrasil	vertical	Zeus and Apex
483	Nidhogg	horizontal	Voyis
485	Gyme	vertical	Zeus and Apex
485	Fenris	vertical	Zeus and Apex
486	Fenris	vertical	Zeus
487	Fenris	vertical & horizontal	Zeus & Voyis
487	Gyme	vertical	Zeus
488	Seep area	horizontal	Voyis
490	Seep area	horizontal	Voyis

Preliminary orthomosaics and 3D models were generated onboard using Agisoft Metashape software. However, to ensure the highest possible accuracy and precision, more refined georeferenced models will be produced following the completion of the cruise. The resulting mosaics offer an exceptional level of detail and clarity, providing invaluable insights into the studied areas. These high-quality images will play a crucial role in advancing our understanding of the seabed's geological features, biological communities, and potential resources.

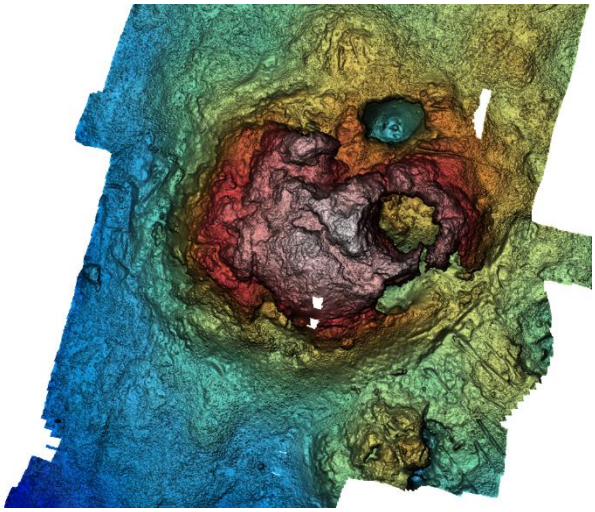

Fig. 5.5.52 Preliminary DEM calculated from the horizontal mosaic at the Molløy flare site GFA, recorded during dive 482 with the Voyis camera.

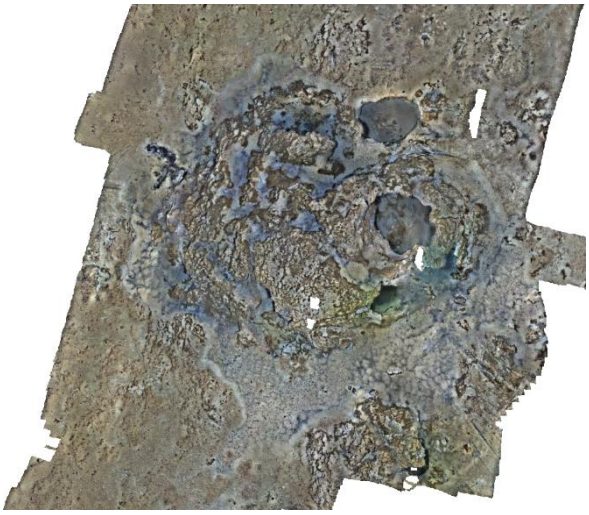

Fig. 5.5.53 Preliminary orthomosaic calculated from the horizontal mosaic at Molløy flare site GFA, recorded during dive 482 with the Voyis camera.

Preliminary Results

In total, ten photomosaic scenes were recorded during MSM131 (Tab. 5.5.12). The flare site GFA in the Molløy area has been recorded for a horizontal photomosaic (Fig. 5.5.52 and 5.5.53), however, Zeus video footage will be added to fill gaps in the Voyis mosaic. Further horizontal mosaics were created from the Nidhogg vent site and the seep area within the Jøtul vent field. The latter was recorded twice during ROV dives 488 and 490, while the first recording during dive 488 covered an area of about ~700 m^2, the second was dedicated to focus on the sampling area, but with high resolution and an altitude of only 1.5 m. The mosaic at the Nidhogg vent site was the smallest with only 5 lines and had some technical problems, resulting pictures with a central shadow due to a loose object in the glass lens.

Vertical mosaics were performed at Yggdrasil (Fig. 5.5.54), Gyme and Fenris. Fenris and Gyme were recorded three and two times, respectively, to illustrate temporal changes. At Fenris it will be also possible to combine a vertical mosaic of the black smoker with a horizontal mosaic covering the mound structure were the smoker is located at.

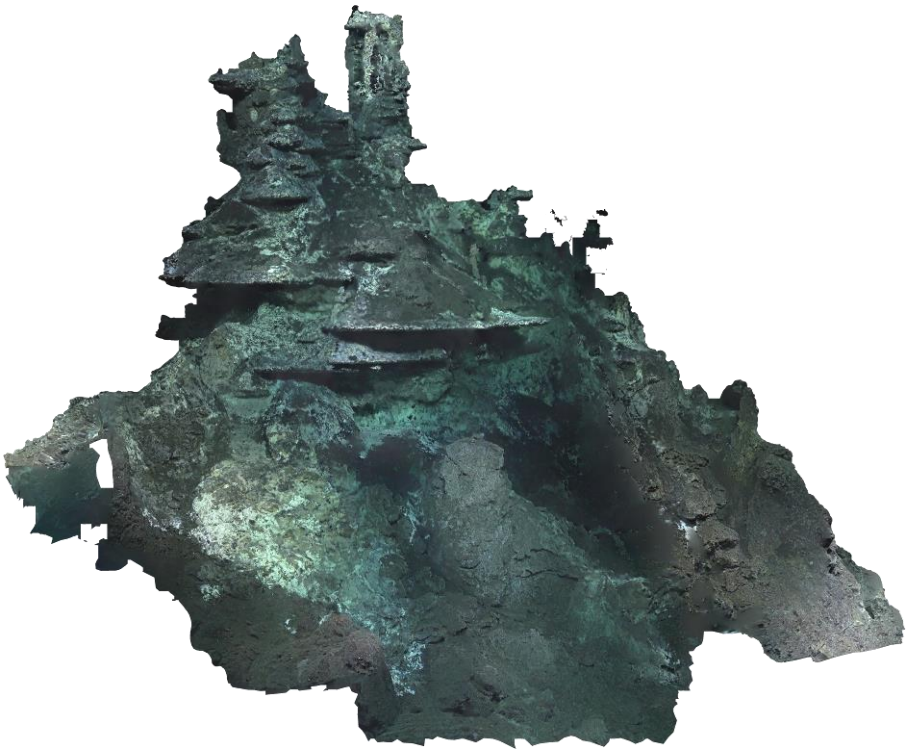

Fig. 5.5.54 Screenshot of the preliminary vertical mosaic of vent site Yggdrasil, recorded during ROV dive 483 using the Zeus camera footage.

5.5.4 Temperature Measurements in the Sediments (T-Stick)

(M. Römer)

The T-stick is a temperature measurement device built by the company RBR Ltd. (Canada). It consists of a lance with temperature sensors and a data-logger (Fig. 5.5.55). The total length and maximum penetration of the lance is 60 cm. Eight temperature probes are evenly spaced with a distance of 8 cm. The device has a measurable temperature range of -5 to 35°C and a resolution of 0.6 mK. Sample period was set to every 10 s. The logger with ID 13116 was used for all deployments.

The device is operated by the ROV and logging throughout the entire dive time. When deployed by the ROV manipulator into the sediments, the temperature probes measure the differences in the specific sediment depth, which reveal temperature profiles for the sampling site. The T-Stick was inserted as vertical as possible into the sediments so that the entire lance was within the sediment. The manipulator was not holding the lance for at least 10 minutes for each measurement to ensure that no frictional heat effects the measurement. The lance was slightly bent during the first deployment, which however did not affect the measurements.

The data were downloaded from the logger after the ROV dive using the RBR software. Further post-processing was done with Microsoft excel. The Raw data of the eight temperature probes were plotted on a time axis for a first quality check. Then, the temperatures were intercalibrated to reveal the same values before the first measurement. To achieve a temperature profile for a

measurement site, the values of the probes close to the end of each measurement were extracted and plotted against depth. The gradient can then also be calculated using the profile values.

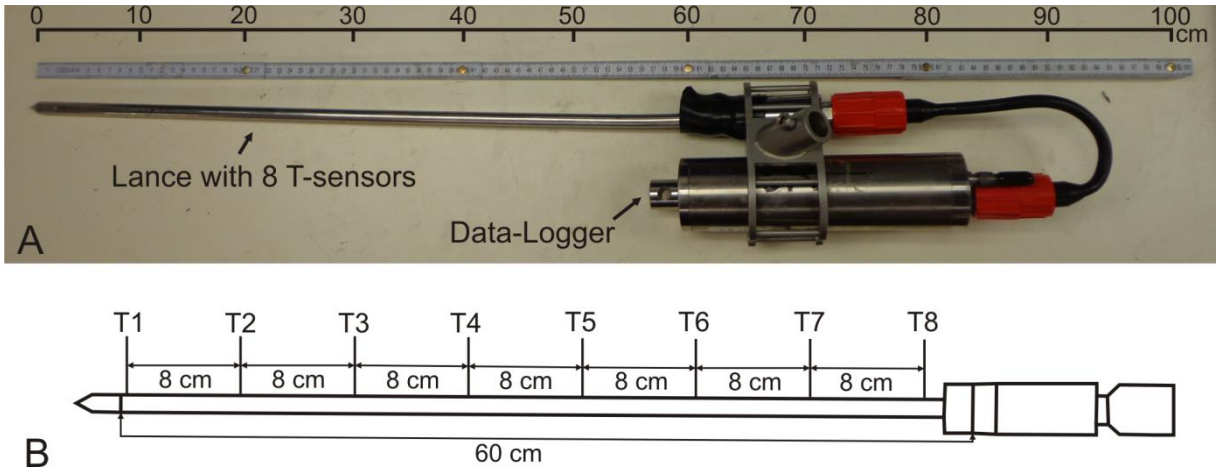

Fig. 5.5.55 A) Photograph of the T-stick consisting of lance and data-logger. B) Schematic drawing of lance showing the positions of the temperature probes (T1 – T8).

Preliminary Results

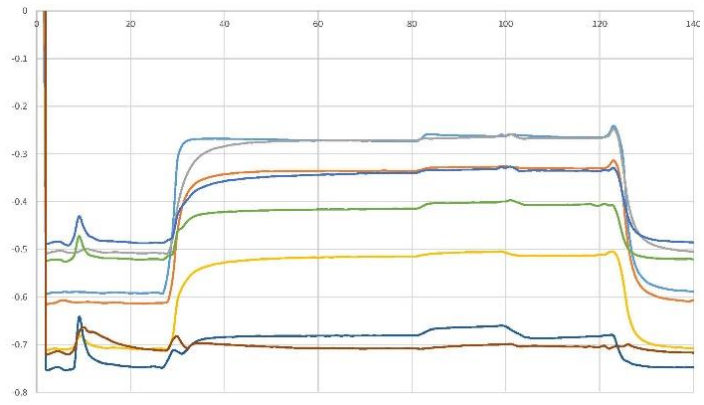

Fig. 5.5.56 Plot of the raw time series of the temperature probes of the deployment during ROV dive 488.

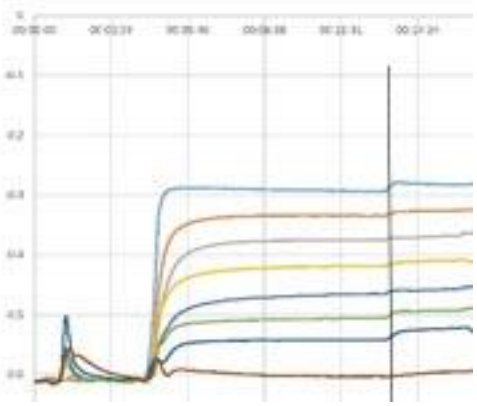

Fig. 5.5.57 Plot of the intercalibrated T series. Black vertical line indicates the values extracted for the temperature profile.

The T-Stick was activated and installed at the ROV for five dives during MSM131. However, it has been only been used for measurements during ROV dives 488 and 490. All measurements were conducted at a seep area about 200 m east of the black smoker Fenris within the Jøtul vent field.

During ROV dive 488, one T-Stick deployment has been conducted within a sea floor area characterized by loose exposed precipitates with a whitish staining, presumably microbial mats. The measurement has been disturbed as the ROV touched the T-Stick during push coring (Fig. 5.5.56), however, already more than 10 minutes have passed, so that the values just before the disturbance were extracted to plot the temperature profile (Fig. 5.5.57). The temperature gradient is almost linear within this 60 cm depth and was calculated at 0.554 K/m (Fig. 5.5.58).

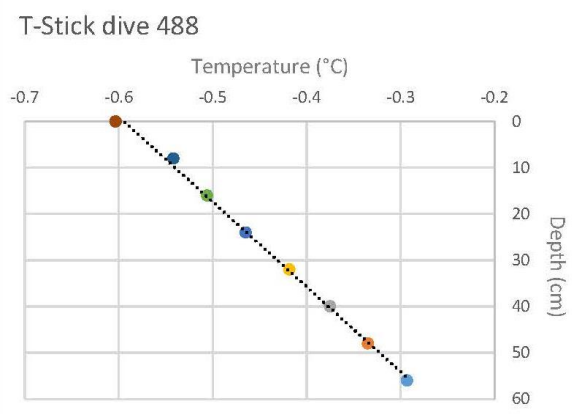

Fig. 5.5.58 Temperature profile of the deployment during ROV dive 488. The calculated gradient (black dotted line) is 0.554 K/m.

During ROV dive 490 a set of T-Stick deployments has been conducted to investigate the seep area in more detail and also to better evaluate the gradient measured during ROV dive 488 related to background. Therefore, four deployments were successfully conducted.

The first deployment failed since the T-Stick was not inserted entirely and fell slightly aside (Fig. 5.5.59). This measurement has to be neglected (Fig. 5.5.60). The T-Stick was replaced within the same habitat, which is also comparable and only few meters next to the sampling site during ROV dive 488. The same patch with loose precipitates and microbial mats was targeted again. The temperature gradient was calculated at 0.858 K/m. The second habitat measured with the T-Stick was only few meters aside within a darkish appearing sediment area with microbial mats. The gradient was calculated at 0.706 K/m. The third measurement was taken again only few meters aside where typical seep characteristics at the sea floor were missing, but still within the circular appearing seep influenced area. The temperature gradient was calculated at 0.486 K/m. The last measurement was taken about 5 meters north outside this seep influenced area and should serve as a background measurement. The temperature gradient was calculated at 0.241 K/m. In conclusion, the four measurements show a clear decrease in temperature gradients related to the seep habitats (Fig. 5.5.61).

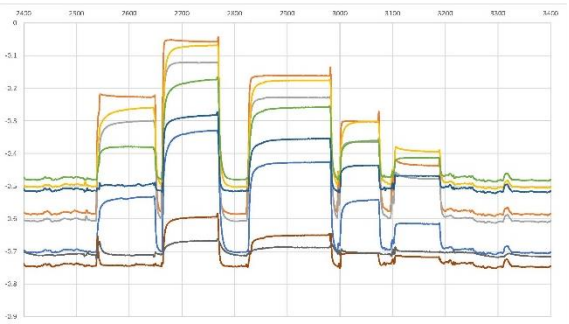

Fig 5.5.59 Plot of the raw time series of the temperature probes of the deployment during ROV dive 490.

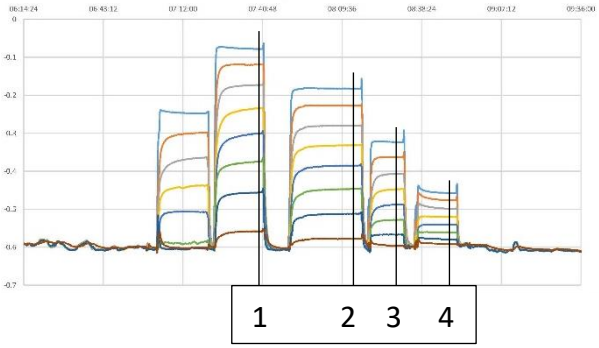

Fig. 5.5.60 T-Plot of the intercalibrated time series of the deployment during ROV dive 490. Black lines and numbers refer to the four successful measurements conducted in different habitats.

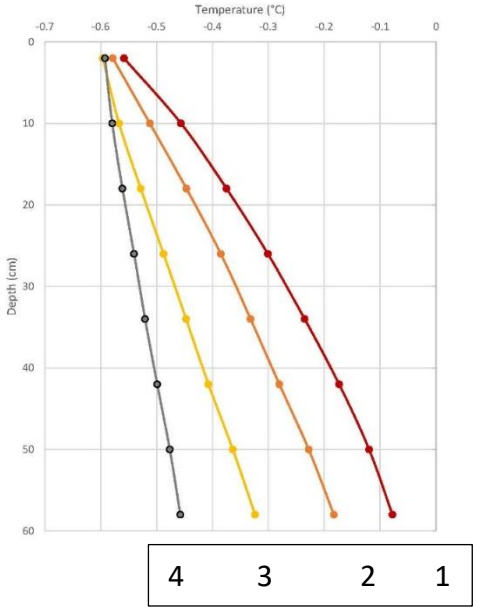

Fig. 5.5.61 Temperature profiles of the four successful deployments during ROV dive 490.

5.5.5 KIPS Sampling

(E. Meckel, E. Anagnostou and J. Kleint)

During 10 ROV QUEST dives at the different working areas in the Jøtul vent field focused on diffuse vent fluids and potential diffuse seep areas were sampled via the Kiel Pumping System (KIPS). In addition, three 5 L Niskin bottles (Fig. 5.5.62) were attached to the starboard side of the ROV for sampling the buoyant plumes above the diffuse vent structures and interesting seep areas.

Fig. 5.5.62 Three 5 L Niskin bottles attached to the starboard side of MARUM ROV QUEST during MSM131

ROV-based sampling of vents and seeps in e.g. hydrothermal systems is essential to constrain physical, chemical, and biological processes in the deep sea. However, sampling of hydrothermal systems is challenging due to mostly extreme temperatures (up to 400°C), high pressure, potentially enormous gas contents and/or highly corrosive fluid properties. For the analyses of particularly rare trace elements and their isotopic systematics, samples were taken by the Kiel Pumping System (KIPS) (Garbe-Schönberg et al., 2006) which had proven ideally suited for varied types of trace element work including hydrothermal fluid and plume studies (e.g., Kleint et al., 2019; Koschinsky et al., 2008). The KIPS is an inert, temperature-resistant, modular, and remotely controlled fluid sampling system for the storage of 4 samples with up to 750 ml volume (Figs. 5.5.63 and 5.5.64).

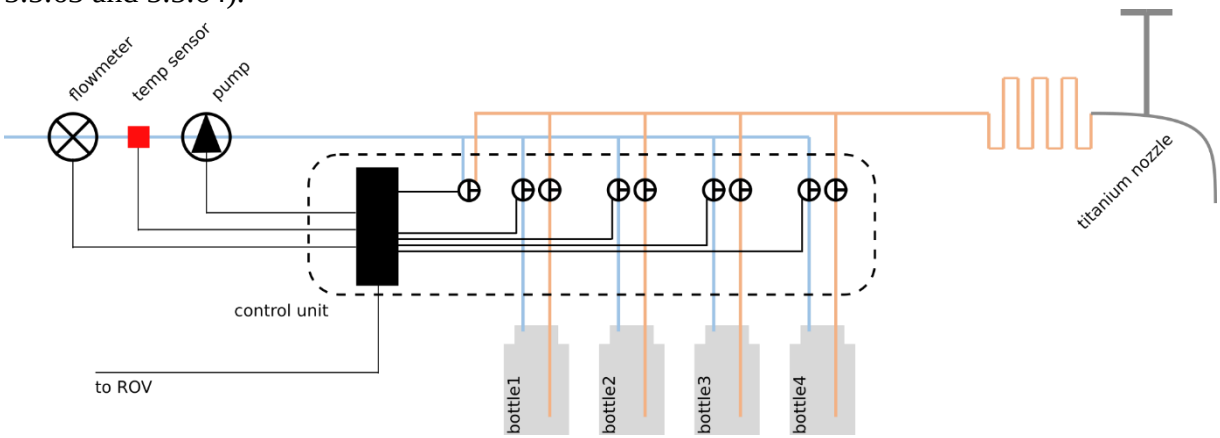

Fig. 5.5.63 The setup of the Kiel Pumping System (KIPS).

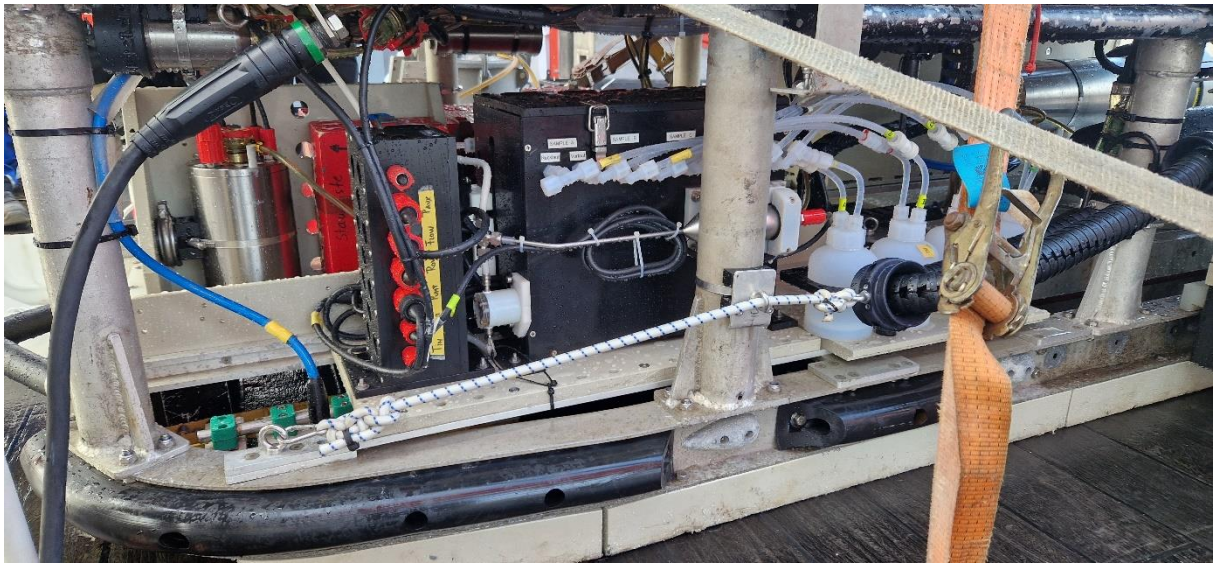

Fig. 5.5.64 The fluid sampling system KIPS deployed from MARUM ROV QUEST during MSM131

During ROV-based sampling, fluids enter the KIPS via a titanium tube, that is guided by the ROV's manipulator to the point of sampling. Sampled fluids are pumped through PFA tubing (3/8" O.D., 6 m length) to the remotely controlled valve pack with 3 sample lines and 1 purge line bottles 3 and 4 were connected allowing the sampling of a bigger volume. The KIPS gear pump (0-1.5 L/min) is mounted downstream, and an in-line flow meter delivers real-time data for flow rate and total fluid volume. In general, sample flasks were prefilled with DI water and sampled fluids are slowly pumped over 5-10 min, giving a > 5-fold exchange of the flask's volume. Immediately

after recovery of the ROV on deck, all KIPS sample flasks were sampled for subsequent gas analyses and were transferred to the ship's laboratory for sub-sampling following the standardized protocols thereafter. During MSM131 the KIPS was deployed on the back (starboard) of MARUM ROV QUEST (Fig. 5.5.64). In total 11 samples were taken with the KIPS and 18 samples were taken with Niskins (see station list), from which aliquots were taken for the further analyses on board and in the home laboratories after the cruise.

In line with the outflow from the KIPS sampling system, an fDOM (fluorescent Dissolved Organic Matter) sensor was installed on the portside in the back of MARUM ROV QUEST. The colored or chromophoric fraction of the dissolved organic matter (DOM) pool strongly absorbs in the ultraviolet spectrum of light. A subset of colored DOM also fluoresces (fDOM). These two pools cannot be directly quantified in chemical terms, i.e. units of moles per volume, but alternatively, the strength of their optical signals obtained via light excitation and emission is used (Dittmar and Stubbins, 2014). In the total pool of DOM, the humic fraction is optically active, and specific wavelength combinations in fluorescence spectroscopy are used to estimate a 'humic-like' component of fDOM, which is supposed to be derived from microbial processing and reworking of biomolecules. As fDOM is a surrogate for cDOM, measurements of fDOM represent a fast and easy means of tracking the fate of DOM in natural waters.

The investigation of the fDOM pool in ocean waters is, however, scarce but has been of more and more concern during recent years. Detection of fDOM in the ocean and at the ocean floor can be performed via discrete water sampling and subsequent analysis in the laboratory or alternatively, by in situ-detection using optical sensors. Data are immediately available on board and will provide information on the 3D distribution of fDOM, its far-field effect and its potential effect on macro- and microbiological life.

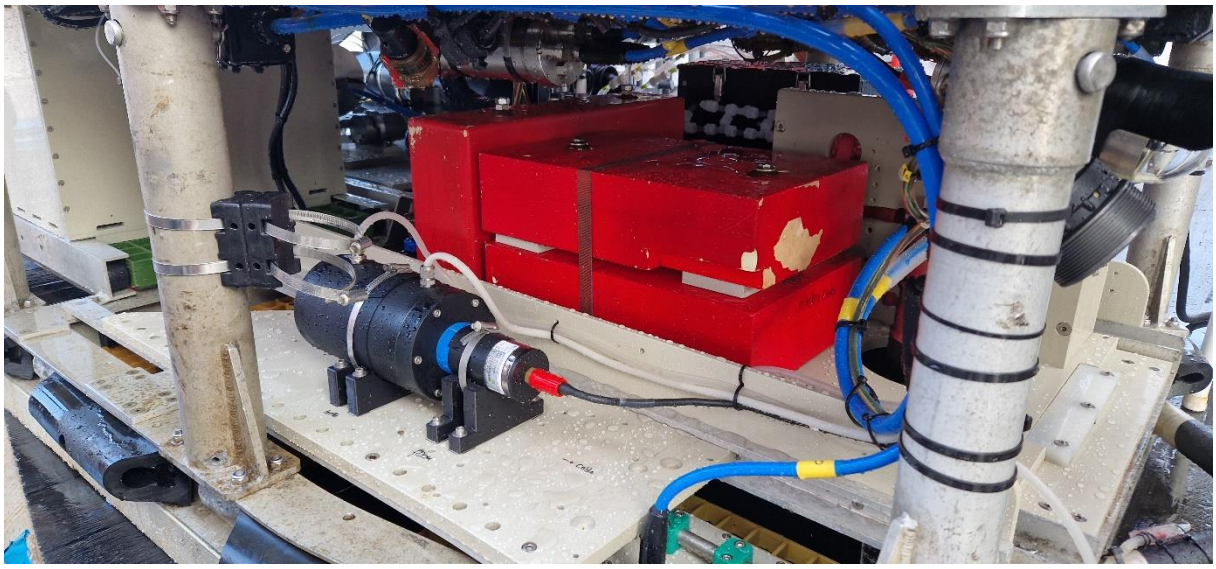

Fig. 5.5.65 The fDOM sensor connected to the outflow of fluid sampling system KIPS deployed from MARUM ROV QUEST during MSM131 (photo: E. Meckel)

5.5.6 IGT Sampling of Fluids and Gases

(A. Diehl)

Dissolved gases in hydrothermal vent fluids provide important constraints on redox processes and fluid rock reactions in the subsurface high-temperature reaction zone in hydrothermal systems. During expedition MSM109 in 2022 hydrothermal fluids from the Jøtul vent field were sampled via the KIPS sample system and showed high concentrations of methane which are typical for sediment-related hydrothermal vent fluids. The concentrations of these samples remain somewhat uncertain as KIPS water bottles are not gas-tight and potentially degas during their ascent from the ocean floor to the ship and during the laboratory work following the recovery. During this cruise, we utilize isobaric gas-tight samplers (IGT's) to improve the quantification of CH_4 and to quantify H_2 and other dissolved gas species to better characterize the vent fluids in this particular region.

IGT Samplers

Two isobaric-gas-tight (IGT) samplers were deployed to recover hot hydrothermal fluids during ROV Quest dives at the Jøtul hydrothermal field. The samplers (Seewald et al., 2002) are equipped with a thermocouple attached to the sampler's snorkel and allow for real time temperature measurements. The samplers' snorkel was brought into the venting orifice and the samplers were fired when the vehicle was positioned and the thermocouple temperature readings showed stable maximum temperatures. Back on deck the samplers were immediately processed and fluids were drawn within some hours after the sampling. Gas analytics and quantification of H_2 and CH_4 were prioritized. pH, conductivity and Eh was measured on board and subsequently aliquots were distributed to the shipboard science party. Samples inside the samplers were kept at 275bar until the gas analytics and on-board measurements were completed. After the sampling the sample chambers were dismantled, thoroughly cleaned, the pistons greased and the samplers were reassembled for the following dive. On overview of the samples is given in Tab. 5.5.13.

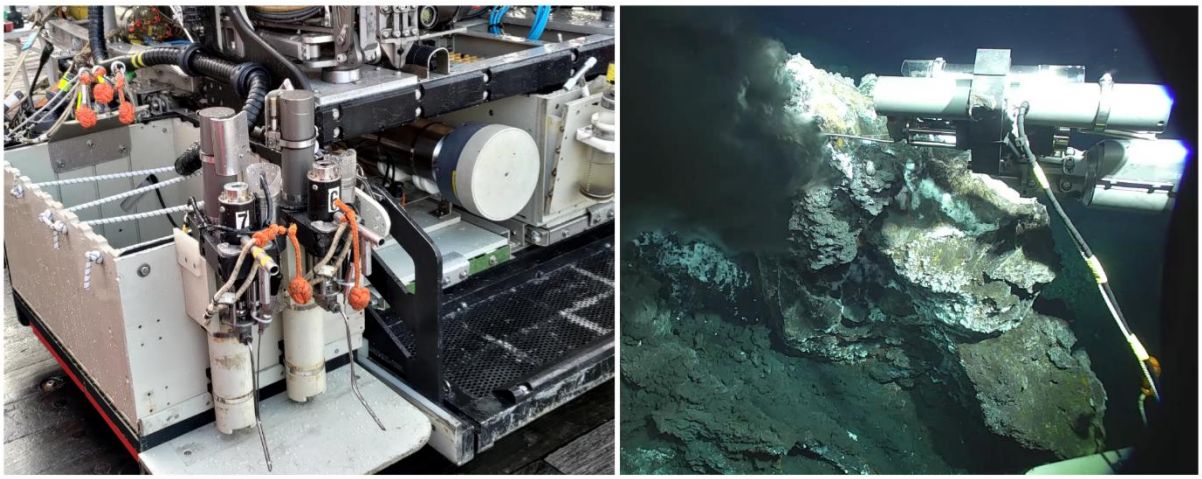

Fig. 5.5.66 left: IGT samplers attached to ROV QUEST 4000; right: IGT sampling at the vigorously venting black smoker Fenris.

Table 5.5.13 IGT samples successfully recovered during MSM131.

GeoB No.	Location	Date	Time (UTC)	Latitude N	Longitude E	Water Depth	Remarks
26235-3	Yggdrasil	**03.09.2024**	10:24	77° 26.195'	07° 42.490'	2954 m	Large flange structure, clear fluid
26252-3	Gyme	**08.09.2024**	08:54	77° 26.414'	07° 42.171'	3021 m	Black smoker chimney, vigorous venting
26269-2	Nidhogg	**13.09.2024**	14:03	77° 26.195'	07° 42.199'	2992 m	Shimmering outflow, clear fluid
26269-4	Fenris	**13.09.2024**	15:58	77° 26.384'	07° 42.514'	2972 m	Black smoker chimney, vigorous venting
26280-2	Yggdrasil	**18.09.2024**	11:26	77° 26.199'	07° 42.510'	2953 m	Large flange structure, clear fluid

Quantification of Dissolved Hydrogen and Methane

For hydrogen (H_2) and methane (CH_4) analysis about 1mL of aqueous solution were transferred from the IGT samplers into gas-tight glass syringes. All samples were particularly gas-rich with resulting headspaces being around two times of the fluid volumes. The gases were extracted via a headspace extraction procedure by equilibration of the samples with a fixed volume of nitrogen gas (typically 2mL) at a pressure of 1 atm. Finally, 250 µL of the gas in the headspace were injected into an Agilent 7820A gas chromatograph (GC) equipped with a Molsieve 60/80 column and a thermal conductivity detector (TCD, for H_2 detection) and a flame ionization detector (FID, for CH_4 detection) using N_2 as carrier gas. Total concentrations of H_2 and CH_4 were then calculated according to Henry's Law, considering the headspace and the aqueous volumes. All samples were measured in triplicates with each measurement performed on individual aliquots.

Preliminary Results

Our onboard analytic results showed consistently high concentrations of H_2 and CH_4 for the different orifices in the Jøtul hydrothermal field (Tab. 5.5.14). We successfully recovered 5 samples in which gas concentrations are much higher than the concentrations reported from KIPS samples recovered during expedition MSM109 in 2022 (Bohrmann et al., 2024). CH_4 concentrations measured during MSM131 range from around 50 mmol/L up to 67mmol/L and are comparable to vent fluids from Guaymas basin (Seewald et al., 2024).

Table 5.5.14 On-board analytical results for IGT hydrothermal fluid samples. Ranges of concentrations for the sediment-hosted Guyamas basin are shown for comparison (Seewald et al., 2024). For Guaymas basin hydrothermal fluid samples with Mg concentrations of less than 10 mmol kg^{-1} were considered.

Location	T (°C)	CH_4 (mmol/L)	H_2 (mmol/L)	H_2/CH_4
Jøtul field	214 – 324	49.7 – 66.3	14.3 – 17.6	0.25 – 0.29
Guaymas basin	249 – 317	36.2 – 61.0	0.5 – 3.1	0.01 – 0.06

In contrast, H_2 concentrations were determined between 14 and 17 mmol/L, which are around one order of magnitude higher than reported for vent fluids from the sediment-hosted Guyamas basin. H_2/CH_4 ratios were determined in a narrow range of 0.25 – 0.30. Our preliminary results put some interesting constraints on the chemical composition of the Jøtul hydrothermal field, and we are looking forward to the upcoming laboratory work where major element-, trace element-, and isotope composition in these fluid samples will be determined.

5.6 Gas Analysis

(T. Pape, J. Malnati, G. Feddersen, M. Meyer, F. Berger, E. Kopiske)

During MSM131, gas samples were prepared to determine the composition of light hydrocarbons and hydrogen in the fluids discharged at the Jøtul hydrothermal field and to monitor the distribution of vent- and seep-derived components in the water column at the Jøtul field and at the Molløy Ridge area. Additional gas samples were prepared from sediment cores from the Jøtul hydrothermal field and the Molløy Ridge area to determine the concentration of methane and its distribution in the pore space.

Sampling of gas in Fluids and Water

Various methods were used to prepare the gases from the fluid, water and sediment samples. Fluid samples were collected precisely at the fluid discharge sites using IGT (Isobaric gas tight) samplers and the KIPS (Kiel Pumping System. Gas subsamples were prepared from five fluid samples that were obtained with the ROV-operated IGT samplers (Tab. 5.6.1). The gas phases were transferred with gas-tight syringes into glass vials that were prefilled with gas-free saturated NaCl solution and closed with butyl stoppers. The composition of the volatile hydrocarbons (C_1-C_6) in the gas phase was determined on board using gas chromatography.

Table 5.6.1 List of fluid samples collected using the ROV-operated isobaric gas-tight (IGT) fluid samplers in the Jøtul hydrothermal field for gas analysis.

ROV Dive	GeoB	Tool	Sampling Site	# samples, C_1-C_6 HCs
484	26235-3	IGT-7	Outflow flange Yggdrasil	1
485	26252-3	IGT-7	Black Sm. West (Gyme)	1
486	26269-2	IGT-6	Nidhogg	1
486	26269-4	IGT-7	Fenris	1
489	26280-2	IGT-6	Yggdrasil flange	1
			Total:	**5**

Subsamples of 11 gas-rich fluid samples obtained with the ROV-Operated Kiel Pumping System (KIPS) were prepared for gas analysis (Tab. 5.6.2) immediately after recovery of the ROV on deck. For this purpose, a connector above the cap of the individual KIPS sampling flasks was opened and a silicone hose connected to a syringe with an open-/close-mechanism was inserted into the connector. The hose was pushed through close to the bottom of the sampling flask, and the syringe was filled with the fluid by pulling the syringe plunger.

The gas phase that formed as a result of the degassing of the fluids in the syringe, was transferred to glass vials prefilled with NaCl. Compositions of C_1-C_6-hydrocarbons were determined on board using gas chromatography. Concentrations of light hydrocarbons on these samples were determined onboard.

Table 5.6.2 List of fluid samples obtained with the ROV-operated Kiel Pumping System (KIPS) in the Jøtul hydrothermal field for gas analysis.

ROV Dive	GeoB	Flask	Sampling Site	# samples, C_1-C_6 HCs
484	26235-2	KIPS A	Outflow flange Yggdrasil	1
484	26235-4	KIPS B	Outflow top Yggdrasil	1
484	26235-7	KIPS C	Nidhogg vent	1
485	26252-2	KIPS A	Black Sm. West	1

485	26252-2	KIPS B	Black Sm. West	1
485	26252-6	KIPS C	Black Sm. East	1
485	26252-6	KIPS D	Black Sm. East	1
486	26269-3	KIPS A	Nidhogg	1
486	26269-5	KIPS B	Fenris	1
486	26269-6	KIPS C	Gyme (?)	1
488	26274-2	KIPS A	presumed seepage area	1
			Total:	**11**

506 water samples (Tab. 5.6.3) were collected at selected water depth in order to determine concentrations of CH_4 and partly H_2 and to follow their individual spread within the water column. The water samples were collected during 22 hydrocasts with the SBE-32 carousel equipped with 23 x 10 L Niskin-type water sampling bottles from OceanTest Equipment Inc. (OTE) that was part of the CTD/ro system onboard (one of the usual 24 sampling bottles was removed and the transponder of the underwater positioning system installed in this place).

Table 5.6.3 List of water samples collected with OTE water sampling bottles during CTD/ro stations for gas analysis. JHF – Jøtul hydrothermal field; MRa – Molløy Ridge area

GeoB	Tool CTD-	Area	# samples, conc. CH_4	# samples, conc. H_2	He isotopes	conc. tritium
26201-1	01	JHF	23			
26216-1	02	JHF	23			
26219-1	03	JHF	23			
26220-1	04	MRa	23			
26221-1	05	MRa	23			
26223-1	06	MRa	23			
26224-1	07	JHF	23	10		
26229-1	08	JHF	23	13		
26234-1	09	JHF	23	8	8	
26241-1	10	JHF	23	12	8	
26246-1	11	JHF	23	14	5	
26251-1	12	JHF	23	18	9	
26253-1	13	JHF	23	17	6	
26262-2	14-2	JHF	23	14	23	
26267-1	15	JHF	23	15	11	
26270-1	16	JHF	23	14	10	
26271-1	17	JHF	23	14	14	
26273-1	18	JHF	23	16		
26275-1	19	JHF	23	16		
26279-1	20	JHF	23	23		
26281-1	21	JHF	23	23		
26283-1	22	JHF	23	23	23	23
		Total:	**506**	**250**	**117**	**23**

Concentrations of dissolved CH_4 and also partly of dissolved H_2 on these samples were determined on board using Off-Axis Integrated Cavity Output Spectroscopy (Greenhouse Gas Analyzer, GGA) and Reducing Compound Photometry (Peak Performer). For quantification of CH_4 with the GGA, 100 mL-aliquots of the water were immediately transferred from each Niskin bottle into two 140 mL-syringes equipped with a Luer Lock connector with twist lock using silicone hoses. The syringes were carefully flushed and filled with water while avoiding turbulence and introduction of bubbles from atmospheric air and closed. A headspace volume was generated in each syringe by drawing 40 mL of 'Zero Air' (hydrocarbon-free air) into the syringe. The syringes were shaken vigorously for more than 1.5 minutes to allow for equilibration between

water and headspace. To minimize the risk of water injection into the measurement chamber of the analytical instrument, the 40 mL headspace gas each from both syringes were collected in another gas-tight syringe via a Luer Lock adapter.

For quantification of dissolved H_2 in water samples with the Peak Performer, 40 mL of bubble-free water from the Niskin bottles were transferred into 50 mL-plastic syringes equipped with Luer Lock 3-way valves using silicone hoses. In the ship's laboratory, an additional 10 ml of nitrogen was filled into the syringe as a headspace volume, and the syringe was vortexed for 1 min. to create equilibrium between water and headspace volume.

In addition, selected water samples were prepared for the analysis of He ($^3He/^4He$) isotopic compositions (117 samples) and concentrations of the radionuclide tritium (23 samples) at the Institute of Environmental Physics, University of Bremen.

18 discrete bottom water samples were collected with three 5 L-Niskin-type water sampling bottles that were attached to the frame of the ROV (Tab. 5.6.4). Those samples were collected in the Molløy Ridge area and from near the hydrothermal fluid emission sites in the Jøtul hydrothermal field. The methods of water subsampling from the ROV-Niskins and CH_4 and H_2 analysis were identical to those for the water samples collected using the CTD/ro system.

Table 5.6.4 List of water samples collected with Niskin-type water sampling bottles attached to MARUM ROV QUEST 4000 for gas analysis. Niskin 1 – ‚white'; Niskin 2 – ‚yellow'; Niskin 3 – ‚green'; JHF – Jøtul hydrothermal field; MRa – Molløy Ridge area

ROV-Dive	GeoB	(Niskin #)	Sampling site	Area	samples, conc. CH_4	samples, conc. H_2
482	26222-2	3	Site of active bubble release	MRa	1	
482	26222-3	2	Site of active bubble release	MRa	1	
482	26222-5	1	Site of active bubble release	MRa	1	
483	26228-6	3	Nidhogg vent	JHF	1	1
483	26228-7	1	~5 m apart from Nidhogg vent	JHF	1	1
483	26228-8	2	~10 m apart from Nidhogg vent	JHF	1	1
484	26235-6	3	1 m above outflow Yggdrasil	JHF	1	1
484	26235-9	2	1.5 m above Nidhogg vent	JHF	1	1
485	26252-7	3	1 m above B.S.	JHF	1	1
485	26252-8	2	3 m above B.S.	JHF	1	1
485	26252-9	1	5 m above B.S.	JHF	1	1
486	26269-7	3	1 m above Gyme	JHF	1	1
486	26269-8	1	3 m above Gyme	JHF	1	1
486	26269-9	2	5 m above Gyme	JHF	1	1
488	26274-8	1	1 m above sf	JHF	1	1
488	26274-9	2	5 m above	JHF	1	1
488	26274-10	3	10 m above	JHF	1	1
489	26280-3	3	~12 m east of Yggdrasil	JHF	1	1
				Total:	**18**	**15**

103 headspace gas samples were prepared from sediment cores obtained with the Multi-Minicorer and ROV-operated push corers in the Jøtul hydrothermal field and with the gravity corer in the Molløy Ridge area (Tab. 5.6.5). The ex situ concentration of dissolved methane was determined on board on all headspace gas samples.

Table 5.6.5 List of surface sediment cores from the Jøtul hydrothermal field analyzed for CH_4 concentrations in headspace gas. MIC – Multi-Minicorer, PC – Push Corer; GC – Gravity Corer, JHF – Jøtul hydrothermal field; MRa – Molløy Ridge area

GeoB	Tool	# headspace gas samples	Area	Sampling Site
26237-1	MIC-09	10	JHF	N of Gyme Black Smoker
26238-1	MIC-10	8	JHF	N of Gyme Black Smoker
26239-1	MIC-11	9	JHF	NE of Fenris Black Smoker
26240-1	MIC-12	9	JHF	NNE of Fenris Black Smoker
26242-1	MIC-13	9	JHF	N of Gyme Black Smoker
26274-5	PC-12	10	JHF	presumed seepage area
26274-6	PC-11	9	JHF	presumed seepage area
26282-4	PC-09	12	JHF	presumed seepage area
26282-7	PC-10	11	JHF	presumed seepage area
26282-10	PC-05	9	JHF	presumed seepage area
26282-13	PC-08	5	JHF	presumed seepage area
26257-3	GC-03	11	MRa	GFA
	Total:	**112**		

Analytical Methods

Compositions of light hydrocarbons (C_1 to C_6) in gas extracted from fluids sampled with the IGT samplers and the KIPS were determined onboard by use of a 7890B (Agilent Technologies) gas chromatograph. Gas chromatography was also used to determine ex-situ concentrations of methane in headspace gas prepared from some bottom water samples and all sediment samples. Light hydrocarbons were separated with a capillary column, and detected and quantified with a Flame Ionization Detector. Calibrations and performance checks of the gas chromatographic system were conducted regularly using commercial pure methane standards and gas mixtures (CH_4 in various concentrations in N_2, C_1-C_6 hydrocarbons in N_2).

Onboard analysis of concentrations of methane dissolved in water samples collected with the CTD/ro system and in some bottom water samples collected with the Niskin water sampling bottles attached to the ROV was carried out with a Greenhouse Gas Analyzer (GGA-30r-EP, Los Gatos Research Mountain View, CA). The instrument uses laser absorption spectroscopy, where the absorption of the infrared laser beam directed through the sample is used to calculate the mole fraction of methane in the gas. The combined headspace gas volume of 80 mL prepared from the two syringes was injected in the GGA. This was followed immediately by injection of 60 mL of 'Zero Air', as needed to provide a gas volume of 140 mL in the measurement chamber required for analysis with the GGA. Precision of the GGA was checked prior to each analytical series with commercial gas standards (CH_4 in various concentrations in N_2).

During the second leg of the cruise, dissolved hydrogen concentrations in selected water samples (CTD/ro stations CTD-07 to CTD-22, ROV-Niskins ROV dives 483 to 489) were also determined onboard using a Peak Performer 1 from Peak Laboratories (Mountain View, CA). The instrument is equipped with a sample loop and a hybrid ultraviolet/HgO photometer. For determination of H_2 concentrations, 4–5 mL of the headspace gas were injected into the sample loop. Performance checks of the instrument were conducted prior to each analytical series with a commercial gas standard (H_2 in N_2).

Preliminary Results

At the 19 CTD/Ro stations conducted at the Jøtul hydrothermal field, significant enrichments of dissolved methane were detected in the water column between approx. 2,260 m and 3,000 m (Fig.

5.6.1, left). Highest CH_4 concentrations of up to 16 µmol/L were measured between approx. 2910 m and 2970 m.

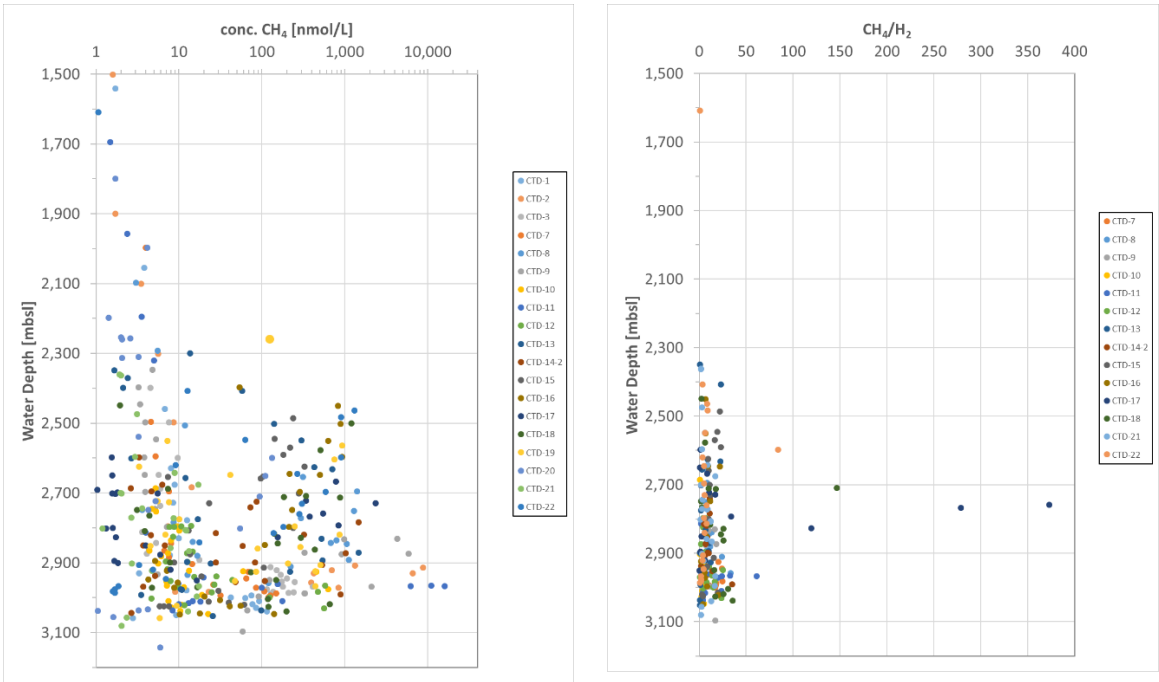

Fig. 5.6.1 Left: Concentration of dissolved methane versus water depth below a water depth of 1500 m for all stations carried out at the Jøtul hydrothermal field. Note the logarithmic scaling of the methane concentration. Right: Concentration of dissolved methane versus water depth below a water depth of 1500 m at the Jøtul hydrothermal field.

In general, the methane distribution pattern is similar to that recorded during MSM109 in 2022 (Bohrmann et al., 2024). However, the maximum CH_4 concentrations during MSM131 were higher than those in 2022, which may have been favored by the high sampling density during MSM131.

The four known fluid emission sites in the Jøtul hydrothermal field are at water depths ranging between approx. 2950 m and 3020m (see station list). Methane enrichments in the water column, which are fed by hydrothermal fluid emissions, could therefore be traced over a vertical distance of at least 760 m. In most cases, enrichments in dissolved methane corresponded to positive temperature anomalies and anomalies detected with the ORP sensor.

In the majority of the samples, concentrations of CH_4 were significantly higher than those of H_2 (CH_4/H_2 between approx. 1 and 36; Fig. 5.6.1, right). Exceptions were individual samples from stations CTD-11, -17, -18, and -22, in which extreme relative enrichments of CH_4 were measured (CH_4/H_2 up to approx. 370). At these stations the hydrothermal plume was crossed a few tens of meters north of Yggdrasil and Niddhog or Gyme and Fenris, respectively.

The extensive data set that was obtained during MSM131 will be used to spatially characterize the individual fate of the CH_4 and H_2 emitted into the water column.

In Fig. 5.6.2 concentration profiles of dissolved methane in gravity core GC-03 from the Molløy Ridge area (left) and in push core PC-5 from the seepage area at the Jøtul hydrothermal field (right) are shown as examples.

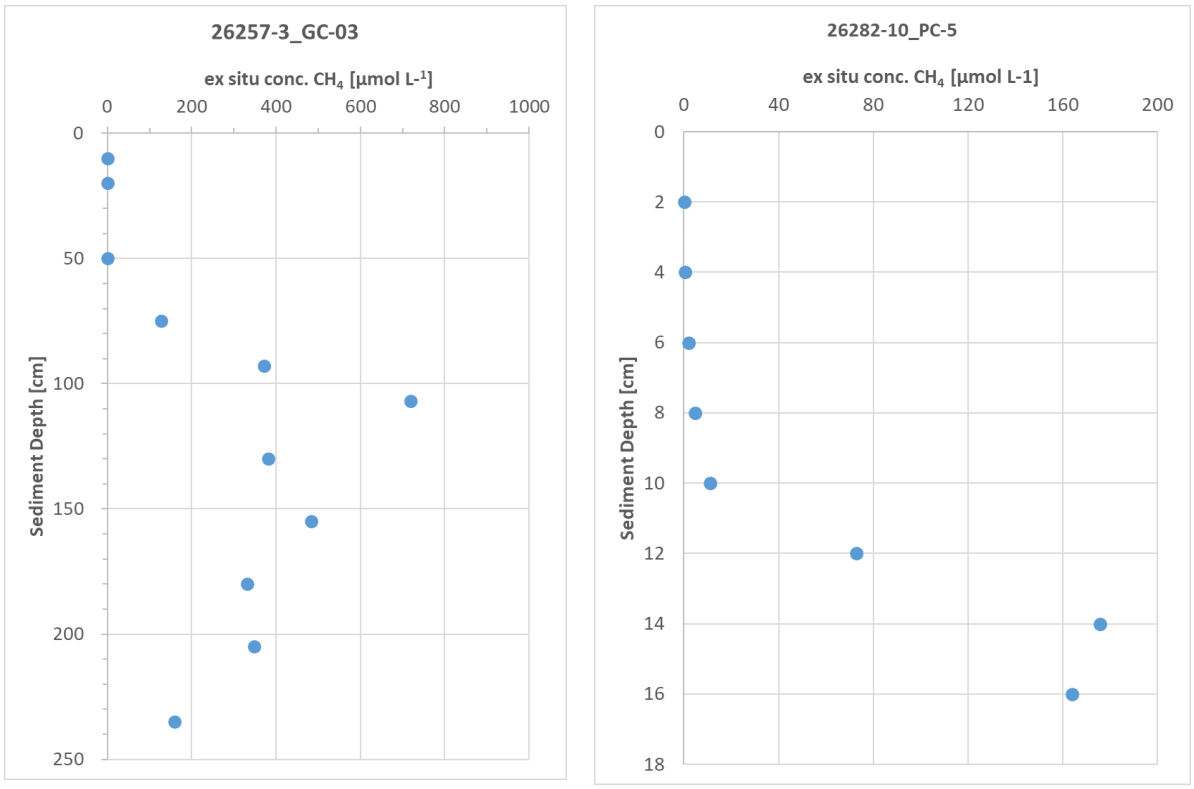

Fig. 5.6.2 Left: Concentration of dissolved methane in gravity core GeoB26257-3, GC-03 from the Molløy Ridge area. Right: Concentration of dissolved methane push core GeoB26282-10, PC-5, collected by means of the ROV from seepage area east of Fenris Black smoker at the Jøtul hydrothermal field.

Near-surface sediments of both cores are relatively depleted in dissolved methane as a result of the anaerobic oxidation of methane. Highest methane concentrations were measured at a sediment depth of approx. 107 cm (GC-03, approx. 720 µmol L^{-1}) and at a sediment depth of approx. 14 cm (PC-5, approx. 175 µmol L^{-1}). Methane-rich samples from the methane zone in the sediment cores will be analyzed in the home laboratory for their signature of methane stable isotopes (C, H) in order to characterize the sources of volatile hydrocarbons at these locations.

5.7 Sediment Sampling

(T. Pape, G. Bohrmann, M. Römer, J. Malnati, G. Feddersen, F. Berger)

Sampling Methods

A Multi-Minicorer (MIC) and a gravity corer (GC), both operated using the ship's own winch, were used to sample sediments. In addition, push corers were deployed during dives with the ROV using the ROVs manipulators. For veering and heaving the MIC, the working winch via the working crane (3) was used. The GC was operated via the large movebar, friction winch F1 and storage winch S1. Acoustic underwater positioning was achieved with the ship's own Sonardyne Ranger 2 Gyro USBL HPT 7000 with the transponder being attached to the cable 50 m above the coring tool.

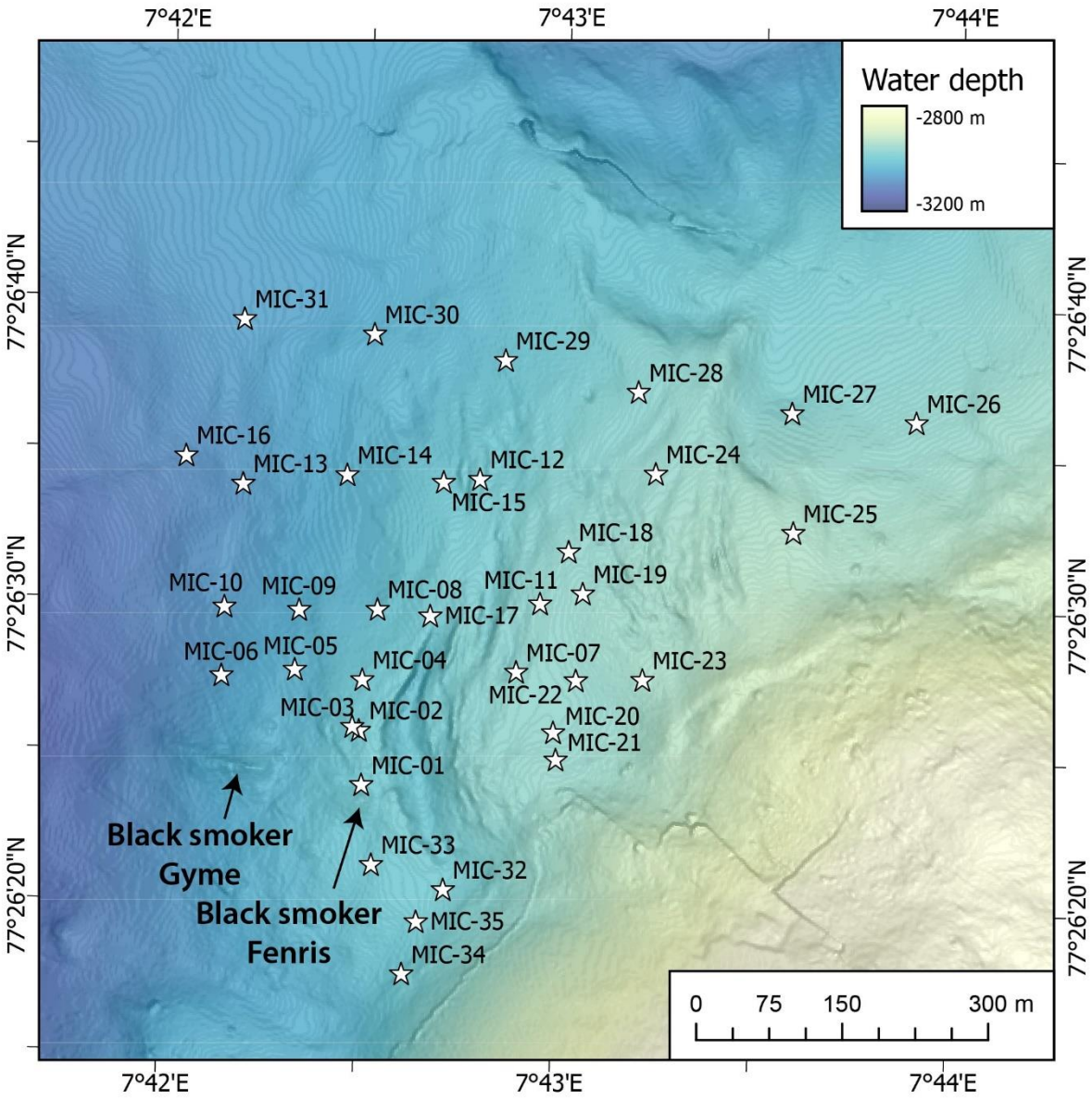

Fig. 5.7.1 Bathymetric map showing positions of the 35 MIC stations carried out during cruise MSM131.

The MIC was equipped with four coring devices and plastic core liners with a length of 61 cm and an inner diameter (ID) of 56 mm. The GC was equipped with 1.5 tons of weight, a 3- or 6-m long cutting barrel (ID ca. 130 mm) and a flexible foil liner in order to ensure rapid access to the sampled material such as gas hydrates. The ROV-operated push corers consisted of plastic core liners with a length of 30 cm and an ID of 78 mm.

MIC cores (Fig. 5.7.1, Tab. 5.7.1) were exclusively taken from the area of the Jøtul hydrothermal field and its vicinity in order to determine the distribution of deposited precipitates originating from the discharge of hydrothermal fluids. Push cores (Tab. 5.7.2) were exclusively collected at the seep area east of the Jøtul hydrothermal field. Those cores were taken to investigate the composition of deposits, vertical distributions of methane, and compositions of pore water ingredients. During ROV-490, cores were collected in pairs at one site to obtain sufficient material for the various analyses. Three gravity corer stations were carried out in the Molløy Ridge area (Tab. 5.7.3) to determine the distribution of methane and to verify the presence of gas hydrates in near-surface sediments close to deep-water hydrocarbon emission sites. In total, 25 MIC cores

(Tab. 5.7.1), 4 push cores (Tab. 5.7.2), and 11 sediment subsamples prepared from gravity core GC-03 (Tab. 5.7.3) are available for analysis in the home lab.

Table 5.7.1 List of surface sediment cores obtained with the Multi-Minicorer (MIC) from the Jøtul hydrothermal field as well as core lengths and number of headspace gas samples prepared. Two cores were stored from station MIC-23. MIC stations without core recovery are not listed. no entry – no samples prepared.

GeoB	Tool	No. headspace gas samples	No. sedi. sample(s)	Length of core frozen (cm)
26225-1	MIC-01		3	23.0
26226-1	MIC-02		3	16.5
26227-1	MIC-03		3	-
26230-1	MIC-04		3	13.6
26231-1	MIC-05		3	11.7
26232-1	MIC-06		1	-
26233-1	MIC-07		1	-
26236-1	MIC-08		3	36.0
26237-1	MIC-09	10	3	32.5
26238-1	MIC-10	8	3	25.6
26239-1	MIC-11	9	3	32.0
26240-1	MIC-12	9	3	32.0
26242-1	MIC-13	9	3	30.5
26243-1	MIC-14		3	25.0
26247-1	MIC-17		3	29.8
26248-1	MIC-18		3	16.3
26249-1	MIC-19		3	24.5
26250-1	MIC-20		1	14.2
26254-1	MIC-21		-	17.5
26255-1	MIC-22		1	-
26256-1	MIC-23		3	15.6 / 17.5
26259-1	MIC-25		1	10.0
26260-1	MIC-26		3	25.0
26261-1	MIC-27		3	27.8
26263-1	MIC-28		3	27.5
26264-1	MIC-29		1	22.0
26265-1	MIC-30		3	31.5
26266-1	MIC-31		1	-
26268-1	MIC-32		1	-
26276-1	MIC-33		-	13.5
26278-1	MIC-35		3	30.4

Of the MIC cores, the longest sediment core at each station was between 10.0 and 36.0 cm long (Tab. 5.7.1). The longest MIC core recovered at each of the stations was frozen immediately upon recovery on deck for storage and analysis of trace metals in the home laboratory. From another of the four MIC cores, slices of near-surface sediments (0–1 cm below seafloor, 1–2 cm, 2–5 cm) were transferred to plastic bags. An additional core was used for foraminiferal studies at almost all stations. MIC cores -09 to -13 were sampled for onboard analysis of dissolved methane using the headspace gas technique.

Table 5.7.2 Push cores collected in the seep area east of the Jøtul hydrothermal field and samples prepared. no entry – no samples prepared

GeoB	ROV Dive	Length of core (cm)	# headspace gas samples	Bulk sedi. sample(s)	Pore water samples	Core kept frozen
26274-5	ROV-488	24	10	8		
26274-6	ROV-488	20	9	9		
26282-3	ROV-490	27			11	X

26282-4	ROV-490	24	12	10		
26282-6	ROV-490	21			10	X
26282-7	ROV-490	22	11	9		
26282-9	ROV-490	22			11	X
26282-10	ROV-490	18	9	6		
26282-12	ROV-490	17			8	X
26282-13	ROV-490	10	5	4		

Table 5.7.3 Stations conducted with the gravity corer (GC) in the Molløy Ridge area and samples prepared. no entry – no samples prepared.

GeoB	**Tool**	**Length core barrel**	**Approx. core recovery**	**Headspace gas samples**	**bulk pp sample**	**Comment**
		[m]	**[cm]**			
26257-1	GC-01	5.75	ca. 75			barrel bent
26257-2	GC-02	3	ca. 65			
26257-3	GC-03	3	ca. 245	11	11	

The length of the ten push cores ranged between 10 and 27 cm. Selected push cores were sampled for onboard analysis of dissolved methane (vertical resolution 2 cm). Such cores from ROV Dive 490 that were sampled for headspace gas analysis were also sampled for foraminiferal studies. 2 cm-slices of the remaining sediment were transferred into plastic bags and frozen for long-term storage. Pore water samples were extracted from the second core of the core pairs collected during ROV dive 490 using rhizon water samplers (Seeberg-Elverfeldt et al., 2005) through the pre-drilled core liners. The intact cores were frozen immediately after completion of pore water extraction.

No intact gas hydrates were observed in the cores at all three gravity corer stations conducted in the Molløy Ridge area. Gravity core GC-03 was sampled to determine concentrations of dissolved methane on board and sediment porosity in the home lab.

5.8 Foraminifera from Jøtul Vent Field

(I. Barrenechea Angeles)

Benthic foraminifera are single-celled protists from the Rhizaria phyla and commonly found in marine environments (Pawlowski et al. 2013). Despite harsh conditions occurring in the hydrothermal vents such extreme temperatures and mineral-enriched waters, many studies have shown their presence in hydrothermal vents (Panieri et al. 2006, Levin et al 2016). Agglutinated species which use particles from their environment, seem to be dominant in these environments but exhibit a low diversity and abundance (Gooday et al. 1999, Panieri et al. 2006).

The study of foraminifera in hydrothermal vents remains limited, especially from a genetic perspective.

Objectives

- Determine the foraminifera assemblages from hydrothermal vents, morphologically and genetically.
- Increase the (genetic) barcoding database
- Understand why some foraminifera thrive in such areas
- Assess recolonization after plume deposition.

Material and Methods

Sediment mini-cores (MIC) taken with the mini-corer around the vents and push cores taken in a seep area.

If two mini-cores were available, the longest one was frozen for further studies using Rose Bengal to analyse living and dead assemblages.

Table 5.8.1 List of cores for foraminiferal studies. The headings indicate which for which type of study the sediments were processed/stored.

GeoB	MIC/Push	Living forams eDNA	Frozen cores assemblages	eDNA
26225	1	x		x
26226	2	X		x
26227	3	X		
26230	4	X	x	
26231	5	X		x
26232	6	x		
26236	8		x	x
26237	9		x	x
26238	10		x	x
26239	11			x
22406	12		x	x
26242	13		x	x
26243	14		x	x
26247	17	X	x	x
26248	18	x		x
26249	19		x	x
26256	23			x
26259	25			x
26260	26		x	x
26261	27		x	x
26263	28		x	x
26265	30		x	x
26278	35		x	
26282-10	ROV490/PC05			x
26282-13	ROV490/PC08			x
26282-4	ROV490/PC09			x
26282-7	ROV490/PC10			x

A subsample for sediment eDNA was taken from the core center using a sterile (previously washed with bleach (10%) 50 mL cut-tip syringe. The small core was sliced every cm with a metallic spatula previously washed with bleach (10%), providing ~ 10cm^3 of sediment material per cm. Each slice was placed in a sterile plastic bag (Whirl-Pak) and immediately frozen at -20°C.

The remaining top 0-1 or sometimes 0-2 cm was used for living foraminifera DNA. The sediment was first sieved through 125µm and 63µm mesh sieves and inspected under a stereomicroscope on board when time and weather allowed.

Only living foraminifera were sorted and preserved for genomics studies, they were washed 3 times with filtered seawater (25 µm). Most of the specimens were preserved in RNA later, a solution preserving the RNA and DNA and stored at -20°C. This solution is acidic and tend to dissolve the calcareous shells. For this reason, some of the calcareous specimens were dried on micropaleontological slides. In other cases, the specimens were just frozen in seawater and stored at -20°C.

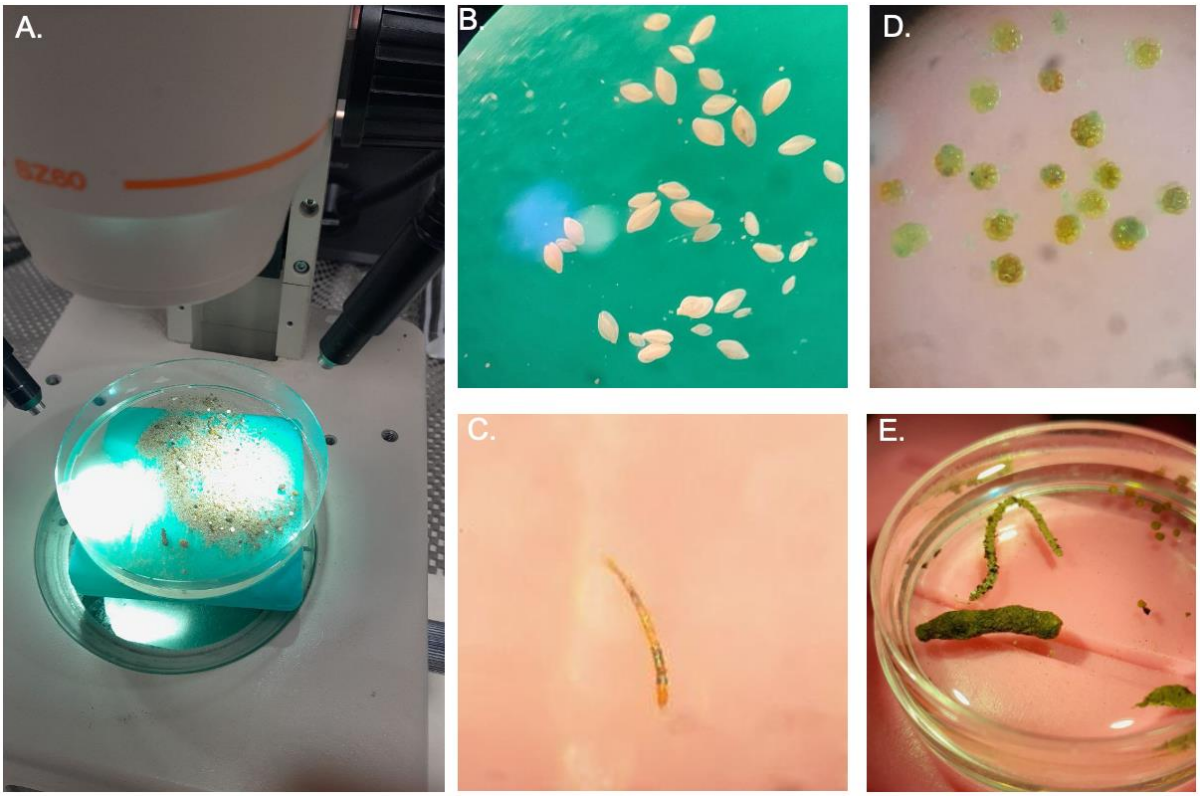

Fig. 5.8.1 Living foraminifera. A. Wet sorting under a steromicroscope using an ice-pack to keep as cold as possible the sea water. B. Miliolids, C. Chitinosiphon sp. D. Ionella tumida, showing a strong coloration of the cytoplasm. E. Other agglutinated monothalamids

Preliminary Results

From the first screening of living forams from the fraction sizes, in general the 125µm fraction had very few living specimen while the 63µm had more living ones. Most of those seemed to not only tiny species but mostly propagules.

Some miliolids were also frozen in seawater and back in the lab are going to be dyed with rose Bengal for a 24h and those turning pink will be selected for DNA barcoding.

A bulk of small rotaliids, most likely propagules were also frozen

A bulk of those propagules were frozen for further studies. From 8/18 cores analyzed on board, 171 specimens were sorted and preserved on RNAl later for DNA or RNA extractions.

Table 5.8.2 Sorted living foraminifera and preserved in RNA late

ID	Station	Number	T°	Individ. #	Description
MSM131_1	GeoB26	226	-20	1	*Mono tube finely agglutinated*
MSM131_2	GeoB26	226	-20	12	*Cribostomoides*
MSM131_3	GeoB26	225	-20	1	*White saccaminid*
MSM131_4	GeoB26	225	-20	1	*C. wuellestorfi*
MSM131_5	GeoB26	227	-20	6	*Elongate Tinollgulmia like (2x), ovammina like (2x), gromid (1x), white saccaminid (1x)*
MSM131_6	GeoB26	230	-20	2	*chitonosiphon*
MSM131_7	GeoB26	230	-20	1	*tube agglutinated (muddy)*
MSM131_8	GeoB26	230	-20	1	*tube agglutinated*
MSM131_9	GeoB26	231	-20	2	*C. wuellestorfi*
MSM131_10	GeoB26	231	-20	2	*groomia like, inside, pellets or stercomata*
MSM131_11	GeoB26	231	-20	1	*Quinqueloculina*
MSM131_12	GeoB26	231	-20	10	*juveniles in vrac (4x Ionella, 3 epistominella, 1 nonionella, 1 rotaliid)*
MSM131_13	GeoB26	231	-20	2	*bathysiphon like*
MSM131_14	GeoB26	231	-20	5	*juveniles in vrac (4x reophax gutiffer, 1x ammodiscus)*
MSM131_15	GeoB26	231	-20	10	*textularids juveniles (Spirolectammina)*
MSM131_16	GeoB26	232	-20	1	*groomia like, inside, pellets or stercomata*
MSM131_17	GeoB26	232	-20	10	*Glomospira, adercotryma*
MSM131_18	GeoB26	232	-20	1	*monothalamid*
MSM131_19	GeoB26	247	-20	22	*chitinosiphon*
MSM131_20	GeoB26	248	-20	9	*chitinosiphon*
MSM131_21	GeoB26	248	-20	1	*elongate saccaminid 2 apertures*
MSM131_22	GeoB26	248	-20	10	*Spirolectammina*
MSM131_23	GeoB26	248	-20	11	*reophax gutiffer*
MSM131_24	GeoB26	248	-20	5	*very elongate, tubular saccaminid white silver*
MSM131_25	GeoB26	248	-20	6	*Ammobaculites*
MSM131_26	GeoB26	248	-20	2	*saccaminid brown with neck*
MSM131_27	GeoB26	248	-20	6	*Adercotryma*
MSM131_28	GeoB26	248	-20	10	*ionella tumida*
MSM131_29	GeoB26	248	-20	1	*tube agglutined only fine grains*
MSM131_30	GeoB26	248	-20	2	*tube agglutinating mainly other forams*
MSM131_31	GeoB26	248	-20	2	*Fissurina*
MSM131_32	GeoB26	247	-20	3	*Ammodiscus*
MSM131_33	GeoB26	247	-20	10	*miliolida, quinqueloculina*
MSM131_34	GeoB26	247	-20	2	*Fissurina*

5.9 Outreach Activities

(U. Prange and J. Nitsch, media office MARUM, G. Bohrmann)

As part of live broadcasts to the ship, three outreach events were held with different project partners during MSM131. On September 8, 2024, 12:30 p.m., with the German Maritime Museum in Bremerhaven (DSM), Ulrike Prange and Jana Nitsch were on site.

At the DSM there were about 20 listeners, tending to be older. The stream stopped running after about 30 minutes, so we ended it soon with a reference to the simulation container and the link to the stream on the homepage. On September 11, 2024, 11:30 a.m., at the Universum Science Museum in Bremen: Ulrike Prange and Bastian Bullwinkel (Universum) were on site.

At the Universum there were about 30 people, a very mixed-age and curious audience, we had shown a recorded dive via stream and also communicated this - because of the weather, diving was not possible that day. Duration approx. 50 minutes, also here the cross-reference to the MARUM content around the corner.

On September 13, 2024 at 10:30 a.m. in the Wilhelmsburg district school in cooperation with the International Maritime Museum Hamburg (IMMH). Ms. Sonja Schäfer from IMMH and students from class 12 A, who have marine sciences as a focus in their curriculum, were there. 20 students took part. They had prepared good questions and presented them in their own words. A diving recording was streamed again (starting at 10:30 a.m., lasting 11:45 a.m.). Reference was made to the exhibition on marine research on deck 7 in the IMMH.

Overall, the offers were very well received - both by colleagues and the audience. The Universum Science Museum had announced the event in advance, and as a result, one group came just for that reason. There were questions from the audience at all events. The expedition was closely monitored by the MARUM media group on social media, and the response was very good on all channels - as is always the case with expedition content. Due to the uncertainties regarding the weather and technical failures, we were only able to announce some of the dives via our channels, and not specifically via other mailing lists. The conclusion is that it is a great, low-threshold offer, even if only for smaller groups, and the content is conveyed very well. Of course, it is more work for everyone involved, especially on the ship, but we would be happy to repeat it if the opportunity arises. Many thanks to everyone, including Sonja Schäfer, Frederic Theis and Bastian Bullwinkel and their colleagues!

6 Station List MSM131

Date	St.	Instrument	GeoB	Location	on	off		Latitude	Longitude	Water	Latitude	Longitude	Water	Remarks
2024	MSM131/		Number		Begin	seafloor	seafloor	End	N	E	depth (m)	N	E	depth (m)	
23.08.2024	1	CTD-01	26201-1	Jøtul Field, north of black smoke	06:17	07:32		09:02	77° 26.426'	07° 42.402'	3059				
	2	OBS JOT03	26202-1	Jøtul Field	10:28		10:43	11:20	77° 25.800'	08°03.530'	2312				
	3	OBS JOT13	26203-1	Jøtul Field	13:07		13:14	14:01	77° 30.397'	08° 11.048'	2351				
	4	OBS JOT02	26204-1	Jøtul Field	14:36		15:43	16:40	77° 30.201'	07° 51.036'	3055				
	5	OBS JOT14	26205-1	Jøtul Field	17:43		17:43	18:35	77° 37.819'	08° 02.600'	2641				
	6	OBS JOT15	26206-1	Jøtul Field	19:32		19:37	20:43	77° 39.999'	07° 30.020'	3464				
	7	OBS JOT01	26207-1	Jøtul Field	21:44		21:49	22:46	77° 33.013'	07° 32.704'	3477				
	8	OBS JOT11	26208-1	Jøtul Field	23:36		23:41	00:42	77° 27.466'	07° 39.058'	2830				
24.08.2024	9-1	ROV-481	26209-1	Fenris Smoker	12:18	15:02	15:50	17:57	77° 26.411'	07° 42.506'	3016	77° 26.411'	07° 42.243'	3041	
	9-2	Beacon	26209-2	Fenris Smoker		15:25			77° 26.389'	07° 42.529'	3010				Dropped for finding position in the future
	10	OBS JOT04	26210-1	Jøtul Field	19:04		19:12	20:02	77° 21.621'	07° 50.448'	2663				
	11	OBS JOT12	26211-1	Jøtul Field	20:40		20:43	21:36	77° 22.746'	08° 07.313'	2136				
	12	OBS JOT09	26212-1	Jøtul Field	22:43		22:47	23:43	77° 14.940'	07° 54.390'	2682				
25.08.2024	13	OBS JOT08	26213-1	Jøtul Field	01:19		01:23	02:21	77° 16.955'	06° 52.894'	2601				
	14	OBS JOT07	26214-1	Jøtul Field	03:11		03:15	04:05	77° 23.014'	06° 59.366'	2662				
	15	OBS JOT06	26215-1	Jøtul Field	04:56		05:00	05:49	77° 28.373'	07° 10.174'	2759				
	16	CTD-02	26216-1	Jøtul Field	07:06	08:35	13:32	14:22	77° 26.101'	07° 42.525'	2933	77° 26.944'	07° 43.152'	2687	Tow-Yo CTD
	17	OBS JOT05	26217-1	Jøtul Field	15:03		15:10	16:16	77° 23.249'	07° 33.633'	3620				
	18	OBS JOT10	26218-1	Jøtul Field	18:07		18:13	18:56	77° 32.990'	06° 25.111'	1993				
26.08.2024	19	CTD-03	26219-1	Jøtul Field	08:20	09:20		10:53	77° 26.390'	07° 42.542'	2993				
27.08.2024	20	CTD-04	26220-1	Molloy Ridge Flare GFA	18:19	19:28		20:47	79° 36.828'	03° 39.716'	3566				
28.08.2024	21	CTD-05	26221-1	Spitsbergen FZ Flare GFB	00:54	02:14		03:49	79° 48.125'	03° 10.706'	3778				
	22-1	ROV-482	26222-1	Molloy Ridge Flare GFA	08:14	11:43	17:33	20:08	79° 36.847'	03° 39.695'	3554	79° 36.862'	03° 39.466'	3552	
	22-2	NIS	26222-2	Molloy Ridge Flare GFA		12:51			79° 36.861'	03° 39.451'	3555				# 3 green
	22-3	NIS	26222-3	Molloy Ridge Flare GFA		12:56			79° 36.861'	03° 39.481'	3550				# 2 yellow
	22-4	SCO	26222-4	Molloy Ridge Flare GFA		13:14			79° 36.862'	03° 39.471'	3554				Portside box, compartment 1
	22-5	NIS	26222-5	Molloy Ridge Flare GFA		17:24			79° 36.862'	03° 39.427'	3554				# 1 white
	23	CTD-06	26223-1	Molloy Ridge Flare GFA	20:51	22:00	23:04	00:17	79° 36.873'	03° 39.632'	3570	79° 36.862'	03° 39.489'	3571	
31.08.2024	24	CTD-07	26224-1	Jøtul Field	07:03	08:46		10:00	77° 26.396'	07° 42.682'	2999				
	25	MIC-01	26225-1	Jøtul Field	10:15	12:19		13:15	77° 26.399'	07° 42.506'	3005				
	26	MIC-02	26226-1	Jøtul Field	13:27	14:38		15:34	77° 26.428'	07° 42.501'	3009				
	27	MIC-03	26227-1	Jøtul Field	15:41	17:03		18:00	77° 26.431'	07° 42.482'	3015				
01.09.2024	28-1	ROV-483	26228-1	Yggdrasil, Nidhogg	06:21	08:49	16:07	18:21	77° 26.201'	07° 42.460'	2965	77° 26.204'	07° 42.227'	2992	
	28-2	SCO	26228-2	Yggdrasil		12:45			77° 26.197'	07° 42.497'	2955				Flange piece Yggdrasil
	28-3	MAN	26228-3	Yggdrasil		13:13			77° 26.195'	07° 42.503'	2950				Flange piece Yggdrasil
	28-4	MAN	26228-4	Yggdrasil		13:29			77° 26.196'	07° 42.501'	2951				Precipitate Yggdrasil
	28-5	MAN	26228-5	Nidhogg		15:03			77° 26.202'	07° 42.202'	2990				Precipitate Nidhogg

					Time (UTC)				Begin / on seafloor			End / off seafloor			
Date	St.	Instrument	GeoB	Location		on	off		Latitude	Longitude	Water	Latitude	Longitude	Water	Remarks
2024	MSM131/		Number		Begin	seafloor	seafloor	End	N	E	depth (m)	N	E	depth (m)	
	28-6	NIS	26228-6	Nidhogg		16:04			77° 26.204'	07° 42.209'	2989				# 3 green
	28-7	NIS	26228-7	Nidhogg		16:05			77° 26.202'	07° 42.229'	2990				# 1 white
	28-8	NIS	26228-8	Nidhogg		16:07			77° 26.206'	07° 42.232'	2992				# 2 yellow
	29	CTD-08	26229-1	Jøtul Field	18:45	20:07	04:36	05:59	77° 26.398'	07° 42.635'	2898	77° 26.408'	07° 42.571'	2863	Tow-Yo CTD
02.09.2024	30	MIC-04	26230-1	Jøtul Field	06:19	07:30		08:25	77° 26.457'	07° 42.504'	3002				
	31	MIC-05	26231-1	Jøtul Field	08:45	10:05		11:01	77° 26.462'	07° 42.332'	3037				
	32	MIC-06	26232-1	Jøtul Field	13:22	14:31		15:32	77° 26.458'	07° 42.146'	3067				
	33	MIC-07	26233-1	Jøtul Field	15:47	17:00		17:57	77° 26.463'	07° 42.894'	3113				
	34	CTD-09	26234-1	Jøtul Field	18:54	19:54	04:36	05:43	77° 26.468'	07° 42.647'	2788	77° 26.408'	07° 42.571'	2863	Tow-Yo CTD
03.09.2024	35-1	ROV-484	26235-1	Yggdrasil, Nidhogg	06:21	08:34	16:00	18:09	77° 26.217'	07° 42.484'	2973	77° 26.192'	07° 42.208'	2998	
	35-2	KIPS A	26235-2	Yggdrasil		09:55			77° 26.193'	07° 42.487'	2953				Outflow flange Yggdrasil
	35-3	IGT 7	26235-3	Yggdrasil		10:24			77° 26.195'	07° 42.490'	2954				Outflow flange Yggdrasil
	35-4	KIPS B	26235-4	Yggdrasil		11:40			77° 26.196'	07° 42.481'	2950				Outflow top Yggdrasil
	35-5	MAN	26235-5	Yggdrasil		12:04			77° 26.194'	07° 42.483'	2950				Outflow top Yggdrasil, precipitate
	35-6	NIS	26235-6	Yggdrasil		12:15			77° 26.192'	07° 42.486'	2948				# 3 green, 1 m above outflow top Yggdrasil
	35-7	KIPS C	26235-7	Nidhogg		13:37			77° 26.200'	07° 42.222'	2992				Nidhogg vent
	35-8	IGT 8	26235-8	Nidhogg		13:58			77° 26.199'	07° 42.189'	2992				Nidhogg vent
	35-9	NIS	26235-9	Nidhogg		14:10			77° 26.201'	07° 42.195'	2992				# 2 yellow, 1.5 m above Nidhogg vent
	35-10	NET	26235-10	West of Nidhogg		15:07			77° 26.205'	07° 42.024'	3024				Hydrothermal precipitates
04.09.2024	36	MIC-08	26236-1	Jøtul Field	06:34	08:01		08:56	77° 26.496'	07° 42.539'	3016				
	37	MIC-09	26237-1	Jøtul Field	09:14	10:36		11:32	77° 26.495'	07° 42.340'	3049				
	38	MIC-10	26238-1	Jøtul Field	11:48	12:52		13:52	77° 26.496'	07° 42.150'	3080				
	39	MIC-11	26239-1	Jøtul Field	14:01	15:09		16:08	77° 26.501'	07° 42.951'	3099				
	40	MIC-12	26240-1	Jøtul Field	16:27	17:37		18:35	77° 26.569'	07° 42.792'	3111				
	41	CTD-10	26241-1	Jøtul Field	19:18	20:02	05:54	06:59	77° 26.316'	07° 44.004'	2714	77° 26.252'	07° 42.043'	3037	Tow-Yo CTD
05.09.2024	42	MIC-13	26242-1	Jøtul Field	07:36	09:10		10:05	77° 26.564'	07° 42.191'	3087				
	43	MIC-14	26243-1	Jøtul Field	10:16	11:58		12:54	77° 26.570'	07° 42.455'	3055				
	44	MIC-15	26244-1	Jøtul Field	13:06	14:36		15:32	77° 26.567'	07° 42.700'	3015				
	45	MIC-16	26245-1	Jøtul Field	15:48	17:19		18:15	77° 26.579'	07° 42.045'	2980				
	46	CTD-11	26246-1	Jøtul Field	18:57	19:53	21:19	22:17	77° 26.236'	07° 42.783'	2796	77° 26.220'	07° 41.967'	3036	Tow CTD
07.09.2024	47	MIC-17	26247-1	Jøtul Field	07:16	10:34		11:28	77° 26.493'	07° 42.673'	2997				
	48	MIC-18	26248-1	Jøtul Field	11:45	12:40		13:35	77° 26.530'	07° 43.021'	2963				Four short cores
	49	MIC-19	26249-1	Jøtul Field	13:48	14:49		15:50	77° 26.507'	07° 43.059'	2957				
	50	MIC-20	26250-1	Jøtul Field	15:56	16:55		17:49	77° 26.430'	07° 42.991'	2962				
	51	CTD-12	26251-1	Jøtul Field	18:19	19:27	02:57	03:54	77° 26.131'	07° 43.252'	3004	77° 26.167'	07° 42.011'	3053	Tow-Yo CTD
08.09.2024	52-1	ROV-485	26252-1	Jøtul Field / Black Smoker	04:17	06:29	15:26	18:01	77° 26.414'	07° 42.265'	3000	77° 26.377'	07° 42.426'	3000	
	52-2	KIPS A + B	26252-2	Gyme Smoker		08:14			77° 26.415'	07° 42.172'	3020				Black Sm. West, max. T = 287°C

					Time (UTC)				Begin / on seafloor			End / off seafloor			
Date	St.	Instrument	GeoB	Location		on	off		Latitude	Longitude	Water	Latitude	Longitude	Water	Remarks
2024	MSM131/		Number		Begin	seafloor	seafloor	End	N	E	depth (m)	N	E	depth (m)	
	52-3	IGT 7	26252-3	Gyme Smoker		08:54			77° 26.414'	07° 42.171'	3021				Black Sm. West, max. T = 296°C
	52-4	NET	26252-4	Gyme Smoker		09:21			77° 26.416'	07° 42.174'	3021				white net, Chimney sample
	52-5	NET	26252-5	Gyme Smoker		09:25			77° 26.416'	07° 42.171'	3021				white net, precipitate
	52-6	KIPS C + D	26252-6	Fenris Smoker		11:09			77° 26.395'	07° 42.547'	2971				Black Sm. east
	52-7	NIS	26252-7	Fenris Smoker		12:53			77° 26.380'	07° 42.582'	2969				# 3 green, 1 m above B.S.
	52-8	NIS	26252-8	Fenris Smoker		12:55			77° 26.376'	07° 42.563'	2967				# 2 yellow, 3 m above B.S.
	52-9	NIS	26252-9	Fenris Smoker		12:57			77° 26.375'	07° 42.561'	2966				# 1 white, 5 m above B.S.
	52-10	MAN	26252-10	Fenris Smoker		14:32			77° 26.379'	07° 42.547'	2975				Rock precipitate
	53	CTD-13	26253-1	Jøtul Field	18:32	19:45	03:22	05:50	77° 26.252'	07° 42.124'	3035	77° 26.530'	07° 42.596'	2927	Tow-Yo CTD
09.09.2024	54	MIC-21	26254-1	Jøtul Field	06:03	07:12		08:07	77° 26.415'	07° 42.999'	2960				one core filled
	55	MIC-22	26255-1	Jøtul Field	08:21	09:26		10:21	77° 26.459'	07° 43.046'	2960				one core with surface sediments
	56	MIC-23	26256-1	Jøtul Field	10:27	11:29		12:24	77° 26.460'	07° 43.215'	2950				
10.09.2024	57-1	GC-1	26257-1	Molloy Ridge Flare GFA	07:26	09:17		10:26	79° 36.857'	03° 39.440'	3567				6 m, bended core
	57-2	GC-2	26257-2	Molloy Ridge Flare GFA	11:28	12:54		14:04	79° 36.854'	03° 39.479'	3567				3 m
	57-3	GC-3	26257-3	Molloy Ridge Flare GFA	14:29	16:05		17:17	79° 36.850'	03° 39.446'	3566				3 m
11.09.2024	58-1	MIC-24	26258-1	Jøtul Field	10:29	11:31		12:26	77° 26.574'	07° 43.238'	2961				
	59-1	MIC-25	26259-1	Jøtul Field	12:41	13:46		14:41	77° 26.543'	07° 43.590'	2936				
	60-1	MIC-26	26260-1	Jøtul Field	14:52	16:03		16:58	77° 26.605'	07° 43.897'	2965				
	61-1	MIC-27	26261-1	Jøtul Field	17:06	18:11		19:11	77° 26.609'	07° 43.581'	2979				
	62-1	CTD-14_1	26262-1	Jøtul Field	19:40	20:34		21:20	77° 26.152'	07° 41.960'	2578				aborted, problems with winch EL2
	62-2	CTD-14_2	26262-2	Jøtul Field	21:37	23:09	06:52	07:59	77° 26.187'	07° 42.131'	3071	77° 27.227'	07° 45.292'	3061	Tow-Yo CTD
12.09.2024	63	MIC-28	26263-1	Jøtul Field	08:35	09:49		10:38	77° 26.619'	07° 43.190'	2983				
	64	MIC-29	26264-1	Jøtul Field	10:58	12:01		12:57	77° 26.635'	07° 42.851'	3021				one core
	65	MIC-30	26265-1	Jøtul Field	13:09	14:13		15:10	77° 26.648'	07° 42.517'	3052				
	66	MIC-31	26266-1	Jøtul Field	15:23	16:30		17:27	77° 26.655'	07° 42.186'	3068				very few cm of sediment
	67	CTD-15	26267-1	Jøtul Field	18:02	19:26	06:54	07:50	77° 27.156'	07° 44.328'	3078	77° 27.086'	07° 45.463'	3043	Tow-Yo CTD
13.09.2024	68	MIC-32	26268-1	Jøtul Field	08:20	09:26		10:20	77° 26.342'	07° 42.720'	2993				
	69-1	ROV-486	26269-1	Nidhogg, Fenris, Gyme	11:01	13:59	18:23	20:36	77° 26.197'	07° 42.193'	2989	77° 26.404'	07° 42.143'	3016	
	69-2	IGT 6	26269-2	Nidhogg		14:03			77° 26.195'	07° 42.199'	2992				max. T = 214°C
	69-3	KIPS A	26269-3	Nidhogg		14:26			77° 26.192'	07° 42.192'	2992				max. T = 210°C
	69-4	IGT 7	26269-4	Fenris Smoker		15:58			77° 26.384'	07° 42.514'	2972				max. T = 313°C
	69-5	KIPS B	26269-5	Fenris Smoker		16:12			77° 26.385'	07° 42.518'	2972				max. T = 309°C
	69-6	KIPS C	26269-6	Gyme Smoker		17:48			77° 26.406'	07° 42.151'	3021				max. T = 301°C
	69-7	NIS	26269-7	Gyme Smoker		18:05			77° 26.404'	07° 42.142'	3020				# 3 green, 1 m above B.S.
	69-8	NIS	26269-8	Gyme Smoker		18:18			77° 26.406'	07° 42.148'	3018				# 1 white, 3 m above B.S.
	69-9	NIS	26269-9	Gyme Smoker		18:23			77° 26.404'	07° 42.145'	SVP				# 2 yellow, 5 m above B.S.
	70	CTD-16	26270-1	Jøtul Field	21:16	23:44	07:13	08:22	77° 27.062'	07° 44.636'	3025	77° 26.667'	07° 42.988'	3005	Tow-Yo CTD

						Time (UTC)			Begin / on seafloor			End / off seafloor			
Date	St.	Instrument	GeoB	Location		on	off		Latitude	Longitude	Water	Latitude	Longitude	Water	Remarks
2024	MSM131/		Number		Begin	seafloor	seafloor	End	N	E	depth (m)	N	E	depth (m)	
14.09.2024	71	CTD-17	26271-1	Jøtul Field	17:05	18:58	07:12	08:23	77° 26.488'	07° 43.218'	2942	77° 26.583'	07° 42.256'	3060	Tow-Yo CTD
15.09.2024	72	ROV-487	26272-1	Jøtul Field	09:14	11:34	17:03	19:31	77° 26.389'	07° 42.515'	2976	77° 26.478'	07° 42.712'	2970	
	73	CTD-18	26273-1	Jøtul Field	19:50	20:54	04:54	06:00	77° 26.779'	07° 42.636'	3031	77° 26.705'	07° 43.186'	3003	Tow-Yo CTD
16.09.2024	74-1	ROV-488	26274-1	Jøtul Field	06:46	08:55	16:26	18:55	77° 26.351'	07° 42.379'	2993	77° 26.410'	07° 43.219'	2924	
	74-2	KIPS A	26274-2	Jøtul Field		14:59			77° 26.404'	07° 42.961'	2935				- 0.7°C
	74-3	T-stick	26274-3	Jøtul Field		15:27			77° 26.405'	07° 42.964'	2935				Vent area
	74-4	NET	26274-4	Jøtul Field		15:31			77° 26.404'	07° 42.969'	2935				Vent area
	74-5	Push corer	26274-5	Jøtul Field		15:36			77° 26.405'	07° 42.964'	2935				Push core 12, center
	74-6	Push corer	26274-6	Jøtul Field		15:36			77° 26.405'	07° 42.964'	2935				Push core 11, rim
	74-7	MAN	26274-7	Jøtul Field		16:15			77° 26.411'	07° 43.210'	2916				Piece of rock
	74-8	NIS	26274-8	Jøtul Field		16:10			77° 26.411'	07° 43.212'	2924				# 3 green, 1 m above seafloor
	74-9	NIS	26274-9	Jøtul Field		16:12			77° 26.411'	07° 43.215'	2919				# 2 yellow, 5 m above seafloor
	74-10	NIS	26274-10	Jøtul Field		16:14			77° 26.412'	07° 43.209'	2914				# 1 white, 10 m above seafloor
	75	CTD-19	26275-1	Jøtul Field	19:27	20:34	04:37	05:47	77° 26.408'	07° 41.940'	3086	77° 26.597'	07° 42.166'	3072	Tow-Yo CTD
17.09.2024	76	MIC-33	26276-1	Jøtul Field	11:16	12:44		13:39	77° 26.355'	07° 42.536'	3005				
	77	MIC-34	26277-1	Jøtul Field	13:53	14:50		15:45	77° 26.295'	07° 42.619'	3001				
	78	MIC-35	26278-1	Jøtul Field	15:49	16:49		17:44	77° 26.324'	07° 42.653'	3001				
	79	CTD-20	26279-1	Jøtul Field	18:23	19:33	04:31	05:44	77° 26.507'	07° 41.441'	3145	77° 26.930'	07° 42.179'	3053	Tow-Yo CTD
18.09.2024	80-1	ROV-489	26280-1	Jøtul Field	07:42	10:33	17:24	19:33	77° 26.197'	07° 42.490'	2950	77° 26.048'	07° 43.815'	2552	
	80-2	IGT 6	26280-2	Yggdrasil		11:26			77° 26.199'	07° 42.510'	2953				
	80-3	NIS	26280-3	Yggdrasil		11:41			77° 26.198'	07° 42.619'	2941				# 3 green
	80-4	MAN	26280-4	Oceanic Core Complex		12:00			77° 26.190'	07° 42.670'	2924				rock
	80-5	MAN	26280-5	Oceanic Core Complex		12:12			77° 26.189'	07° 42.680'	2923				rock
	80-6	MAN	26280-6	Oceanic Core Complex		12:34			77° 26.176'	07° 42.755'	2893				rock
	80-7	MAN	26280-7	Oceanic Core Complex		12:59			77° 26.171'	07° 42.792'	2878				rock
	80-8	MAN	26280-8	Oceanic Core Complex		13:39			77° 26.145'	07° 43.005'	2805				rock
	80-9	MAN	26280-9	Oceanic Core Complex		14:19			77° 26.122'	07° 43.184'	2747				rock
	80-10	MAN	26280-10	Oceanic Core Complex		14:43			77° 26.107'	07° 43.321'	2709				rock
	80-11	MAN	26280-11	Oceanic Core Complex		15:10			77° 26.093'	07° 43.377'	2689				rock
	80-12	MAN	26280-12	Oceanic Core Complex		15:43			77° 26.086'	07° 43.540'	2638				rock
	80-13	MAN	26280-13	Oceanic Core Complex		16:23			77° 26.092'	07° 43.385'	2680				two rocks
	80-14	MAN	26280-14	Oceanic Core Complex		16:47			77° 26.058'	07° 43.662'	2604				rock
	80-15	MAN	26280-15	Oceanic Core Complex		17:16			77° 26.047'	07° 43.816'	2552				two rocks
	81	CTD-21	26281-1	Jøtul Field	20:04	21:06	04:26	05:50	77° 26.878'	07° 41.460'	3083	77° 26.822'	07° 44.776'	2970	Tow-Yo CTD
19.09.2024	82-1	ROV-490	26282-1	Jøtul Field	06:17	08:57	14:25	16:57	77° 26.414'	07° 42.274'	3002	77° 26.453'	07° 43.005'	2937	Venting area
	82-2	T-stick	26282-2	Jøtul Field		12:18			77°26.40'N	07°42.95'E	2954				
	82-3	Push corer	26282-3	Jøtul Field		12:23			77°26.40'N	07°42.95'E	2954				R1, white

					Time (UTC)				Begin / on seafloor			End / off seafloor			
Date	St.	Instrument	GeoB	Location		on	off		Latitude	Longitude	Water	Latitude	Longitude	Water	Remarks
2024	MSM131/		Number		Begin	seafloor	seafloor	End	N	E	depth (m)	N	E	depth (m)	
	82-4	Push corer	26282-4	Jøtul Field		12:27			77°26.40'N	07°42.95'E	2954				9, yellow
	82-5	T-stick	26282-5	Jøtul Field		12:45			77°26.40'N	07°42.95'E	2954				
	82-6	Push corer	26282-6	Jøtul Field		12:49			77°26.40'N	07°42.95'E	2954				R2, white
	82-7	Push corer	26282-7	Jøtul Field		12:57			77°26.40'N	07°42.95'E	2954				10, yellow
	82-8	T-stick	26282-8	Jøtul Field		13:14			77°26.40'N	07°42.95'E	2954				
	82-9	Push corer	26282-9	Jøtul Field		13:16			77°26.40'N	07°42.95'E	2954				R3, white
	82-10	Push corer	26282-10	Jøtul Field		13:18			77°26.40'N	07°42.95'E	2954				5, yellow
	82-11	T-stick	26282-11	Jøtul Field		13:31			77°26.40'N	07°42.95'E	2954				
	82-12	Push corer	26282-12	Jøtul Field		13:34			77°26.40'N	07°42.95'E	2954				R4, white
	82-13	Push corer	26282-13	Jøtul Field		13:36			77°26.40'N	07°42.95'E	2954				8, yellow
	82-14	NET	26282-14	Jøtul Field		14:15			77°26.40'N	07°42.95'E	2954				Surface sample
	83	CTD-22	26283-1	Jøtul Field	17:12	18:27		19:46	77° 26.486'	07° 42.750'	2989				

				ROV Quest:	ROV				CTD + Rosette:	CTD					
				Orion manipulator:	MAN				OBS recovery:	OBS					
				Net sample:	NET				Gravity corer:	GC					
				Scoop:	SCO				Mini-Corer:	MIC					
				Fluid sampler:	KIPS										
				Niskin bottle:	NIS										

7 Data and Sample Storage and Availability

Metadata of the cruise, as well as the station list, were submitted to Pangaea data bank (https://www.pangaea.de/). Samples collected during the ROV dives are under investigation at the Department of Geosciences, University of Bremen (gbohrmann@marum.de). Non-cruise participants can request samples after the moratorium of three years. In addition, data (raw and processed) will be submitted to Pangaea along with the scientific publication.

Table 7.1 Overview of data availability.

Type	**Database**	**Available**	**Free Access**	**Contact**
Sediment echosounder (Parasound P70 raw data)	PANGAEA	https://doi.pangaea.de/10.1594/PANGAEA.973990	December 2027	gbohrmann@marum.de
Water column data, (Kongsberg EM122)	PANGAEA	https://doi.pangaea.de/10.1594/PANGAEA.973989	December 2027	gbohrmann@marum.de
Multibeam bathymetry data (Kongsberg EM122)	PANGAEA	https://doi.pangaea.de/10.1594/PANGAEA.973988	December 2027	gbohrmann@marum.de
Multibeam bathymetry Raw data (EM711)	PANGAEA	https://doi.pangaea.de/10.1594/PANGAEA.974044	December 2027	gbohrmann@marum.de
CTD-RO data (CTD 911)	PANGAEA	https://doi.pangaea.de/10.1594/PANGAEA.974381	December 2027	gbohrmann@marum.de

8 Acknowledgements

We scientists are very happy about the new scientific findings from the Jøtul hydrothermal field with many new measurement results, data, samples and observations. We scientists are very happy about the goals we have achieved and are returning home with very good results. We owe the success of the scientific work to the excellent and friendly support of the ship's crew in all areas (nautical, WTD, deck crew, engine and service area, etc.), the shipping company and the employees of the German Research Fleet Coordination Centre as well as the colleagues from MARUM logistics. We would especially like to thank Captain Björn Maass and his entire crew, who were always friendly and helpful in all matters. The ship time was provided by the Deutsche Forschungsgemeinschaft within the METEOR/MERIAN core program. Funding of the cruise was performed by the Bremen Cluster of Excellence "The Ocean Floor – Earth's Uncharted Interface".

9 References

Bohrmann, G., Streuff, K., Romer, M., Knutsen, S. M., Smrzka, D., Kleint, J., Rohler, A., Pape, T., Sandsta, N. R., Kleint, C., Hansen, C., Dos Santos Ferreira, C., Walter, M., de Paula Santos, G. M., & Bach, W. 2024, Discovery of the first hydrothermal field along the 500-km-long Knipovich Ridge offshore Svalbard (the Jøtul field). Sci Rep, 14(1), 10168. https://doi.org/10.1038/s41598-024-60802-3

Chand, S., Knies, J., Geissler, W.H., Plaza-Faverola, A., & Thorsnes, T. (2024). Acoustic evidence of hydrocarbon release associated with the Spitsbergen Transform Fault, north of the Molloy Ridge, Fram Strait. Frontiers in Earth Science, 12, doi: 10.3389/feart.2024.1347252.

Dittmar T and Stubbins A, 2014, Dissolved Organic Matter in Aquatic Systems, Reference Module in Earth Systems and Environmental Sciences, Treatise on Geochemistry (second edition), Vol. 12, Pages 125-156; https://doi.org/10.1016/B978-0-08-095975-7.01010-X

Edmonds et al., 2003, Discovery of abundant hydrothermal venting on the ultraslow-spreading Gakkel ridge in the Arctic Ocean, Nature, Vol. 421, 252-256, https://doi.org/10.1038/nature01351

Garbe-Schönberg, D., Koschinsky, A., Ratmeyer, V., Jähmlich, H., Westernstroeer, U. 2006, KIPS – a new multiport valve-based all-Teflon fluid sampling system for ROVs. Geophys. Res. Abstracts, Vol. 8, 7032

German et al. 2022, Volcanically hosted venting with indications of ultramafic influence at Aurora hydrothermal field on Gakkel Ridge, Nature Communications, 13:6517, doi: 10.1038/s41467-022-34014-0

Gooday, A. J., & Rathburn, A. E. 1999, Temporal variability in living deep-sea benthic foraminifera: a review. Earth-Science Reviews, Vol. 46 (1-4), 187-212, https://doi.org/10.1016/S0012-8252(99)00010-0

Kleint C., Bach W., Diehl A., Fröhberg N., Garbe-Schönberg D., Hartmann J.F., de Ronde C.E.J., Sander S., Strauss H., Stucker V.K., Thal J., Zitoun R., Koschinsky A., Geochemical characterization of highly diverse hydrothermal fluids from volcanic vent systems of the Kermadec intraoceanic arc, Chemical Geology, 2019, Vol. 528, 119-289, https://doi.org/10.1016/j.chemgeo.2019.119289

Knies, J., E. Damm, J. Gutt, U. Mann, and L. Pinturier (2004), Near-surface hydrocarbon anomalies in shelf sediments off Spitsbergen: Evidences for past seepages, Geochem. Geophys. Geosyst., 5, Q06003, doi:10.1029/2003GC000687

Koschinsky A., Garbe-Schönberg D., Sander S., Schmidt K., Gennerich H.-H., Strauss H.; Hydrothermal venting at pressure-temperature conditions above the critical point of seawater, 5°S on the Mid-Atlantic Ridge. Geology 2008; 36 (8): 615–618, doi: https://doi.org/10.1130/G24726A.1

Levin, Lisa A., et al., 2016, Hydrothermal Vents and Methane Seeps: Rethinking the Sphere of Influence. Frontiers in Marine Science, Vol 3, doi: 10.3389/fmars.2016.00072

Liira, M., Noormets, R., Sepp, H., Kekišev, O., Maddison, M., & Olaussen, S. (2019). Sediment geochemical study of hydrocarbon seeps in Isfjorden and Mohnbukta: a comparison between western and eastern Spitsbergen, Svalbard. *arktos*, *5*, 49-62

Panieri, G. (2006) The effect of shallow marine hydrothermal vent activity on benthic foraminifera (Aeolian Arc, Tyrrhenian Sea) Journal of Foraminiferal Research, v. 36, no. 1, p. 3–14

Pawlowski et al., 2013, New supraordinal classification of Foraminifera: Molecules meet morphology, Marine Micropaleontology, Vol. 100, Pages 1-10, https://doi.org/10.1016/j.marmicro.2013.04.002

Pilot et al. 2024, Microseismicity around Loki's Castle Hydrothermal Vent Field Reveals the Early Stages of Detachment Faulting at the Mohns-Knipovich Ridge Intersection, Geochemistry Geophysics Geosystems, in review

Roy, S., Senger, K., Braathen, A., Noormets, R., Hovland, M., Olaussen, S., 2014. Fluid migration pathways to seafloor seepage in inner Isfjorden and Adventfjorden, Svalbard. Norwegian Journal of Geology 94, 99-119

Roy, S., Hovland, M., Noormets, R., Olaussen, S., 2015. Seepage in Isfjorden and its tributary fjords, West Spitsbergen. Marine Geology 363, 146-159. DOI: 10.1144/GSL.SP.1993.070.01.06

Rudels, B., Björk, G., Nilsson, J., Winsor, P., Lake, I., & Nohr, C. (2005). The interaction between waters from the Arctic Ocean and the Nordic Seas north of Fram Strait and along the East Greenland Current: results from the Arctic Ocean-02 Oden expedition. Journal of Marine Systems, 55(1), 1-30, doi: 10.1016/j.jmarsys.2004.06.008.

Schlichtholz, P., & Houssais, M.-N. (1999). An inverse modeling study in Fram Strait. Part II: Water mass distribution and transports. Deep Sea Research Part II: Topical Studies in Oceanography, 46(6), 1137-1168, doi: 10.1016/S0967-0645(99)00017-X.

Seeberg-Elverfeldt, J., Schlüter, M., Feseker, T., & Kölling, M. 2005, Rhizon sampling of porewaters near the sediment-water interface of aquatic systems. Limnology and Oceanography: Methods, 3, 361-371, doi: 10.4319/lom.2005.3.361.

Seewald, J. S., Doherty, K. W., Hammar, T. R., & Liberatore, S. P. 2002, A new gas-tight isobaric sampler for hydrothermal fluids. Deep Sea Research Part I: Oceanographic Research Papers, 49(1), 189-196. https://doi.org/10.1016/s0967-0637(01)00046-2

Seewald, J. S., Geoffrey Wheat, C., Reeves, E. P., Tivey, M. K., Sievert, S. M., Stakes, D., Sylva, S. P., Lilley, M. D., & Heuer, V. B. 2024, Spatial evolution and temporal stability of hydrothermal processes at sediment-covered spreading centers: Constraints from Guaymas Basin, Gulf of California. Geochimica et Cosmochimica Acta, 367, 87-106. https://doi.org/10.1016/j.gca.2023.12.006

Appendix

App. 1 List of all MAPR and ORP deployments. Geographic coordinates are not given for Tow-Yo CTD casts and ROV dives, since the position varied during the deployments.

Station	Device	GeoB	Area	Lat	Lon	ORP-Anomaly	Comment
1	CTD-01	26201-1	Jøtul field	77° 26.426'	07° 42.402'	Yes	
9	ROV-481	26209-1	Jøtul field	77° 26.411'	07° 42.506'		No records
16	CTD-02	26216-1	Jøtul field			Yes	Several
19	CTD-03	26219-1	Jøtul field	77° 26.390'	07° 42.542'	Yes	
20	CTD-04	26220-1	Molløy Flare	79° 36.828'	03° 39.716'	No	
21	CTD-05	26221-1	Molløy Flare	79° 48.125'	03° 10.706'	No	
22	ROV-482	26222-1	Molløy Flare	79° 36.847'	03° 39.695’	Yes	Several
23	CTD-06	26223-1	Molløy Flare	79° 36.873'	03° 39.632'	No	
24	CTD-07	26224-1	Jøtul field	77° 26.396'	07° 42.682'	Yes	
25	MIC-01	26225-1	Jøtul field	77° 26.399'	07° 42.506'	No	
26	MIC-02	26226-1	Jøtul field	77° 26.428'	07° 42.501'	No	
27	MIC-03	26227-1	Jøtul field	77° 26.431'	07° 42.482'	No	
28	ROV-483	26228-1	Jøtul field	77° 26.201’	07° 42.460’	Yes	Several
29	CTD-08	26229-1	Jøtul field			Yes	
30	MIC-04	26230-1	Jøtul field	77° 26.457'	07° 42.504'	Yes	
31	MIC-05	26231-1	Jøtul field	77° 26.462'	07° 42.332'	Yes	
32	MIC-06	26232-1	Jøtul field	77° 26.458'	07° 42.146'	No	
33	MIC-07	26233-1	Jøtul field	77° 26.463'	07° 42.894'	No	
34	CTD-09	26234-1	Jøtul field			Yes	Several
35	ROV-484	26235-1	Jøtul field	77° 26.217’	07° 42.484’	Yes	
36	MIC-08	26236-1	Jøtul field	77° 26.496'	07° 42.539'	Yes	Weak
37	MIC-09	26237-1	Jøtul field	77° 26.495'	07° 42.340'	No	
38	MIC-10	26238-1	Jøtul field	77° 26.496'	07° 42.150'	No	
39	MIC-11	26239-1	Jøtul field	77° 26.501'	07° 42.951'	No	
40	MIC-12	26240-1	Jøtul field	77° 26.569'	07° 42.792'	No	
41	CTD-10	26241-1	Jøtul field			Yes	Several
42	MIC-13	26242-1	Jøtul field	77° 26.564'	07° 42.191'	No	
43	MIC-14	26243-1	Jøtul field	77° 26.570'	07° 42.455'	No	
44	MIC-15	26244-1	Jøtul field	77° 26.567'	07° 42.700'	Yes	
45	MIC-16	26245-1	Jøtul field	77° 26.579'	07° 42.045'	Yes	
46	CTD-11	26246-1	Jøtul field			Yes	Several
47	MIC-17	26247-1	Jøtul field	77° 26.493'	07° 42.673'	Yes	
48	MIC-18	26248-1	Jøtul field	77° 26.530'	07° 43.021'	Yes	Weak
49	MIC-19	26249-1	Jøtul field	77° 26.507'	07° 43.059'	Yes	
50	MIC-20	26250-1	Jøtul field	77° 26.430'	07° 43.991'		No records
51	CTD-12	26251-1	Jøtul field			Yes	Several
52	ROV-485	26252-1	Jøtul Field	77° 26.414’	07° 42.265’	Yes	
53	CTD-13	26253-1	Jøtul Field			Yes	
54	MIC-21	26254-1	Jøtul Field	77° 26.415'	07° 42.999'	Yes	
55	MIC-22	26255-1	Jøtul Field	77° 26.459'	07° 43.046'	Yes	
56	MIC-23	26256-1	Jøtul Field	77° 26.460'	07° 43.215'		No records

58	MIC-24	26258-1	Jøtul Field	77° 26.574'	07° 43.238'	Yes	
59	MIC-25	26259-1	Jøtul Field	77° 26.543'	07° 43.590'	Yes	
60	MIC-26	26260-1	Jøtul Field	77° 26.605'	07° 43.897'	Yes	
61	MIC-27	26261-1	Jøtul Field	77° 26.609'	07° 43.581'	Yes	
62-1	CTD-14_1	26262-1	Jøtul Field	77° 26.152'	07° 41.960'	No	Aborted
62-2	CTD-14_2	26262-2	Jøtul Field			Yes	
63	MIC-28	26263-1	Jøtul Field	77° 26.619'	07° 43.190'	Yes	
64	MIC-29	26264-1	Jøtul Field	77° 26.635'	07° 42.851'	No	
65	MIC-30	26265-1	Jøtul Field	77° 26.648'	07° 42.517'	No	
66	MIC-31	26266-1	Jøtul Field	77° 26.655'	07° 42.186'	No	
67	CTD-15	26267-1	Jøtul Field			Yes	
68	MIC-32	26268-1	Jøtul Field	77° 26.342'	07° 42.720'	Yes	
69	ROV-486	26269-1	Jøtul Field	77° 26.197'	07° 42.193'	Yes	
70	CTD-16	26270-1	Jøtul Field			Yes	
71	CTD-17	26271-1	Jøtul Field			Yes	
72	ROV-487	26272-1	Jøtul Field	77° 26.389’	07° 42.515’	Yes	
73	CTD-18	26273-1	Jøtul Field			Yes	
74	ROV-488	26274-1	Jøtul Field	77° 26.351'	07° 42.379'	Yes	
75	CTD-19	26275-1	Jøtul Field			Yes	
76	MIC-33	26276-1	Jøtul Field	77° 26.355'	07° 42.536'	Yes	
77	MIC-34	26277-1	Jøtul Field	77° 26.295'	07° 42.619'	Yes	
78	MIC-35	26278-1	Jøtul Field	77° 26.324'	07° 42.653'	No	
79	CTD-20	26279-1	Jøtul Field			Yes	
80	ROV-489	26280-1	Jøtul Field			Yes	
81	CTD-21	26281-1	Jøtul Field			Yes	
82	ROV-490	26282-1	Jøtul Field			Yes	
83	CTD-22	26283-1	Jøtul Field			Yes	